

System level Analysis of advanced a-Si:H flexible and lightweight PV

Emilio J. Manrique Ambriz



System level analysis of advanced a-Si:H flexible and lightweight PV modules

Emilio J. Manrique Ambriz

by

to obtain the degree of Master of Science
at the Delft University of Technology,
to be defended publicly on Monday November 25, 2019 at 10:30 AM.

Student number: 4746309
Project duration: February 11, 2019 – November 25, 2019
Thesis committee: Prof. dr. ir. Arno Smets, TU Delft, supervisor
Dr. Gregory Pandraud, TU Delft, PVMD
Dr. ir. Babak Gholizad, TU Delft, DCE&S
Dr. Davide Bartesaghi, HyET Solar
Dr. Gianluca Limodio, TU Delft, PVMD

This thesis is confidential and cannot be made public until November 25, 2021.

An electronic version of this thesis is available at <http://repository.tudelft.nl/>.

Preface

To my parents, who have shaped me with their love into the person I am today, and whose support helped me to be in the place I am today. To my Godfathers, who supported me to pursue my studies abroad in the moment I needed it the most. To Gris. Thank you for joining me on my crazy adventures. And to my Grandma. Q.E.P.D. ...

Delft, November 2019

Acknowledgments

This work, which I am very proud of, would not have been possible without the help of many people. I would like to spend some lines thanking them for their support.

I would first like to thank my supervisor Prof. Dr. Ir. Arno Smets. He might not know it but his online EDX courses inspired me to join the master in science in Sustainable Energy Technology in TU Delft. Two years later I know I took the best possible decision. He also, he helped me to get an interesting thesis project which I very much enjoyed and I learned a lot from. And, to my surprise, even though his busy agenda, he always found time to discuss with me.

I would also like to thank my two company supervisors. First Ir. Robin Quax, he knew how to steer the project in the right direction, allowing me to work independently developing a lot of skills. He also believed in my capacity to accomplish the project. Thank you. Second but not last, Dr. Davide Bartesaghi. I'm pretty sure he spent much more time correcting my thesis than it would be politely acceptable. Thank you for helping me improve my writing.

Of course, this work involved a lot of physical work and diverse technical knowledge, which would not be possible for a single person to successfully accomplish in a 9 month period. Therefore I would like to thank everybody at HyET Solar for supporting me on the completion of this project. I believe you all gave valuable input for the "Outdoor system", A.K.A "The Emilio system." First, thank to Furkan, John Paul and Davide, even if you didn't notice, you were my Phd's daily supervisors. Thanks to Zafar and Maureen, experts on the practical matters involved and successfully making the work environment very pleasant. Thanks to Edward for giving valuable insights on the modules operation. Thanks to everybody from the production team, with your help I managed to accomplish the deadlines, and I forced myself to improve my Netherlands. Special thanks to Eberth and Jan, who greatly helped with the fabrication of physical components for the monitoring station, and the electrical connections. Also they didn't kill me after taking their tools and leaving the ladder outside for one month. Big thanks to Maurice and Lorenzo for volunteering their time for the project. Particular thanks to Devika for helping with the reflection measurements. Without you I would have finished the project easily one week after. Thanks to Mark and Joost for the technical insights. Oscar and Peter for the business insights. To Katerina for being a great office mate. And of course thanks to Quentin, Alexis and Max for helping with the build up of the system and the ordering of components. Very much appreciated.

I would also like to thank every at TU Delft that helped me with the project and build the model. Of course a big thanks to my daily supervisor Dr. Gianluca, who always helped me with a big smile. Special thanks to Stefaan, he greatly helped shape the data acquisition system. Thanks to Juan Camilo for his support, always willing to help. Thanks to Hesam for his support with the horicatcher and meteorology. And thanks to Rudi for patiently helping with the theory required for the reflection measurements and the reflection section in the model. Thanks to Arturo and Lory for their help with the PV lab. And a big thanks to Anthony for helping me build the computer model. Thank you.

I would also like to thank all my friends for helping me survive through the master and particularly through the thesis, and also for helping with the integration on the Dutch culture. Special thanks to the Heineken group, Josu, Rayen, Ricky, Bonny Budez, Marianita, Andrew, Lukas, Carolina, Berend, Charly, Espi, Elisa, Federico, Kritika, Bobby, Stella and Thomas. You made this 2 couple of years an unforgettable experience. Special thanks for the thesis support group A.K.A "Thesis Warriors", comprised of Josu, Rayen and Senja. Our daily routine helped me keep my mental sanity. And to my roomies Anthony, Ursula, Noelia and Rogier.

I would also like to thank for the support of the Mexican government that supported me during my master through the CONACYT-SENER scholarship, and the Central Bank of Mexico for supporting me with the FIDERH scholarship.

A big thank you to all my family for supporting me accomplish my dreams, particularly my father and my mother.

And last but not least, A big thank you to Gris for supporting me through the thesis with her love and affection.

Abstract

Thin film amorphous silicon based PV systems are a rather new and promising photovoltaic technology with plenty field for technological development and potential for unique applications such as integration within the built environment. Nevertheless, in order for the technology to be established, further technical development is required and economical aspects should be tackled, both in the module and system level.

From a commercial point of view, the ultimate goal of a PV system, once installed, is to cost effectively deliver the highest possible energy yield. In reality, the actual energy yield every system delivers is lower than the theoretical rated performance. Location and environmental factors, such as heating of the modules, irradiance, dirt accumulation, angle of incidence, Etc. affect the performance of the systems. Understanding the behaviour of this new technology under real operation conditions can provide reliable insights for its further development, help better estimate the energy yield amorphous silicon systems can provide and perhaps, help the technology differentiate itself from the better commercially established crystalline silicone based one.

This work investigates the effect of most of the location and environmental factors affecting the performance and the ultimate energy yield of an photovoltaic system comprised of flexible and lightweight amorphous silicon modules. The factors responsible for this performance decrease are individually investigated, and its effects are quantified by addressing in which manner they decrease the performance ratio of the system. A performance monitoring system was built expressly for this purpose, which data acquisition plan was based on the IEC 61724 -1 (2017) standard. A computer model with the capability of simulate the performance of the system after correcting for the evaluated mechanism was also constructed as part of this work using Matlab. This model was based on an experimental characterization of the modules, using live performance data as an input to give a performance ratio, and an assessment of the effect of loss factors.

The results allocated the source of the system losses up to a 78% of the total power decrease, considering the rest of the unexplained observed losses as effects of the active material degradation. The performance ratio of the system was reported on a daily basis for the evaluated period, concluding a strong correlation between a high irradiance and a high performance ratio. The common literature claim of a better behaviour of thin film a-Si:H technologies compared to c-Si was verified under this study, and the effects of system operation under low irradiance conditions was identified as the dominant loss mechanism.

Contents

Acknowledgments	v
Abstract	vii
1 Introduction	1
1.1 Motivation: Why studying thin film a-Si:H is relevant?	1
1.2 HyET Solar: A brief summary of the company	1
1.3 Relevance of performance monitoring for product development and improved reliability.	3
1.4 Work Objectives	3
1.5 Thesis outline	3
2 Performance Metrics for PV Systems	5
2.1 IEC 61724-1:2017, Photovoltaic system performance monitoring	5
2.2 Performance Ratio	6
3 System Level Loss Mechanisms of Thin film a-Si:h modules	7
3.1 Temperature	8
3.2 Irradiance intensity variations with respect to STC	8
3.3 Ohmic losses	8
3.4 Power conversion losses.	9
3.5 Reflection losses	9
3.6 Soiling.	9
3.7 Partial shading	9
3.8 Spectral Mismatch	10
3.9 Degradation.	10
4 Methodology	13
4.1 General Methodology Description	14
4.2 Temperature effects	15
4.2.1 Measuring the temperature coefficient	15
4.2.2 Measuring the array module temperature	19
4.2.3 Temperature corrected performance model.	21
4.3 Angle of Incidence (AOI).	21
4.3.1 Calculating the position of the Sun and AOI	21
4.3.2 Calculating the AOI.	23
4.3.3 Calculating the correction for reflection losses	23
4.4 Low irradiance	25
4.5 Power Conversion and Ohmic Losses	30
4.6 Soiling losses	31
4.7 Partial shading	32
5 Photovoltaic and Data Acquisition System Design	35
5.1 Design Considerations	35
5.1.1 IEC 61724-1 class A Standard.	36
5.1.2 Data Resolution.	37
5.1.3 Modularity.	38
5.1.4 Available Resources	38
5.1.5 Level of monitoring	38
5.1.6 Monitoring compatibility between c-Si and a-Si:H technology	39
5.1.7 Design for Performance	40
5.1.8 Availability of resources	40

5.2	Analyzed design proposals	40
5.3	Selected equipment	43
5.3.1	Electrical System	43
5.3.2	Data Acquisition System	45
5.3.3	Crystalline silicone photovoltaic modules	52
5.3.4	Mounting System	52
5.4	Modules	55
5.5	Final System	56
6	Data Analysis	59
6.1	Temperature losses	60
6.2	Angle of incidence losses	62
6.3	Low irradiance losses	64
6.4	Power conversion and ohmic losses	65
6.5	Intra-day Analysis	66
6.6	Full Period Analysis	71
A	Power Optimizers Datasheets	81
B	Solar edge SE2200H Datasheet	85
C	Datalogger	89
D	Crystalline silicon modules data sheet	99
	Bibliography	103

Introduction

1.1. Motivation: Why studying thin film a-Si:H is relevant?

Hydrogenated amorphous silicon photovoltaic devices are a second generation photovoltaic technology that has been studied for over 40 years. Unlike its crystalline based first generation counterpart, a-Si:H devices require a considerably thinner absorbing layer in the order of a few μm , compared to the traditional wafer thickness of c-Si devices. This could prove to be an advantage on reducing production costs as less material can be used, and a simpler production procedure can be followed. Nevertheless, this technology still requires further research to reach a maturity level that allows it to compete with crystalline silicon, being some of the main drawbacks of the technology a lower initial efficiency and higher degradation rate than c-Si and even than other thin film technologies such as cadmium tellurium and copper indium gallium selenide based devices [25].

Regardless of the apparent drawbacks, the technology presents a positive outlook as it offers unique possibilities, highly regarded in a future scenario where carbon neutral energy production technologies will have a larger share on the energy mix. In a future scenario where the implementation of photovoltaics is being done on a considerably larger scale, additional considerations need to be addressed such as the availability of the used materials for the manufacture of the solar modules, the toxicity of these materials, and the environmental impact of its disposal after their productive lifetime is over. Here, a-Si:H based technologies appear as a suitable response for these considerations as the materials used for their fabrication are highly abundant and do not present toxic effects, a factor that cannot be said of the CIGS and CdTe technologies. This claim can be noted on Figure 1.1. Additionally, the processing temperatures required for the manufacture of the photo-active layers and contacts is low, having a reduced energy payback time. Depending on the used procedure for processing a-Si:H modules, the highest used temperature can be well below $200^{\circ}C$.

These environmental factors make the research and development of a-Si:H modules an interesting approach to foster the energy transition into renewable energy technologies. If the technology reaches a maturity level when it can be economically attractive to use a photovoltaic alternative to produce energy, being it massively on a large solar farm, or at a local distributed scale such as in the integration with the built environment, a positive impact on keeping a livable planet for future generations would be done.

1.2. HyET Solar: A brief summary of the company

HyET Solar is a Dutch owned company located in Arnhem, the Netherlands. It was founded in 2012 after a private investor acquired the company, formerly known as Helianthos. Helianthos was a daughter company of the Akzo Nobel corporation, starting operations in 1997. Some time after, it operated jointly under the umbrella of Akzo Nobel and Shell, and finally it was taken over by the company Nuon, now part of the Vattenfall group. Currently, the company is comprised of a small production line operating under the unique Roll-to-Roll production process, where thin film a-Si:H solar modules can be created in a virtually uninterrupted process, which allows the fabrication of custom lengths to be produced. At

	Materials	Abundance	Toxic	scale to TW
Substrate	glass, plastic or metal foil	high	No	easy
TCO	ZnO:B, ZnO:Al, Sn ₂ O ₃ :F	high	No	easy, adapted by industry
	In ₂ O ₃ :Sn, In ₂ O ₃ :H	low (In)	No	strongly limited by In
p-layer	p-SiC:H, p-SiO _x :H	high	No	easy
absorber layers	a-Si:H, nc-Si:H	high	No	easy
	a-SiGe:H, nc-SiGe:H	high	No	easy
n-layer	n-SiO _x :H, n-a-Si:H	high	No	easy
Back contact & reflector	ZnO:B+WP	high	No	easy, adapted by industry
	Ag	medium	No	limited

Figure 1.1

A list of materials used for thin-film silicon solar cells. Extracted from Materials and Light Management for High-Efficiency Thin Film Silicon Solar Cells, TAN, 2015.

the moment of writing this work, the company is undergoing a scale-up process where the production facilities are being quadruplicated in size, expecting to drastically increase the produced yield.

The current business model of the company focuses on a continuous development of the product, looking to increase the rated efficiency of the end module, and improve the reliability (or stability) of operation through the expected lifetime of the module. For this, a large share for the work done at the company focuses on the research and development of their proprietary product. Going deeper into the main product, HyET solar produces an advanced flexible and lightweight thin film solar module, based on a-Si:H. By having a polymer as a top encapsulant instead of glass, the modules have bending capabilities and a reduced weight, making them an optimum product for integration with the built environment. The current base model is based on a single layer of an a-Si:H semiconductor material, nevertheless the company also offers a tandem device with combines an a-Si:H and μ c-Si semiconductor material.

The HyET Solar product is still being sold in a niche market, nevertheless the implications of the physical characteristics of the product make it interesting for mass commercialization if certain efficiency and reliability milestones are reached, that would make this technology more competitive with respect to the already established c-Si technology. Knowing this, HyET Solar is directing its efforts towards the improvement of the initial efficiency delivered by the modules, straight out of the production line, and by performing a quantity of standard test in the photovoltaic industry it is trying to understand the behaviour of the modules after long periods of operations, looking for causes for performance decrease and malfunction. The later effort aims to improve the reliability of the product, assuring that the product will operate in a continuous and reliable way for the stated lifetime.

1.3. Relevance of performance monitoring for product development and improved reliability

Having an improved product reliability in mind, the first stage to improve a product is to know the sources influencing its behaviour, and then understanding how and to what extent they affect the product. By knowing where the product currently stands, its strengths and weaknesses can be addressed. Here is where this project stands for HyET Solar. By obtaining reliable performance data of their newest product under real operation conditions, faults can be identified and a latter research can focus on tackle the most pressing issues limiting performance, helping with the decision making process on development by knowing the hierarchy of performance limiting factors. On the other hand, having a proven empirical documentation of the claimed advantages of the product, can be beneficial for merchandising the product.

Furthermore, having a clear understanding of the influence of factors expected during normal operation conditions on energy production would allow the company to identify the most suitable applications and environments in which the HyET modules would yield higher amounts of energy per kilowatt installed.

Although plenty of research and experimentation is being and has been done by HyET Solar on their modules, mostly of the analysis performed so far were limited to a module level. Having a way to monitor the performance of the HyET Solar modules on their intended application environment, meaning jointly performing on a photovoltaic system, would present high value for the company as these data were scarce at the time the project, on which this thesis work is based, started.

1.4. Work Objectives

The main objective of this work is to answer the research question. How would a photovoltaic system comprised of HyET Solar advanced a-Si:H flexible and lightweight PV modules will perform under real operation conditions in Arnhem, the Netherlands? In order to answer this question, sub objectives need to be accomplished and sub questions need to be answered, being them the following:

- Which factors (environmental, location or electrical) affect the system level performance of a photovoltaic system comprised of HyET Solar a-Si:H flexible and lightweight modules?
- What is the quantitative influence of these factors on the decreased performance experience by an a-Si:H based system, located in Arnhem, the Netherlands?
- What would be the performance ratio of an a-Si:H based system, located in Arnhem, the Netherlands?
- How would the performance ratio of an a-Si:H based system, located in Arnhem, the Netherlands compare to the performance ratio on an c-Si based system, located in Arnhem, the Netherlands?

1.5. Thesis outline

The current work is organized as follows. Chapter 2 and 3 serve as an introductory section to the topics discussed across this work, and together summarize the literature review stage of it. First, Chapter 2 will introduce the main metrics used to evaluate the performance of photovoltaic systems among the academic community and the industry. Following on the introduction, Chapter 3 will discuss the factors that commonly modify the performance of a photovoltaic system. The second stage of the work is the description of the methodology used to answer the research questions here described, which is presented in Chapters 4 and 5. Chapter 4, explains the experimental procedure followed to characterize the module behaviour when exposed to a particular loss factor, presents the logic behind the analysis, introduces the approach of using a real time analysis of the measured parameters, and discloses the essence of the mathematical model constructed to perform this analysis. Following with the methodology section, Chapter 5 explains the technical considerations followed on building a monitoring stations with the sufficient capabilities to obtain relevant data for this and future work. The last stage of this work, the analysis of the model, is composed by the Chapter 6 and the Conclusions. To finalize, an outlook on this work is presented.

2

Performance Metrics for PV Systems

The industry standard to measure the performance of photovoltaic systems is the performance ratio [27] [13]. This widely used metric is a normalized approach used both by industry and academia to describe the goodness of a photovoltaic system operation, either by design, technology or location. Being a normalized metric, it allows the comparison between photostatic systems regardless of size, application, selected power electronics, topology, irradiance conditions, technology, and to a certain extent even location. While there is common ground among the reviewed literature on measuring this metric, the assessing of the data and the complexity levels seen between various sources highly varies according to applications of the results. For this reason, this work uses the standard definition published by the International Electrotechnical Commission (IEC), IEC 61724-1 2017.

As the goal of this work is to obtain results that can be easily comparable between different HyET Solar a-Si:H module generations, different HyET Solar photovoltaic systems and between the performance of other photovoltaic technology, the performance ratio is selected as the main metric.

While this will be the primary metric, other performance metric will be used through this work, the main ones being:

- The standard test conditions power P_{STC} .
 P_{STC} refers to an ideal power obtained by multiplying the rated efficiency η_{STC} times the irradiance received by the module array, or plane of array irradiance Irr_{POA} , times the active area of the module.
- The real power DC P_{DC} .
 P_{DC} refer to the maximum power point power delivered by the modules before any power conversion is effected, and before the electrical energy flows through any cable, being therefore exempt from resistive losses and power conversion losses.
- The real power AC P_{AC} .
 P_{AC} refers to the maximum power point power delivered by the modules after flowing through the system cables, and after being converted from direct current DC into alternate current AC. This power is also referred to as the power delivered by the inverter to the grid or house appliance.

2.1. IEC 61724-1:2017, Photovoltaic system performance monitoring

To facilitate the electrical performance analysis effectuated, this work used, when possible, the described methodology presented by the IEC 61724-1:201 standard on photovoltaic system performance monitoring. This is a standard defined by the IEC to design, build and operate performance monitoring stations under a standardized level of quality.

The International Electrotechnical Commission is an international organization in charge of standardizing industrial practices regarding electrical technology. On 1998 the IEC developed a standard on performance monitoring of photovoltaic systems. The IEC 61724 -1 (2017) is the updated version, finished on 2017. It discusses the best practices of PV Systems monitoring and the minimum requirements in order to unbiasedly compare the performance of the monitored system. The standard outlines equipment, methods and terminology for performance monitoring. It includes the required accuracy and suggested sensors. The main advantage of the standard is that it defines a performance ratio.

2.2. Performance Ratio

The IEC standard 61724-1 2017 defines the performance ratio as the ratio between the PV system real energy yield and the reference Yield [9]. This can be easily seen on equation 2.1, where Y_F accounts for the PV system real yield, and Y_R accounts for the reference yield.

$$PR = \frac{Y_F}{Y_R} \quad (2.1)$$

The ratio can be expressed in practical terms as seen on equation 2.2, 2.3 and 2.4, where E stands for the net power output, P_0 stands for rated power, H_{POA} stands for the total inplane irradiance, and G_{POA} stands for the PV reference irradiance, which is normally $1,000 \frac{W}{m^2}$.

$$PR = \frac{E_{Specific}}{H_{Specific}} \times 100\% \quad (2.2)$$

$$E_{Specific} = \frac{E}{P_0} = \frac{kWh}{kW} = h \quad (2.3)$$

$$H_{Specific} = \frac{H_{POA}}{G_{STC}} = \frac{\frac{kWh}{m^2}}{\frac{kW}{m^2}} = h \quad (2.4)$$

3

System Level Loss Mechanisms of Thin film a-Si:h modules

As noted in Chapter 2, the real performance of any PV system will often differ from the rated performance. While cell-level performance loss mechanisms account for a large percent of the mismatch between the input and output energy delivered by the solar cells, these mechanisms should not be included on a system level analysis of losses as their effects are already taken into account on the module rated efficiency η_{STC} . This way, when a module operates at conditions that differ from the rated operation conditions (also referred as standard test conditions), additional factors influence the performance of the modules.

Standard test conditions (STC) are operation conditions easy to replicate in a laboratory, therefore they are used to characterize the module operation performance. These conditions often reflect beneficial operation conditions for the module performance, and typically yield high power outputs from the modules. The STC refer to an irradiance level of $1,000 \frac{W}{m^2}$, a module temperature of $25^{\circ}C$, and an incident light spectrum corresponding to Air Mass (AM) 1.5.

Typically, the real operation conditions that the modules are exposed to are far from standard conditions and tend to reduce the performance of the modules as many factors not considered in the rated efficiency η_{STC} come into play. The main factors associated to a lower output than the one expected at STC operational conditions are listed next:

- Temperature
- Lower than STC irradiance
- Conduction losses
- Power conversion losses
- Reflection losses
- Soiling
- Partial shading
- Spectral mismatch
- Degradation

3.1. Temperature

The detrimental effect that the temperature has on the performance of PV modules has been broadly documented by plenty of authors, such as King [11], Perez [17], Riesen [18], Dubey [7], DU [6] and Buday [4]. Modules are usually optimized to work at STC and present higher energy yields at lower temperatures, while showing lower yields at higher operational temperatures. This effect can partially be explained by the fact that the recombination rate of charge carriers increases when the temperature in the semiconductor increases as the charge carrier concentration in the absorber layer increases [7]. This lower energy yield can be expressed as a lower than STC temperature operational efficiency expected for a PV system under real operation conditions.

Under normal operation conditions, a PV system will be exposed to a number of factors that will determine its operational temperature. Some of the most important factors are the average irradiance the system receives, the ambient temperature, the wind speed and wind direction, and the heat dissipation characteristics of the mounting. Irradiance can be accounted as the main heat input to the system while all other factors will influence the ability that the system has to dissipate the heat to the environment. It is therefore not a surprise that the system location has a large influence on the expected operational temperature of the system. A location closer to the equator will probably receive higher levels of irradiance and possibly present higher average ambient temperatures than a further location. As an additional consideration, empirical studies suggest that the average wind speed to which the system is exposed has a greater effect on heat dissipation than the ambient temperature itself [18], therefore making the location average wind speed of particular interest.

The above cited literature suggests an approximation for evaluating the performance of photovoltaic modules exposed to higher than STC temperatures, the temperature coefficient k_T . This is a linear rate of change that approximates the real variation on performance of the module with respect to temperature, by decreasing the module efficiency with respect to temperature. There are two ways of reporting the temperature coefficient, one being the direct efficiency variation of the efficiency with respect to temperature, units $\frac{\%}{K}$, and the second one being the normalized variation of efficiency with the STC efficiency η_{STC} , with respect to temperature, units $\frac{1}{K}$.

3.2. Irradiance intensity variations with respect to STC

Solar modules are designed to operate at irradiance levels close to STC or higher, showing a higher charge carrier generation rate when exposed to higher irradiance levels. On the contrary, the operation at lower irradiance than STC is reported to yield lower efficiencies than rated [29]. As the incident irradiance level decreases, other factors appear dominant on the module, such as internal resistive losses that otherwise would have a relative low impact on the lower decrease, however see their impact increased as the relative difference between the losses and the incident energy decrease.

The variations in efficiency due to low irradiance follow an exponential decrease as the incident irradiance approaches minimum levels, therefore this variations are usually described with power curves.

3.3. Ohmic losses

The electrical current delivered by the solar modules travels from the output connectors to the inverter through cables, where resistive or ohmic losses are present. As this is an inherent characteristic of electrical current through a conductor, there are few things that can be done to prevent it. The amount of losses related to the resistance presented on the cables will depend on the thickness of the cables, with cables of lower diameters having a larger resistance per unit length. A second factor will be the total length of the cabling used from the modules to the inverter, being this of higher concern for large systems such as PV farms.

An easy way to estimate the share of losses a PV system due to cable resistance is to refer to the cable properties, where the resistance per unit length is stated. A simple calculation on the overall used cable length will output the amount of losses.

3.4. Power conversion losses

The ever-present loss mechanisms on a photovoltaic system is the effect of power conversion. This losses are present on the power conversion devices such as power optimizers and inverters. The losses accounted to power conversion usually increase as the power conversion drifts further from the rated power of the equipment, and are lower when the system power operates closer to the rated power of the inverter. A good photovoltaic system design will therefore try to approximate the rated power of the inverter, trying to minimize the periods of losses related to a larger mismatch between the inverter rated power, and the actual power delivered by the system.

3.5. Reflection losses

While optical losses are one of the most important loss factor in photovoltaic cells, their effect is already accounted for in the rated efficiency η_{STC} of the modules. Nevertheless, under real operation conditions, the photovoltaic systems operate at a varying angle of incidence of light, as the sun position changes through the day. This factor promotes an increment on the total reflection on the modules surface, making the losses grow larger than the rated value. This increment in the losses usually increases as the angle of incidence increases, being maximum at the maximum possible angle of incidence between the modules and the Sun.

3.6. Soiling

The term soiling refers to the natural accumulation of polluting particles on the module surface. The size and origin varies drastically as it includes natural particles such as dirt and sand, as well as anthropogenic particles such as fumes, carbon, concrete, etc. The soiling occurs during normal operation conditions for photovoltaic systems without programmed module surface cleaning on their maintenance schedule, and it tends to decrease its concentration after being exposed to rain, nevertheless while rain naturally decreases the effect of soiling, it has been reported that certain particles do not get detached without a more thorough cleaning. The effect of soil accumulation on the surface modules causes a decreased performance as the module is partially shaded. Other reported effects include the amplification of reflection losses related to the angle of incidence of light on the modules [26].

The impact of soiling on module performance has been documented in multiple studies [31], [3], and it has been demonstrated that the average impact is location dependant. This can be understood as the soiling rate varies with the environment, and the rain rate also does. Therefore, it can be expected to have higher losses due to this loss mechanism in dry desert areas, compared to locations that receive large amounts of rain.

3.7. Partial shading

The term partial shading refers to two main factors, the first one being a lower performance ratio obtained in a photovoltaic array as part of the array is not exposed to sunlight, decreasing the input energy on the array, while the irradiance measurement instrument is not exposed to it. This combination causes a false reading of input power for a whole array, as in reality a lower influx of light is being received by the array, than that reported by the measurement instrument. This effect is usually greater on large photovoltaic arrays such as photovoltaic farms [5].

The second factor is the partial shading experienced by a single module. This condition causes a mismatch on the power production among the module cells, as different irradiance levels are being fed to the cells composing the module. This causes an effect in which the cells exposed to a shade absorb the electric power generated by the unshaded cells, which causes that the shaded cells dissipate this power in the form of heat, usually in a localized section of the cell [30]. This effect is known in the industry as a hot spot and is reported to cause great damage to solar cells [19]. Most PV modules include bypass diodes to counter the effect of partial shading on hot spot formation. Bypass diodes redirect the flow of current by changing their polarity, allowing current to flow through them instead of through the cell in shaded conditions.

3.8. Spectral Mismatch

Solar modules are designed to work optimally at a specified Air Mass, being the most widely used for module characterisation the Air Mass 1.5, which refers to the resulting incident spectral pattern received at Earth's surface after traveling a distance equal to 1.5 times the atmospheric thickness if the most direct route would be followed, which usually happens at 12:00 on the earth equator. Figure 3.1 shows the spectral distribution from the AM 0, AM 1.5 G and D (where G and D stand for Direct nad Global, respectively). It can be seen that the spectral available power decreases as the air mass increases. This can be explained as the atmosphere is formed by small particles that reflect or absorb certain wavelengths from the incident irradiance, resulting in the fact that a longer path travel by the light across the atmosphere will result in a lower resulting spectral power density.

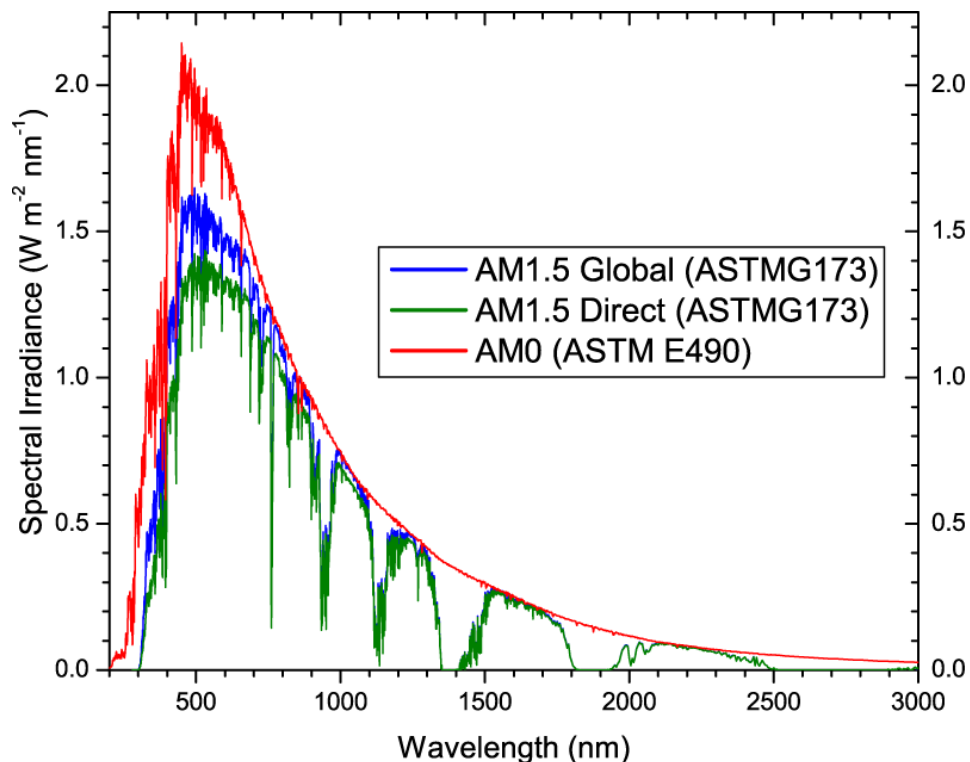


Figure 3.1

Spectral irradiance of Air Mass 1.5 and 0. The red curve represents the AM 0 spectrum, which relates to the incident solar spectrum experienced outside the earth's atmosphere. AM 1.5 global and direct relates to the solar spectrum experienced at the Earth's surface with an atmosphere thickness of 1.5 times the direct normal atmospheric thickness, experienced due to an incidence of the light of 48°.

A higher Air Mass is experienced during sunrise and sunset conditions, involving effects like Mir and Rayleigh scattering in the incident light, and modifying the spectral pattern and power density received by the modules at these periods. This in return causes a decreased performance of the PV modules, which is band-gap dependant.

3.9. Degradation

Degradation is a factor that affects the chemical composition of the semiconductor materials involved in the generation and transport of charge carriers as a consequence of the photovoltaic effect. this re-composition propitiates a reduced generation and/or an increased recombination of charges, therefore reducing the energy conversion efficiency. The term degradation also infers the effect of its dependence with time, making a photovoltaic material lose power at different rates after initial production.

There are plenty of factors involved in degradation of photovoltaic materials. For a-Si:H modules, one of the most studied, and currently unavoidable, mechanisms is the light induced degradation (LID), also known as the Staebler–Wronski effect as it was first studied in 1977 by David L. Staebler and

Christopher R. Wronski. The light incident in the semiconductor creates metastable defects that promote recombination of the electric charges, thus lowering the amount of charges that can be collected and resulting in a lower photogenerated current. [22].

While LID is present in all photovoltaic technologies, it plays a prominent role in a-Si:H, for reasons not fully understood yet [23], [21]. It is reported to have a large influence on decreasing the initial performance of the a-Si:H modules after few hours of exposure to sunlight, and its influence continues over the years, although at a lower rate. For this reason, this technology usually accounts for his quick drop in efficiency by having an averaged performance drop already integrated in their rated efficiency.

4

Methodology

Chapter 2 explained the industry standard for assessing the performance of a photovoltaic system and Chapter 3 showed the mechanisms responsible for performance losses. This Chapter refers to the methodology used to answer the following 3 questions: i) Quantitatively assess to which extent each mechanism is affecting the power performance of a photovoltaic system comprised of HyET Solar flexible and lightweight hydrogenated amorphous silicon solar modules. ii) How losses can be translated into a decreased share of an a-Si:H system Performance Ratio. iii) How the performance ratio of an a-Si:H based system would compare to that of a c-Si based one, when both systems operate in the same location, being this the Netherlands.

The first requirement to answer these questions was to have the performance data and know the characteristics of the modules to be evaluated. This proved an initial challenge for two main reasons. Firstly, although HyET Solar placed modules under monitored systems in the past, issues external to the company made the data impossible to retrieve. Secondly, the inherent nature of the state of the product means that improvements are done on a constant basis. This leads to have a different baseline product after a short period of time, in particular when compared to the variations done on more established technologies. As a result of the aforementioned factors, the procurement of proper real conditions performance data from the current baseline product was the first topic to be addressed. Chapter 5 will refer to the manner this first technical challenge was overcome. For the module characterization, this Chapter will refer to the manner the experiments were conducted when a required module characteristic was unknown.

This Chapter starts by explaining the general methodology used to assess the whole system level losses and thereafter the particular share of losses associated to each of the studied loss mechanisms or factors. Following, the particular methodology followed to assess each particular loss factor will be explained in detail, including, when required, the theoretical or experimental manner a particular parameter, associated to the studied loss mechanism, was characterized for the HyET Solar modules.

4.1. General Methodology Description

In order to assess the performance of the system comprised of HyET Solar a-Si:H modules, the real system output power P_{AC} has to be known. This parameter refers to the amount of power delivered by the inverter to either the local appliances or the grid, and the current is measured in an AC form. Equation 4.1 illustrates this parameter. Following, the predicted standard test conditions performance P_{STC} was to be known. This time dependent parameter refers to the ideal power the system would deliver if it would be operating under standard test conditions (Ideally), if no power losses would occur on the DC side cables (Resistance losses), if no power losses would occur during the power conversion (Inverter and/or power conversion losses), and if the effect of dust, rain and/or snow are not to be considered. Equation 4.2 shows this relationship and equation 4.3 illustrates the expected energy output the system would deliver following ideal STC considerations, E_{STC} .

$$P_{AC}(t) = V_{oc}(t)I_{sc}(t)FF(t) - L_{system}(t) \quad (4.1)$$

$$P_{STC}(t) = Irr_{POA}(t) \times \eta_{STC} \quad (4.2)$$

$$E_{STC} = \int_{t_1}^{t_2} \eta_{STC} Irr_{POA}(t) dt \quad (4.3)$$

As disclosed on Chapter 2, by knowing the P_{AC} and the P_{STC} , the system Performance Ratio PR can be obtained. As both parameters are time dependant, two types of PR can be obtained, a dynamic or time dependent $PR(t)$ and, by averaging the $PR(t)$ over a period of time, a general PR . By the calculation of this parameter, the system performance can be analysed over different period of time such as the sunrise, midday or sunset period, a particular sunny day, an average operational day or a mostly cloudy day, a week or month of the year or a particular season.

The difference between the P_{STC} and the P_{AC} show the system level losses L_{system} as defined by this work, equation 4.4. Similarly to the PR , this parameter can be used as instantaneous or time dependent power losses, or by averaging it through a defined time period it is possible to obtain the whole share of energy losses the system presents.

$$L_{system}(t) = P_{STC}(t) - P_{AC}(t) \quad (4.4)$$

The objective of this study is to determine the contribution of each particular loss factor to the complete share of the system losses. In order to solve this question, this work makes the assumption that each factor has one related module loss characteristic or parameter that can relate the influence of the given factor to the power output and is only dependent of the loss factor. This is, of course, a simplified analysis as the impact of the loss factors can be also be interdependent of additional loss factors but for the scope of this work, and as suggested by an initial literature review, it was idealized in such a way. Whenever possible, this loss parameter is linearized for convenience of calculation. Aided by the acquired loss parameter, a predicted STC performance $P_{STC\alpha}(t)$, corrected for the given loss factor, can be estimated. This is be an estimation of the dynamic power output the system delivers under the STC idealization, but subtracting the amount of power that is lost due to the influence of the loss factor. Equation 4.5 refers to this parameter.

$$P_{STC\alpha}(t) = \alpha \times Irr_{POA}(t) \times \eta_{STC} = \alpha P_{STC}(t) \quad (4.5)$$

Where

$\alpha =$ Loss factor coefficient

By contrasting the $P_{STC}(t)$ with the $P_{STC\alpha}(t)$, the share of losses associated to the studied loss factor would be visible. Additionally, the time dependence of this 2 parameters would allow for a dynamic analysis of the effects of the studied factor, which in turn would allow to indicate the time periods during which its effects are largest. If this procedure is repeated for each loss factor, the theoretical result would approximate the real performance curve of the system. Finally, the model can be validated by

comparison with the measured, real performance.

If all the known factors that affect the system performance are taken into account, the result should be theoretically very close to the P_{Real} with a very small amount accounted to unexplained losses. As it can be seen later on this Chapter, this work analyzed the impact of degradation the HyET a-Si:H modules. For this, the approach followed was to analyse all the expected loss factors for the given a-Si:H technology excluding degradation. Once the performance could be explained for all the factors, the remaining share could be attributed to the effect of degradation on the modules and unexplained losses.

4.2. Temperature effects

The effects of temperature on PV modules and systems is interesting as it has been reported by plenty of works as the main factor for a decrease of the PR [11] [16], particularly on high irradiance intensity, warm locations. While literature suggest this is also true for a-Si:H modules, the study of the effects of temperature versus electrical performance is of particular interest for this technology as some studies suggest the technology has a lower temperature coefficient K_T when compared to c-Si technology. This can be translated as an expected better performance than c-Si under high operational temperatures [18] [13]. This factor, if confirmed, could signify a performance advantage of the a-Si:H technology over c-Si.

Literature suggests that the most straight forward approach for predicting the temperature corrected performance of a PV system is to understand the rate of change of the modules performance parameters with respect to temperature (such as V_{oc} , I_{sc} , fill factor, η), and to measure or estimate the modules real operational temperature through the day.

As explained on Chapter 3, the rate of change versus temperature or temperature coefficient k_T , can be established for each of the modules parameters, but as this work is not focusing in only one loss factor but the whole of them, the temperature coefficient was determined only for the power output variation or plainly said, for its direct effect on the module efficiency. This approach was taken from [20] and it can be better appreciated in equation 4.6 where $\eta(T_m, Irr_{POA})$ stands for the corrected efficiency with respect to the module temperature, T_m stands for the module temperature, and $\eta(25^\circ C, Irr_{POA})$ stands for the STC efficiency, (the efficiency if the T_m is assumed to be $25^\circ C$ and under a 1 Sun irradiation at AM1.5G, or rated efficiency (also referred in this work as η_{stc}).

$$\eta(T_m, Irr_{POA}) = \eta(25^\circ C, Irr_{POA}) [1 + k_T (T_m - 25^\circ C)] \quad (4.6)$$

Based on equation 4.6 it can be seen that $\eta(T_m, Irr_{AOI})$ is defined with 3 parameters. While η_{stc} is easily obtained by either addressing the manufacturer rated efficiency or performing a flash test at STC, k_T and T_m are less straightforward to obtain. The procedures and consideration taken for their acquisition will be referred in subsection 4.2.1 and 4.2.2.

4.2.1. Measuring the temperature coefficient

Based on [11], [18] and internal documents within the HyET Solar company [8], it was decided to measure the temperature coefficient in-house by performing a test with all parameters fixed to STC with the exception of the temperature, where it was varied in a controlled manner. By fixing all the parameters with the exception of the module temperature, a performance curve was obtained with the variation of the output power with respect to temperature. By analyzing the linearized curve, the slope shows the efficiency rate of change with respect to temperature in terms of $[\frac{\%}{^\circ C}]$. By normalizing this rate of change by means of the rated efficiency η_{STC} , the k_t is obtained.

A class AAA solar simulator was used for performing the test with an irradiance level fixed at $1,000 [\frac{W}{m^2}]$. The ambient temperature T_{amb} inside the measuring place ranged from $23^\circ C$ to $25^\circ C$ for the measuring period. The sample module used to perform the test was a HyET Solar 30x30 cm (internally referred as "XL") baseline single junction a-Si:H module, without connectors attached. Figure 4.1 shows the used module. To modify the temperature of the module in a controlled manner, a steel vacuum bed with an internal coil was used as a heat exchanger. The forced vacuum on the device

helped to keep the flexible module flat and therefore at an angle of incidence 0° . The internal coil was wired to a device with the capacity of heating up, again in a controlled manner, a water reservoir and then, pumping it to the vacuum bed/heat exchanger. Once the temperature was set at the device side, it would take some time for the reservoir to get to the selected temperature and once it did, the bed would also take some time to reach its peak temperature. As there were some heat losses to the environment from the heating device and from the hoses wired to the bed, the measuring bed and module temperature was expected to be lower than the set temperature. To accurately report the module temperature, type J thermocouples were used to measure the front surface module temperature in 4 points: middle, bottom, next to positive connector and next to negative connector. Once the recorded temperature among the 4 points stabilized to a point, no increases were detected for at least 1 minute. Then, the flash test was performed and the performance characteristics were recorded. This procedure was repeated in 5°C increments from 25°C to 80°C following the recommendation listed in [9]. As the "XL" module had no connectors, an alligator measuring probe was attached to the copper contacts of the module. In order to discard any variations during the test, 3 measurements were made at the same temperature and then averaged to get the final value. Figures 4.1, 4.2 and 4.3 illustrate this procedure.

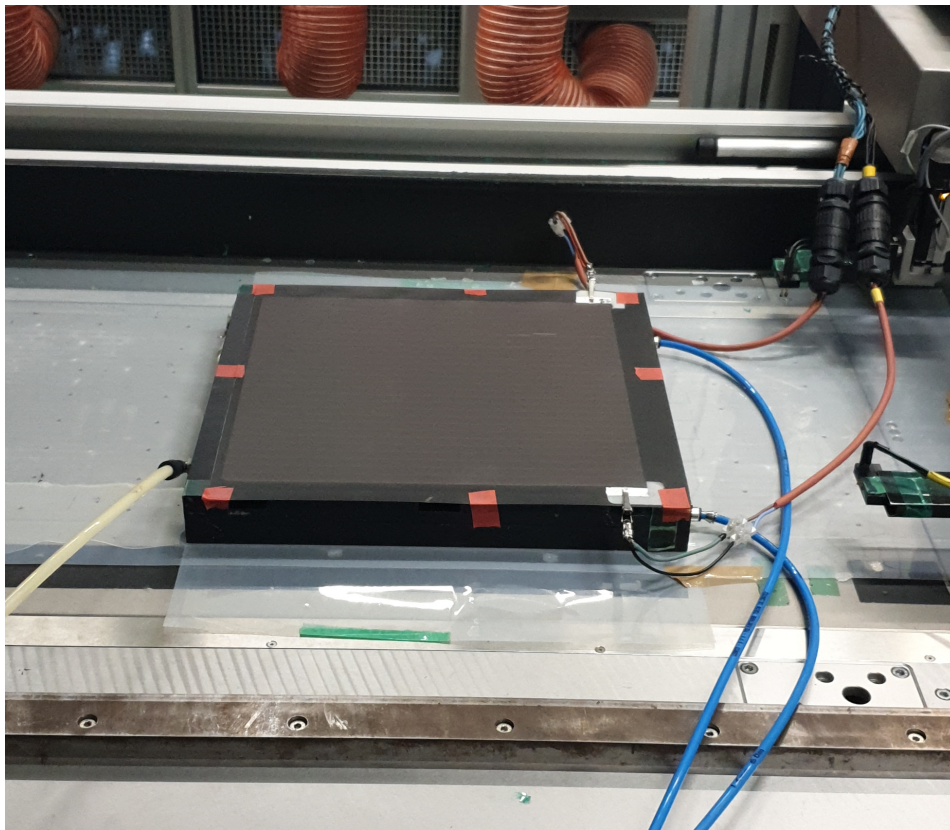


Figure 4.1

Temperature coefficient Setup placed in the class AAA solar simulator flasher "Pulsar". The "XL" module is fixed to the vacuum/heat-exchanger bed. On the left hand side, the pneumatic outlet can be seen. On the right hand side, the water inlet and outlet can be seen. The electrical properties are being sensed by alligator clamps due to the lack of connectors on the module.

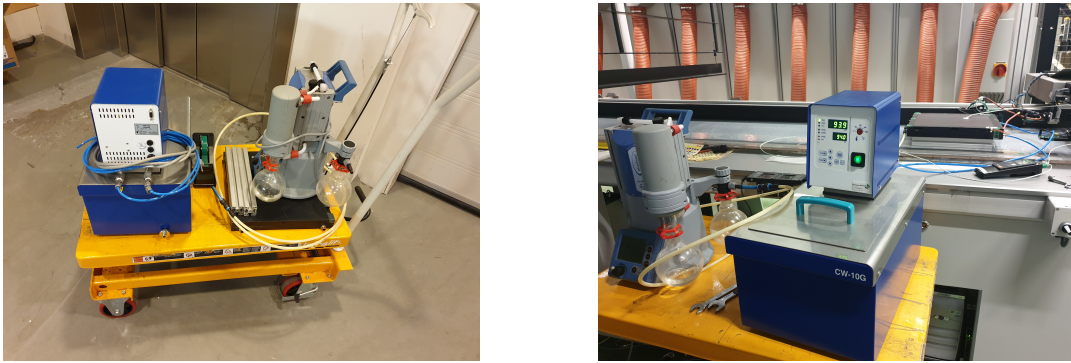


Figure 4.2
Equipment used for the experiment before and during the test. From left to right, temperature regulating device, scotch tape, vacuum/heat-exchanger bed, aluminum stands for minimizing heat loss due to conduction to back surface, vacuum, working table with regulating positions.

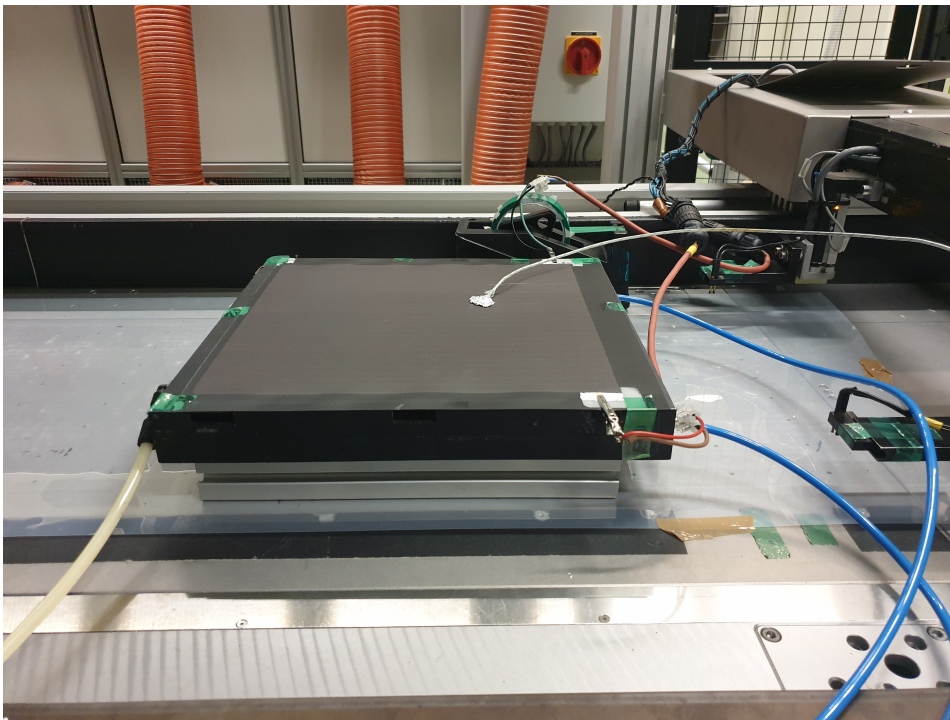


Figure 4.3
Temperature being measured on the front surface of the module. The thermocouple tip has an aluminum extension to better measure surface temperatures.

Once the full set of measurements was performed, the data were plotted, linearized, and the value for of the slope was obtained, figure 4.4 shows the results. The k_t for the 25°C - 80 °C range was obtained, obtaining a value of $-0.0093 \left[\frac{\%}{^\circ K} \right]$.

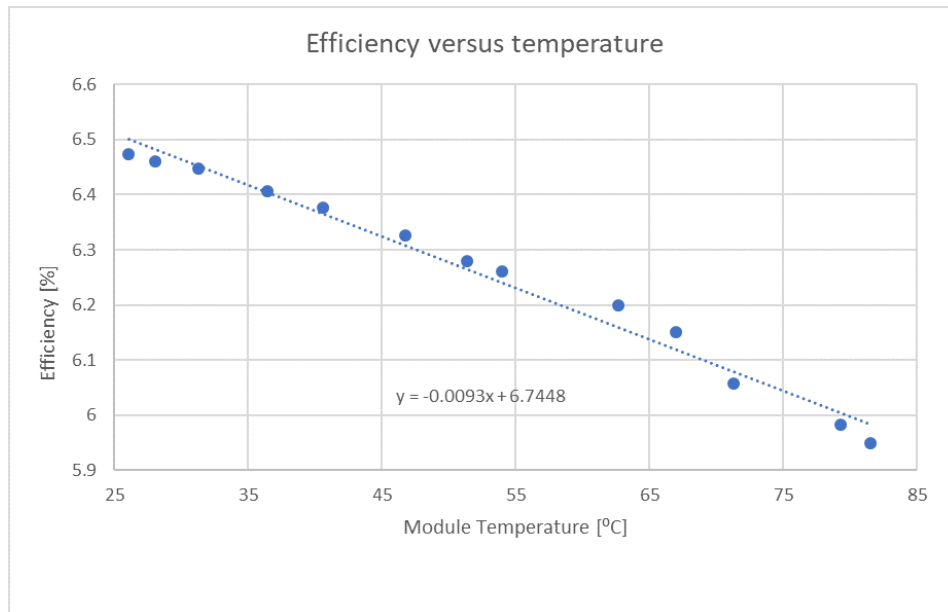


Figure 4.4

Efficiency variation with module temperature. Complete temperature range from 25 °C to 82 °C. The slope of the linearized approximation shows the non normalized temperature coefficient $K_t \left[\frac{\%}{^\circ C} \right]$.

After analyzing the trend shown in this plot, it was realized that the speed of the variation of η versus T_M presented a different trend for the sub-range of 25°C - 40 °C than to the 40°C - 80 °C. As the goal of obtaining this parameter was to include it in the performance model, it was concluded that having a more accurate coefficient per sub-range would result in a more accurate model. Therefore, 2 temperature coefficients where obtained from this experiments, $k_{t_{low}}$ figure 4.5 and $k_{t_{high}}$ figure 4.6.

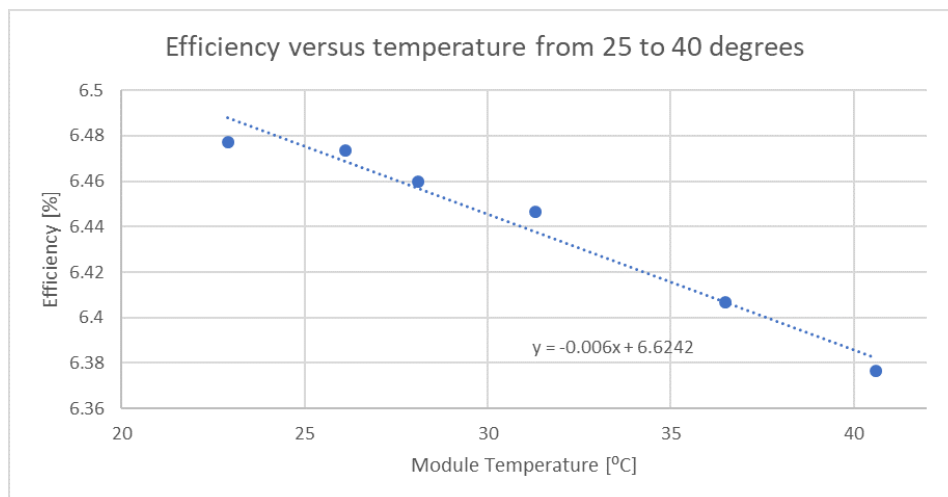


Figure 4.5

Efficiency variation with module temperature. Temperature range from 25 °C to 40 °C. The slope of the linearized approximation shows the non normalized temperature coefficient $K_{t_{low}} \left[\frac{\%}{^\circ C} \right]$.

Finally, the obtained coefficients compared to the temperature coefficients measured 5 years ago for a previous baseline model. A variation was observed on the coefficients obtained in 2019 as the values show a better performance of the modules under high temperature conditions than their 2014 counterparts. The fact that the newly measured coefficients where in the same order of magnitude than

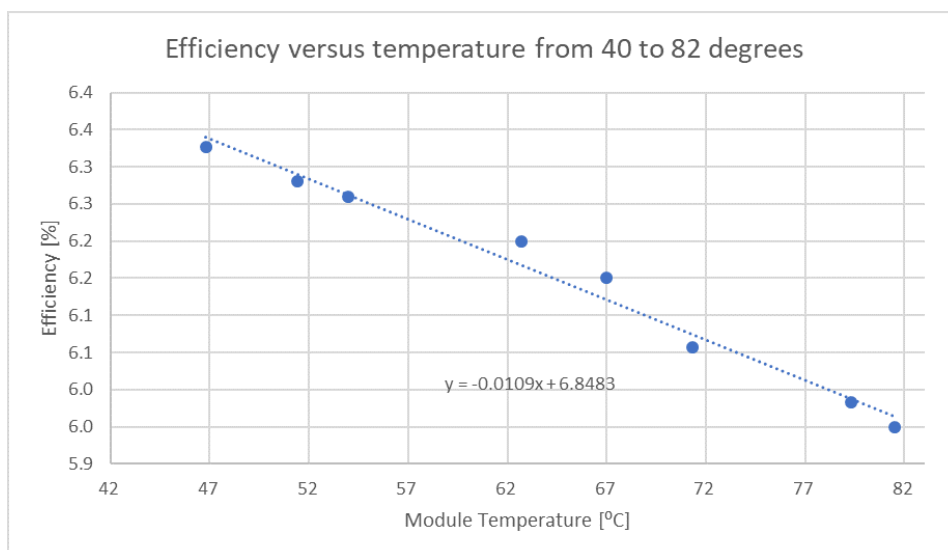


Figure 4.6
Efficiency variation with module temperature. Temperature range from 40 °C to 82 °C. The slope of the linearized approximation shows the non normalized temperature coefficient $K_{t_{high}} [\frac{\%}{^{\circ}C}]$.

the 2014 ones served as an internal validation for the correctness of the procedure. Table 4.1 shows the measured temperature coefficients and, where applicable, their comparison with the 2014 ones.

Table 4.1
Measured HyET Solar temperature coefficients for 2014 and 2019 production lines.

	Temperature Coefficients	
	2014 line	2019 line
$K_t [\frac{\%}{^{\circ}C}]$	-0.01121	-0.009
$K_t [\frac{1}{^{\circ}C}]$	-0.00158	-0.00139
$K_{t_{low}} [\frac{\%}{^{\circ}C}]$	N/A	-0.006
$K_{t_{low}} [\frac{1}{^{\circ}C}]$	N/A	-0.00093
$K_{t_{high}} [\frac{\%}{^{\circ}C}]$	N/A	-0.0109
$K_{t_{high}} [\frac{1}{^{\circ}C}]$	N/A	-0.00168

4.2.2. Measuring the array module temperature

Two approaches were considered for obtaining the T_M , via calculation using a module temperature model or via direct measurements. Reference [20] presents 3 models for indirectly estimating the module temperature, the Installed Nominal Operational Temperature model, the Duffie-Beckman model and the Fluid Dynamic model. These models range in complexity and precision from a very basic approach to a precise one and are based on parameters such as Irr_{AOI} , wind speed, cloud cover factor, layer absorption coefficient, layer transmittance, etc. As it will be explained in Chapter 5, there were additional reasons to build a performance measuring setup in accordance to the IEC 61724-1:2017 standard, in particular under the class A classification. The standard suggested preferably directly measuring the T_M before estimating it, therefore it was decided to follow this approach.

Once it was decided to measure the module temperature, the manner to do it was determined. References [20], [11] and [9] suggest that the actual relevant temperature is the one of the active layer of the photovoltaic module. For thin film amorphous silicon, the active layer is the intrinsic a-Si:H layer sandwiched between the p and n layers. As actually measuring this layer without compromising the integrity of the module would be impossible, an indirect approach was followed. Reference [9] states that a good practice for measuring the T_M is to measure the temperature of the back layer and then correcting it for the temperature difference between the module layers. According to an internal heat transfer model [24], the temperature gradient between the layers is dismissible, therefore no correction factor was applied to the back layer measurements.

As the modules are particularly large, a different temperature across the module surface could be expected, therefore the approach of measuring 4 points across the module and the averaging the end temperature was followed, equation 4.7. The chosen sensing points can be appreciated in figure 4.7 and are one in the middle of the module, one in the farthest horizontal plane from the connectors, one in the farthest vertical plane from the middle point and the last one next to a connector as the current flow could cause an increase on the temperature in that position.

$$T_M = \frac{T_{MP1} + T_{MP2} + T_{MP3} + T_{MP4}}{4} \quad (4.7)$$

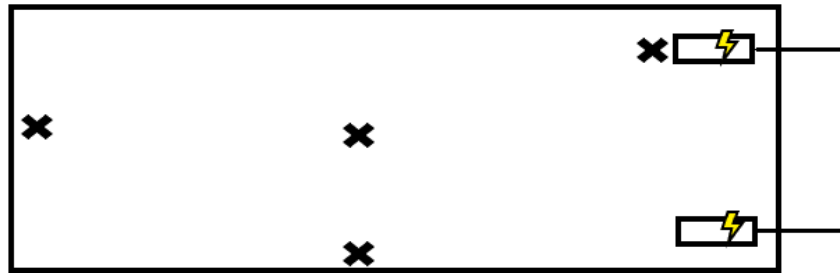


Figure 4.7
Diagram of the position of the temperature sensors on the module

By analyzing the difference between the average module temperature T_M and the measured temperature at the midpoint of the module T_{MP1} , a correction factor that allowed for a more precise measurement of other modules on the system by just measuring one point was determined, equation 4.8.

$$CF = \frac{1}{t_f} \sum_{t_1}^{t_f} \left[\frac{T_M(t) - T_{MP1}(t)}{T_{MP1}(t)} \right] \quad (4.8)$$

With the correction factor CF , the average temperature of the other modules within the array was estimated as described by equation 4.9, where T_{MXP1} refers to the temperature of the module "x" measured in the middle point, and T_{MX} represents the average temperature of the same module X . This allowed to have a better estimation of the temperature in different sections of the array using only one temperature sensor.

$$T_{MXP1} CF = T_{MX} \quad (4.9)$$

A final average between the temperature was performed as modules from opposite sides of the system had temperature sensors attached. This allows to confirm or discard that an even module temperature is being experience across the system.

4.2.3. Temperature corrected performance model

The temperature corrected performance model was created based on $Irr_{POA}(t)$ and a variable system efficiency dependent on the system temperature $\eta(T_M)$, which was subsequently based on $T_M(t)$. Equation 4.10 shows the temperature corrected performance model and equation 4.11 shows the variable efficiency based on the 2 temperature coefficients and the module

$$P(T_M, Irr_{POA}) = A * Irr_{POA}(t) * \eta(T_M) \quad (4.10)$$

Where

$$\eta(T_M) = \begin{cases} \eta_{STC}, & \text{for } T_M \leq 25^\circ C \\ \eta_{STC}[1 + k_{t_{low}}(T_M - 25^\circ C)], & \text{for } 25^\circ C < T_M \leq 40 \\ \eta_{STC}[1 + k_{t_{low}}(40^\circ C - 25^\circ C) + k_{t_{high}}(T_M - 40^\circ C)], & \text{for } 40^\circ C < T_M \leq 85^\circ C \end{cases} \quad (4.11)$$

4.3. Angle of Incidence (AOI)

The AOI is expected to be of high relevance on the performance ratio of PV systems during early and late operational times through the year, particularly sunrises and sunsets, as literature suggests its effect on the modules exponentially lowers the performance after a value of 50° is reached [10]. This effect can be expected to be higher for latitudes farther from the equator.

In order to assess the effect of the AOI on HyET modules, its effect needs to be empirically researched. Although there exists already plenty of empirical and theoretical models on the performance variation with respect to AOI, most of them are based on glass encapsulated technologies [4],[10], [12]. For HyET modules, the layers used to manufacture them differ from both conventional c-Si and other thin film manufacturers, particularly on the top encapsulant used. For the [12] study, it was concluded that glass determined the detriment in the efficiency of the studied modules regardless of the technology as all of them had glass as a top encapsulant and the reported variations were similar, figure 4.8. This suggested that using these models for HyET modules could derive in erroneous results.

The followed approach to establish a new model of AOI versus performance was to relate the performance to the increase in the reflectivity value associated to a variation of the AOI. As explained in chapter 3, the total reflection, and therefore optical losses associated to a module, is related to the interaction of each different layer that composes the module with the incident light. For this reason, the effect the AOI has in the reflectivity parameter of the modules was experimentally obtained at the facilities of the faculty of Electrical, Electronic, Mathematics and Computer Sciences of TU Delft. As the loss of power due to the reflected normal incidence of an AM1.5 source is already accounted for in the rated efficiency, the variation of this value was related to the variation of power due to a different than normal (or zero) AOI. The full procedure will be described in 4.3.3.

Now, apart from getting the AOI coefficient, knowing the exact position of the sun with respect to the studied system was required. As the AOI for a fixed tilt PV system depends uniquely on the sun path through the day, the AOI on the system could be established for every period of time from the exact position of the sun in the sky at the system location. The full procedure will be described in 4.3.1.

4.3.1. Calculating the position of the Sun and AOI

To establish the position of the sun in the celestial sphere as being experienced by an observer at a given location, the spherical horizontal coordinates *Azimuth of the Sun* A_S and *Altitude of the Sun* a_S are helpful. Figure 4.9 illustrates this coordinate system. For establishing the position of the sun during the studied period at the given location of Arnhem, the Netherlands, this work uses the approach proposed by [20], Annex E.1. Equations 4.12 to 4.22 refer to the equations used to compute the Sun position. The computation was performed on Matlab, where a code was written to track the position of the Sun.

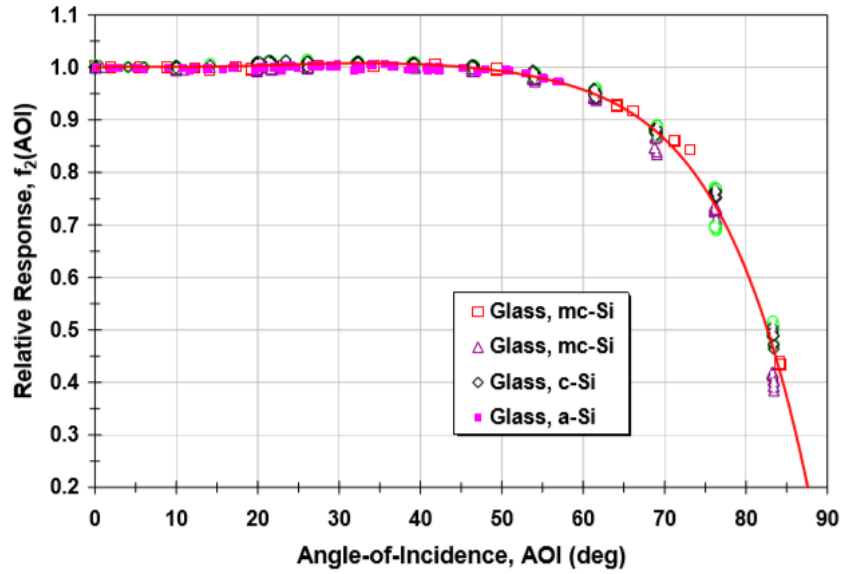


Figure 4.8

Typical empirical relationship of the influence of AOI on a module's short circuit current. Results measured at the Sandia National Laboratories for four different module manufacturers. The effect is reported to be dominated by the reflectance characteristics of the glass surface. (King et al. 2004)

The input parameters were the latitude ϕ_0 and longitude λ_0 of the system (51.9688002° , 5.947664°), and the Azimuth A_m and Altitude a_m of the system.

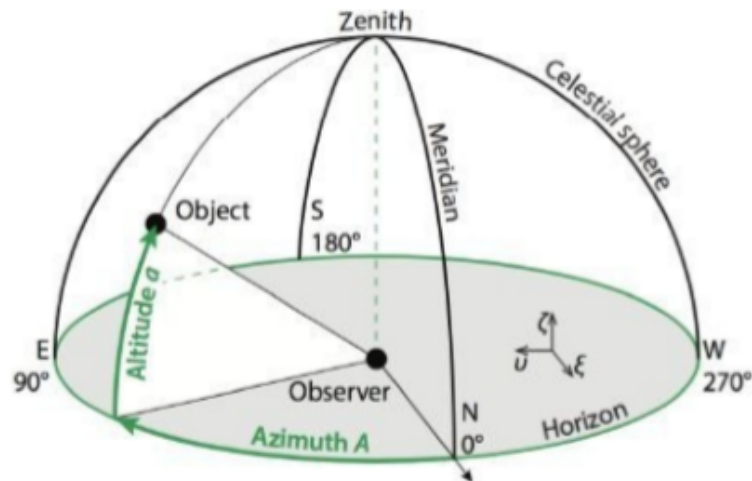


Figure 4.9

The horizontal coordinate system. Azimuth and Altitude in the Celestial sphere. From: Solar Energy. The physics and Engineering of photovoltaic conversion technologies and systems.

First, the time was expressed as the elapsed time in days D since Greenwich noon, terrestrial time, 1 January 2000. It was related to the Julian date JD as suggested by [20].

$$D = JD - 2451525.0 \quad (4.12)$$

Then, the *mean longitude* of the sun corrected to for the aberration of the light q and the *mean anomaly* of the sun g was defined based on the time D .

$$q = 280.459^\circ + 0.98564736^\circ D \quad (4.13)$$

$$g = 357.529^\circ + 0.98560028^\circ D \quad (4.14)$$

The ecliptic longitude of the Sun λ_S was defined based on q and g , the ecliptic latitude was approximated as shown and the axial tilt was defined based on D .

$$\lambda_S = q + 1.915^\circ \sin(g) + 0.020^\circ \sin(2g) \quad (4.15)$$

$$\beta_S = 0 \quad (4.16)$$

$$\epsilon = 23.429^\circ - 0.00000036^\circ D \quad (4.17)$$

The *Local mean sidereal time* was defined based on the *Greenwich mean sidereal time*, which was based on D and T , the number of centuries past since Greenwich noon, Terrestrial time, 1 January 2000.

$$T = \frac{D}{36525} \quad (4.18)$$

$$GMST = 18.697374558 + 24.06570982441908D + 0.000026T^2 \quad (4.19)$$

$$LMST = GMST \frac{15^\circ}{hour} + \lambda_0 \quad (4.20)$$

Finally, the $\tan(A_S)$ and $\sin(a_S)$ are defined as shown on equations 4.21 and 4.22. By applying the *arctan* and *arcsin* to 4.21 and 4.22 respectively, the final values of the A_S and a_S can be obtained. For the purposes of this work, this was computed on the same steps as the output data from the performance of the system, on 15 seconds intervals.

$$\tan(A_S) = \frac{-\sin(LMST)\cos(\lambda_S) + \cos(LMST)\cos(\epsilon)\sin(\lambda_S)}{-\sin(\phi_0)\cos(LMST)\cos(\lambda_S) - [\sin(\phi_0)\sin(LMST)\cos(\epsilon) - \cos(\phi_0)\sin(\epsilon)]\sin(\lambda_S)} \quad (4.21)$$

$$\sin(a_S) = \cos(\phi_0)\cos(LMST)\cos(\lambda_S) - [\cos(\phi_0)\sin(LMST)\cos(\epsilon) + \sin(\phi_0)\sin(\epsilon)]\sin(\lambda_S) \quad (4.22)$$

4.3.2. Calculating the AOI

Once the Sun position with respect to the studied PV system was known for the whole examined period, knowing the AOI was possible. For this task, the equation 18.3 presented on [20] was used as a starting point. By comparing the horizontal coordinates of the system, fixed for the whole computing process, and the time-dependent coordinates of the Sun presents during the same period, equation 4.23 presents the AOI based on A_S and a_S , as explained on 4.3.1 are based on D , therefore obtaining a value of AOI with respect to time $AOI(t)$.

$$AOI = \arccos[\cos(a_M)\cos(a_S)\cos(A_M - A_S) + \sin(a_M)\sin(a_S)] \quad (4.23)$$

4.3.3. Calculating the correction for reflection losses

The procedure followed to relate the effect of a different than normal irradiance incidence, on the fixed positioned modules, due to the movement of the sun in the celestial sphere through the day was performed in controlled lab conditions to isolate this effect from the spectral mismatch losses, which effect is noted to increase during morning and evening periods, the same time periods where the AOI is greater and higher reflection associated losses are expected.

To establish the associated losses in performance due to angular incidence of light, two tests were performed. On a first instance, a reflection test was performed on a *PerkinElmer Lambda 950 spectrophotometer* with a fixed sample holder at a 0° Angle of Incidence. This test shots a beam of monochromatic light programmed at a chosen wavelength distribution. It measures the specular and diffuse reflected component, and returns the values of the transmitted and reflected light, equation

4.24. Once integrated this values over the complete range of wavelengths λ it is programmed to, a total reflection value could be established. The goal of this test is to get reference values of reflection at 0° AOI R_0 , which are assumed to be already accounted for in the η_{STC} , and serve as reference for the second test, equation 4.25.

$$I_0 = I_{R0} + I_{T0} \quad (4.24)$$

$$\frac{I_{R0}}{I_0} = R_0 \quad (4.25)$$

The reflectivity reported at an AOI of 0° was taken as the reference value and its variations with respect to the AOI were recorded. As a higher reflectivity value would mean higher optical losses, resulting in a lower short circuit current [20], then, the rate of change between the reflectivity with the AOI was correlated to the rate of change between the instant efficiency with the AOI. In order to get the variation of reflectivity with respect to AOI R_{AOI} , a second test, a *Variable Angle Spectroscopy* (VAS) was done on an *Automated Reflectance Transmittance Analyzer* (ARTA).

$$R_{AOI\lambda_i-\lambda_f} = \frac{I_{RAOI}}{I_0} - R_0 \quad (4.26)$$

The ARTA setup consist on an addition to the *PerkinElmer Lambda 950 spectrophotometer* where a rotating detector mounted inside a spherical chamber is set in a way that it can measure the reflected component of the incident light from a sample that can also be positioned at a variable angle with respect to the incident beam. The detector has a small integrating sphere for additional precision, which is equipped with a photomultiplier for the Ultra violet and visible region, and a Peltier cooled PbS cell for the NIR region. The detector is attached to a mechanically controlled rotating drum which allows it to be positioned circumferential to the sample within a range of 15° to 345° considering a 0° position as the direction of incident light. The sample is fixed in the center of the chamber and it has the ability to rotate between 0° and 180° . Figure 4.10 and 4.11 better illustrates the working principle.



Figure 4.10
Photograph of the Automated Reflectance Transmittance Analyzer (ARTA) installed in the *PerkinElmer Lambda 950 Spectrophotometer*. From: Zhao, Enhancement of Light Trapping in Thin Film Silicon Solar Cells.

Expecting a band gap of around 1.6 to 1.8 eV for a-Si:H [20], the useful wavelength was concluded to be lower than $850nm$, therefore the spectral range of the ARTA was set from $300nm$ to $850nm$. The set AOI ranged from 10° to 90° having a lower resolution on the 20° to 50° range by performing a measurement every 15° , and having a higher resolution on the 50° to 90° by performing a measurement every 5° . The detector was set to cover the specular and diffuse reflection following Snell's law at an angle of double the AOI and within a range of plus minus 5 degrees from the theoretical value. The measured points were taken every 2 degrees for a total of 10 different measurement points per AOI. In total, 462 points were taken.

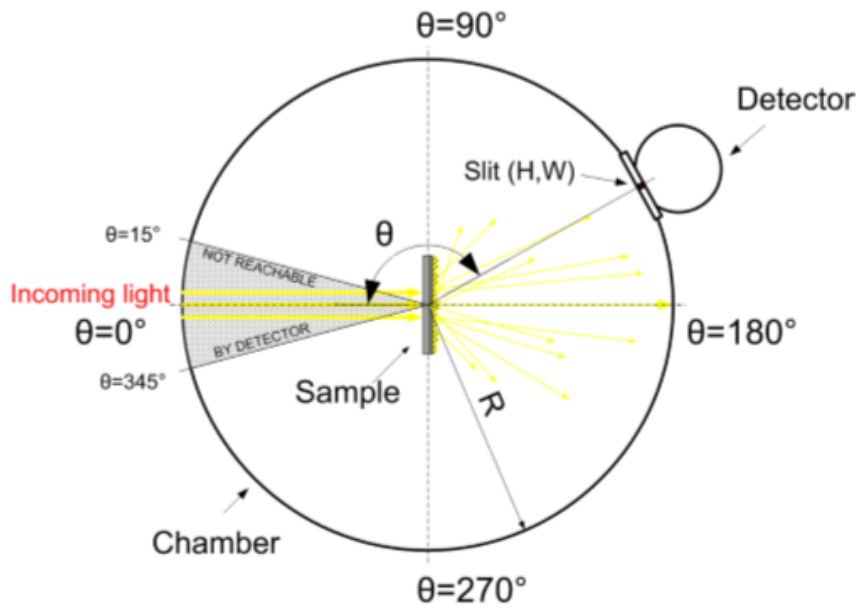


Figure 4.11
Schematic cross section of ARTA chamber along the measuring plane. From: Zhao, Enhancement of Light Trapping in Thin Film Silicon Solar Cells.

$$R_{AOI}(\lambda) = \sum_{i=2AOI-5^{\circ}}^{n=2AOI+5^{\circ}} R_{iAOI}(\lambda) \quad (4.27)$$

Where

$I_{300nm-850nm}$ = Total Effective Irradiance for HyET modules

$$\frac{I_{\lambda_1-\lambda_2}}{I_{300nm-850nm}} = \alpha_{\lambda_2} \quad (4.28)$$

$$R_{Eff}(\lambda_2) = R_{AOI}(\lambda_2) \times \alpha_{\lambda_2} \quad (4.29)$$

$$R_{AOI} = \frac{I_{RAOI}}{I_0} - R_0 \quad (4.30)$$

4.4. Low irradiance

HyET modules, as most of the commercially available PV modules, have a rated performance at STC irradiance of $1,000 [\frac{W}{m^2}]$. At this input irradiance level, the internal characteristics of the module operate in such a way that This means than a less efficient behaviour is obtained when the input irradiance is lower than this value. As explained on Chapter 3, a decrease in the incident irradiance has a linear decreasing effect on the short circuit current J_{sc} , a logarithmic decreasing effect on the V_{oc} and an overall decreasing effect on the fill factor FF . If we take this 3 parameters into consideration, it can be concluded that the overall effect on the module efficiency of a decreased irradiance will be an exponential decrease. By definition, any effect that lowers the performance efficiency of the modules during normal operation conditions can be considered as system level losses and will show a reduction on the performance ratio. Figure 4.12 illustrates this effect on a c-Si module exposed to a lower than standard irradiance.

By analysing Figure 4.12, roughly 3 regions can be seen in the plot. The first is present on the 100% to 40% region. Although exponential, when analysed independent form the whole range, this region shows a somehow linear behaviour. The second range is present on the 40% to 25% region. This

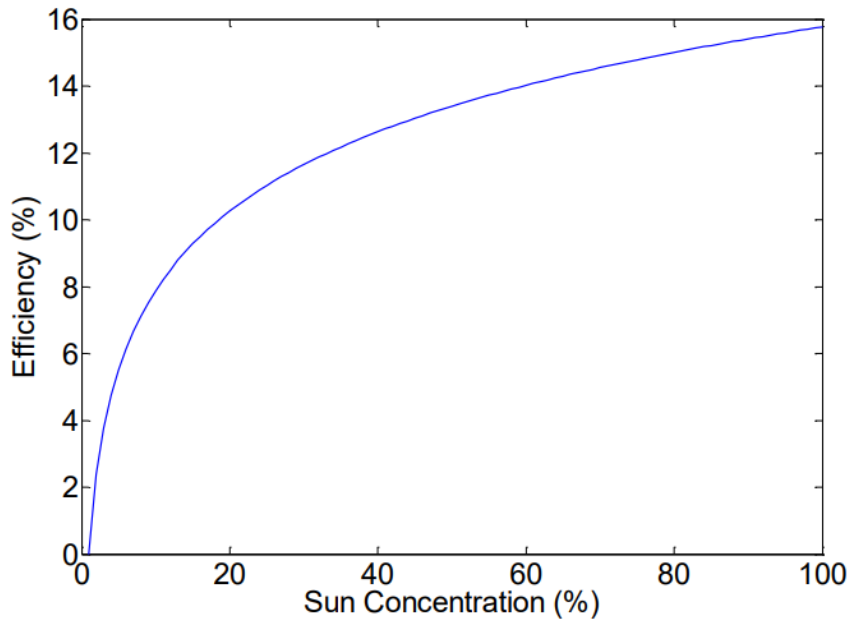


Figure 4.12
Irradiance level versus efficiency. From [1]

region shows steeper curve than the first region but it can, to a certain extent, be idealized as a linear behaviour. The third and final region is present on the 25% to 0% range and it clearly shows drastically exponential behaviour.

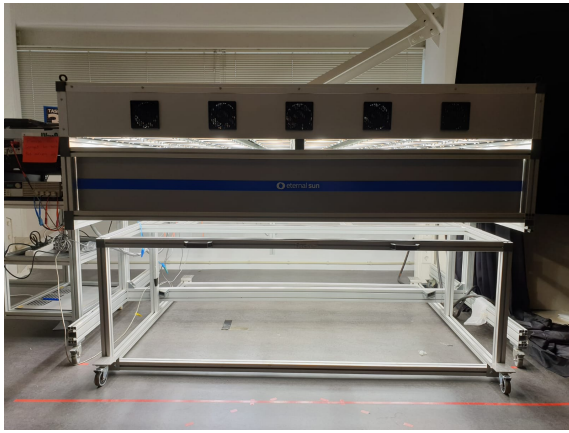
To model the electrical performance of the analyzed a-Si:H modules, the "Irradiance versus efficiency" function is required. This function could be approached by using literature as a reference for a-Si:H behaviour under low irradiance conditions, nevertheless as this loss mechanism was expected to have a large impact in the reduction of the performance ratio at low light conditions, the experimentally measured behaviour of the particular analyzed modules was desired.

The performance data was retrieved by 2 experimental approaches for this work, as the first approach had plenty of uncontrollable variables which lowered the certainty of the results. This factor was reflected in the values obtained under the first experimental approach, as they greatly differed from values suggested by literature, and were impossible to replicate after the experiment was repeated.

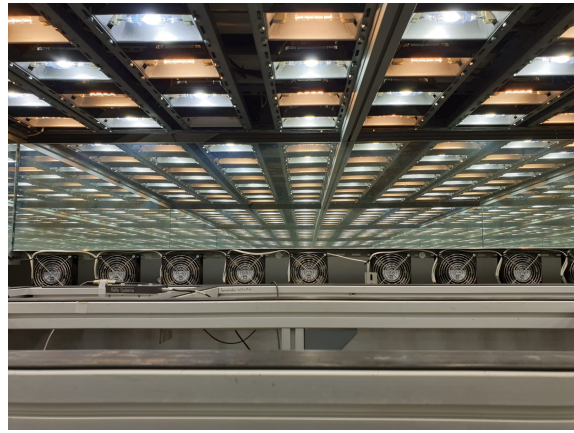
This first experimental approach consisted on using 5 light filters, with increasing shading characteristics, to partially reduce the incident irradiance on the modules in controlled steps, obtaining electrical performance data at different irradiance levels. As the exact filtering value per filter was unknown, a measurement was performed to measure this value. Using the facilities of the Photovoltaic laboratory of EEMCS at TU Delft, a test to measure the filters was performed using the Eternal Sun Large Area Solar Simulator, the reference cell attached to the setup, an aluminum frame for the filters and the filters itself, Figure 4.13.

The value of the incident irradiance on the reference cell surrounded by the frame without any filter was measured. This value served as the reference value for maximum irradiance. Then, the incident irradiance on the reference cell surrounded by the frame with a filter attached to it was measured. This value was contrasted to the reference value and the relative light filtered was obtained. Figure 4.14 shows a variation of filter used for the test. As the maximum filtered value obtained by the filters was 40 %, groups of filters on top of each other were measured to reach a relative light filtering of 80%, value considered to show a rapid decrease in efficiency with respect to irradiance [29].

The measurements were then performed on the modules using the filters to vary the input irradiance while measuring the electrical performance of the modules. While performing the experiment, different



(a)



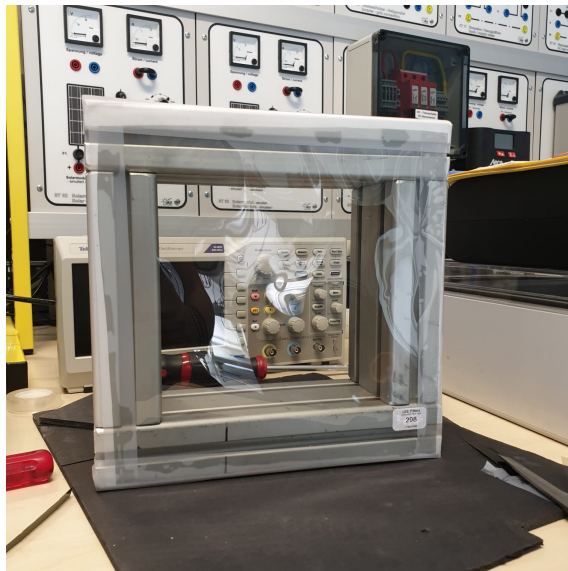
(b)



(c)

Figure 4.13
Experimental procedure to obtain the low irradiance performance.

test conditions added variations to the initially intended procedure. A different aluminium frame was used as the first frame was too small for the size of the sample modules (30x30 cm). The used frame was 35x35 cm, which blocked the incident light coming from an angle different than normal to the module plane. The measurements were performed with all the filters and combinations of superimposed filters up to the combination that reported a decrease of 80%. When the combination of superimposed filters was used, the surface of the filters started to get more wrinkles which might have added to the reflected incident light. Finally, the Large Area Solar Simulator increased the temperature of the module between each measurement, which resulted on a very different module temperature on the last measurement when compared to the first. The procedure of the experiment can be appreciated in Figure 4.15.



(a)



(b)

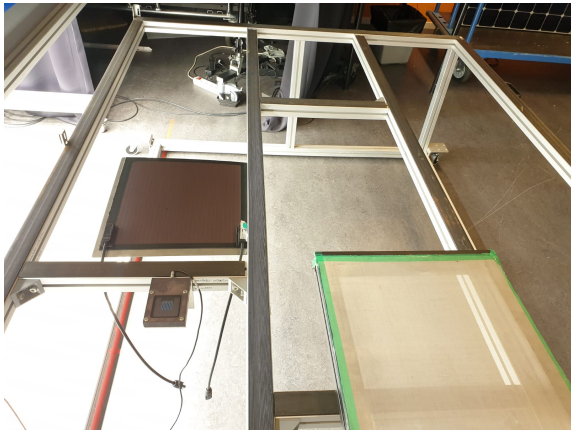


(c)

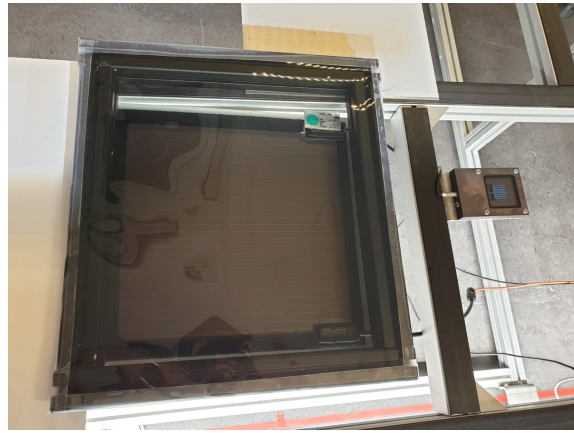
Figure 4.14
Filters used for the experiment.

After analyzing the results of the measurements, the data appeared to be inconclusive and was decided to not be used for the construction of a low irradiance versus efficiency function. An alternative approach for performing the measurements was required. Fortunately, a parallel collaboration project between NREL and HyET Solar allowed to get performance data of the a-Si:H modules at different irradiance intensities. An experiment was performed on two HyET Solar a-Si:H modules where the irradiance was varied on $200 \frac{W}{m^2}$ steps, from $1,200 \frac{W}{m^2}$ to $200 \frac{W}{m^2}$. The spectral pattern was kept constant at AM 1.5 and the module temperature was also kept constant at 25°C .

The efficiency change with respect to the irradiance level was normalized with respect to the STC efficiency. This normalized change was then averaged between both examined modules, ending up with an average normalized efficiency change with respect to the incident irradiance. The variation curve was then approximated by means of a quadratic fit, having a coefficient of determination R^2 of 0.995.



(a)



(b)



(c)

Figure 4.15
Experimental procedure for low irradiance performance.

Figure 4.16 shows the efficiency variation quadratic function. By using this variation function, the expected delivered power after a correction for low irradiance could be obtained, and therefore the associated losses due to performance at low irradiance conditions. Equation 4.31 and 4.32 show the expected power corrected for Low Irradiance performance. Equation 4.32 shows the efficiency variation with respect to the irradiance level, while equation 4.32 shows the power correction approached by the measured Low Irradiance variation function $\alpha_{LI}(Irr_{POA})$. Equation 4.33 shows the time dependant power losses associated to low irradiance. By integrating this function over a defined time period, the energy yield losses due to Low Irradiance can be obtained.

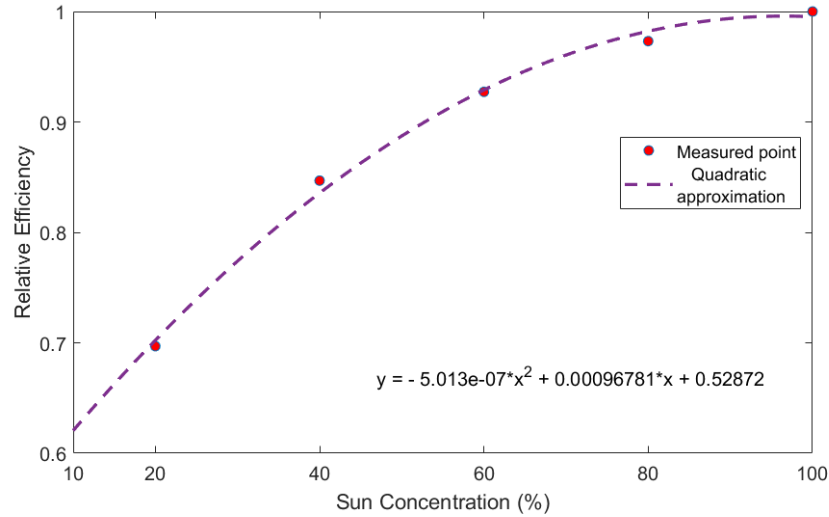


Figure 4.16

Measured Variation of HyET Solar a-Si:H modules efficiency with respect to Irradiance level. The X axis describes the sun concentration where a 100% concentration represents STC irradiance levels. The Y axis describes the normalized efficiency measured in the modules.

$$P_{LIC}(Irr_{POA}) = A * Irr_{POA}(t) * \eta(Irr_{POA}) \quad (4.31)$$

$$P_{LIC}(Irr_{POA}) = P_{STC}(Irr_{POA}) * \alpha_{LI}(Irr_{POA}) \quad (4.32)$$

$$Loss_{LI}(t) = P_{STC}(t) - P_{LIC}(t) \quad (4.33)$$

Where

$$\alpha_{LI}(Irr_{POA}) = -5.013 * 10^{-7} Irr_{POA}^2 + 0.00096781 Irr_{POA} + 0.52872 \quad (4.34)$$

4.5. Power Conversion and Ohmic Losses

The design approach to estimate the share of system losses due to power conversion was to aim the design and therefore power conversion equipment selection, to be as efficient as possible. Chapter ?? will refer to the design considerations followed. As it can be noted on the system design section, the system topology (Central inverter plus power optimizers) means that 2 types of power conversion losses are expected, DC/AC conversion at the inverter side and DC/DC conversion at the power optimizer side.

For assessing the DC/AC power conversion losses (Inverter losses), two time dependent measurements were taken. The former at the DC side and the latter one at the AC side of the system. $P_{Loss_{Inv}}$ was obtained by calculating the difference between these 2 readings. By contrasting the power loss with the power produced over a period of time, a DC/AC conversion efficiency was obtained η_{Inv} . Figure 4.17 shows both measurements on a day.

For assessing the DC/DC power conversion losses (Power optimizer losses), the optimizer power curve was consulted to estimate the loss factor due to conversion. As it can be seen in figure 4.18, the power curve for the SE P405 power optimizer shows an average efficiency at an operation point higher than 25 % of the rated power. As per the sizing of the subsystem connected to the optimizer, under maximum irradiance, the maximum power the subsystem can deliver is 75 % of the rated power for the power optimizer. An assumption was made to establish that the power optimizer would operate on average at an efficiency regime of $\eta_{PO} = 98.6 \%$.

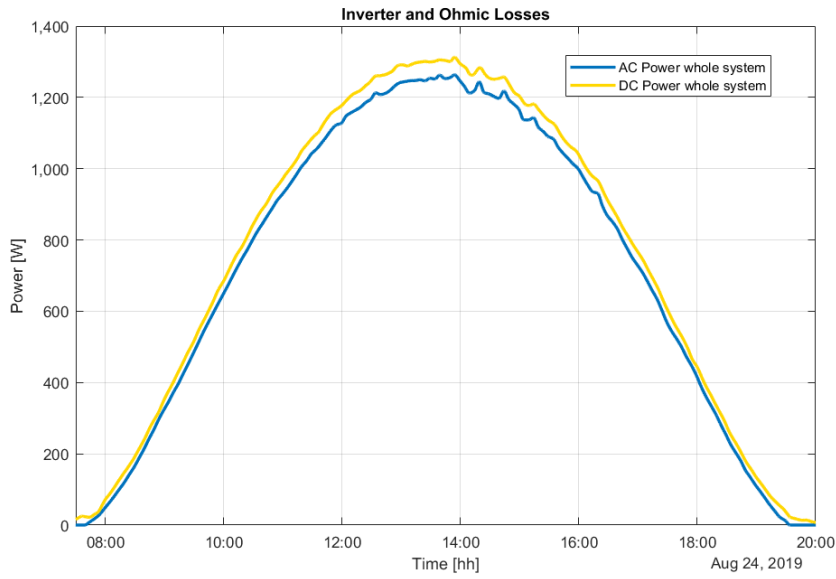


Figure 4.17 Output AC and DC power from the HyET monitoring station. The difference between both curves can be seen as power losses due to power conversion at the inverter side and ohmic losses on the cabling.

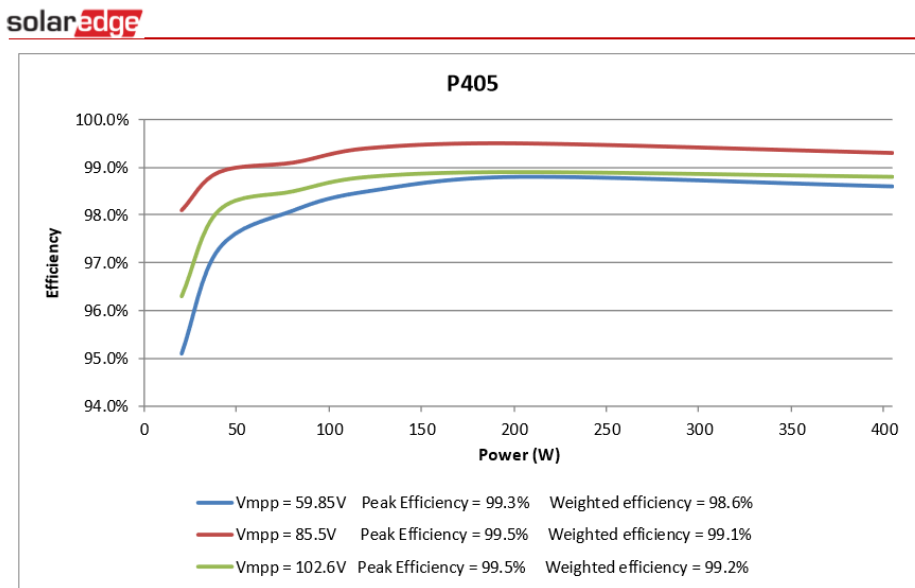


Figure 4.18 Power curve of the Solar edge P405 power optimizer. For an $V_{MPP} = 59.95V$, a weighted efficiency of 98.6 % is defined. It can be seen how the efficiency behaviour is stable up to a 15% of the rated power

4.6. Soiling losses

The IEC 61724-1:2017 standard suggests two approaches for assessing the share of losses related to soiling on a PV System. The first one consists on building a second monitoring prototype using the same solar modules exposed at the same azimuth, tilt and height, and at the same location as the examined PV system. This dummy system would need to be kept clean for the whole examined period of time as the main monitoring station, and assessing the difference in the power generated by both systems. By contrasting both yields, a location and technology dependant soiling coefficient can be obtained and furthermore, the data by itself would allow for a precise estimation of the power lost due to soiling on the system [9].

This procedure implies a high capital expenditure, in case an automated device is used to keep the dummy system clean, or a high operational cost in case manual labor is used to do it. Nevertheless, the IEC 61724-1:2017 standard allows for the use of an annual losses estimated value in case this value is lower than a 2% of the total annual yield. While the average annual losses due to soiling for PV systems range from 1% to 7 % according to Oozeki [16], the work of Nepal [15] and Van Sark et al. [28] provides sufficient data to estimate a value for the Netherlands.

Van Sark et Al al. provides a particular *Yearly specific yield for the Netherlands* Y_{SpNL} 4.35. This parameter estimates the average yield an optimally tilted PV system will deliver in the Netherlands. Additionally, Van Sark et All provides a regional *Yearly specific yield for Arnhem* $Y_{SpArnhem}$ 4.36

$$Y_{SpNL} = 875 \left[\frac{Kwh}{Kwp} \right] \quad (4.35)$$

$$Y_{SpArnhem} = 865 \left[\frac{Kwh}{Kwp} \right] \quad (4.36)$$

To estimate the soiling ratio $\alpha_{Soiling_{Yr}}$, the work of Nepal [15] provides the value for the annual losses $L_{Soiling_{Yr}}$ a system, similar in size to the evaluated HyET one ($1.62Kwp$, **presents installed** in Delft, the Netherlands. To estimate the ratio, the Y_{SpNL} provided by Van Sark 4.35 was used to assume an *Annual system Yield* for the system of Nepal E_{NeYr} , equation 4.37. Once established, the $\alpha_{Soiling_{Yr}}$ was defined as can be seen in equation 4.38.

$$Y_{SpNL} * P_{rated} = E_{NeYr} \quad (4.37)$$

$$\alpha_{Soiling_{Yr}} = \frac{L_{Soiling_{Yr}}}{E_{NeYr}} = \frac{16.22 \left[\frac{KwH}{Yr} \right]}{1,417.5 \left[\frac{KwH}{Yr} \right]} = 1.1442\% \quad (4.38)$$

As the **resulting** $\alpha_{Soiling_{Yr}}$ value **resulted is** lower than 2%, the use of the estimation *was allowed to be can be* used and still complies with the A classification of the IEC 61724-1:2017 standard for the monitoring system, as intended in the original system design. The considerations taken can be further seen in chapter 5.

4.7. Partial shading

The consideration of whether partial shading would affect the system was done by performing an on-site assessment aided by the use of an *Horcatcher*. This device allows for a 360° shot to be taken of the horizon to be later analyzed. The image can be latter digitally converted to view the 360° in a single horizontal plane. Once the picture is digitally converted, the coordinates of the location, direction with respect to the north, time and date are set. This allows for the *Meteonorm* software to determine the sun path the system will experience through the year. The digitalized horizon allows to identify the obstacles, such as buildings and trees, that affect the system view. By contrasting the sun path with the horizon, it is possible to determine which objects in the horizon will contribute to block the direct sun beam the system receives at a particular time of the day and depending on the day of the year.

For this work, shading is only relevant on a situation where the modules are completely or partially exposed to a shading condition, and simultaneously the irradiance sensor, in this particular case the *Kipp & Zonnen CM 21* pyranometer, would not be exposed to it. This situation would result in an erroneous assumption in which a higher energy input is recorded while in reality part of the modules are being shaded. In order to quickly establish the likelihood this situation would present, 2 set of images where taken at different height levels, one at ground and another at the top level of the system. By contrasting the shade profile obtained by both images, an estimation on the partial shading losses experienced by the system was obtained.

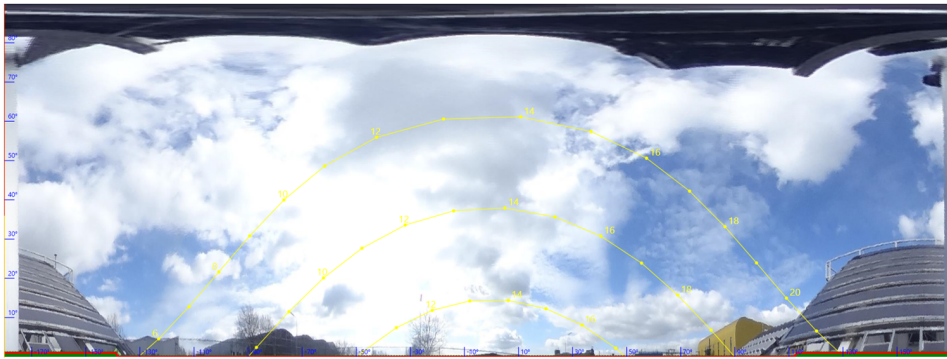


Figure 4.19
Horizon view of the HyET Solar performance monitoring system. Bottom section of the system. It can be appreciated how the sun path is blocked during sunset during the spring and autumn period. The sun path is mostly free during winter periods.

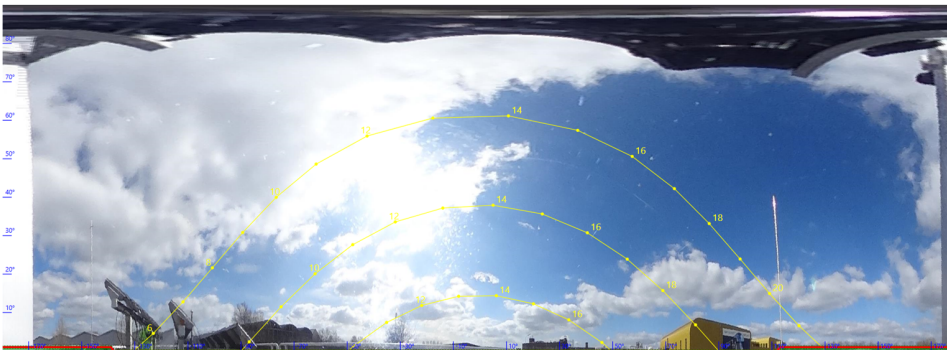


Figure 4.20
Horizon view of the HyET Solar performance monitoring system. Top section of the system. It can be appreciated how the sun path is less constrained by objects than from the bottom view.

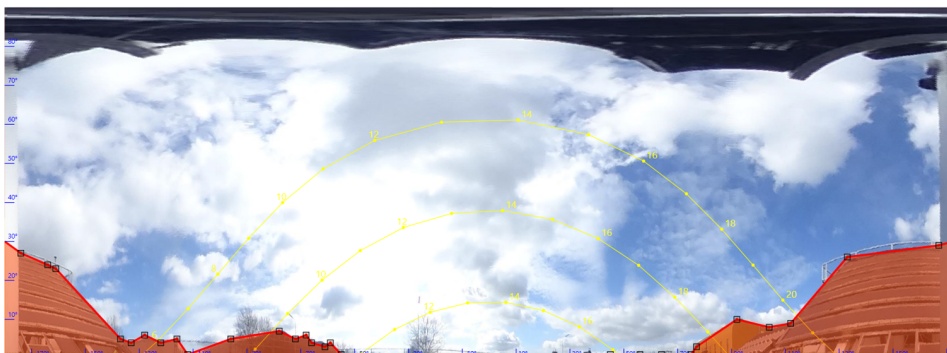


Figure 4.21
Horizon view of the HyET Solar performance monitoring system. Bottom view. Horizon is marked for an easier assessment of its impact on received irradiance through the year

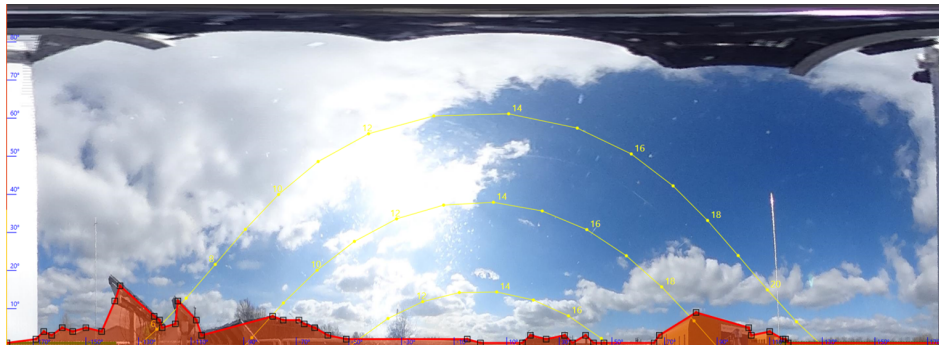


Figure 4.22
Horizon view of the HyET Solar performance monitoring system. Top view. Horizon is marked for an easier assessment of its impact on received irradiance through the year

5

Photovoltaic and Data Acquisition System Design

Following an extensive literature review, the environmental and location factors affecting photovoltaic performance on a system level were identified on Chapter 3. By convenience, and following the names used by certain revised literature, **this** factors are identified as *loss mechanisms* or *loss factors* by this work. **This** factors are known to alter, and particularly reduce, the relative power output a photovoltaic system produces in relation to the solar energy received by the system. This relative output is also known as the photovoltaic system performance and its better described by the parameter known as *Performance Ratio*, mentioned in Chapter 2. An in-depth review of **this** loss mechanisms at an earlier stage of the reported project allowed to identify the measurable parameters required to explain the performance of a photovoltaic system comprised of a-Si:h modules, **installed** in the Netherlands. Now, in order to perform a robust analysis of the newest HyET Solar baseline modules under real operation conditions, a data acquisition plan for modules under real operation conditions needs to be devised.

During an earlier stage of the *benchmark project*, the construction of a photovoltaic system with data acquisition capabilities was **decided indicated** as the solution for acquiring the required performance data to *be analyzed analyze*. This Chapter will describe the *techno- technical and* economic considerations steering the design of the system on section 5.1. Following, a brief description of the first photovoltaic system proposals will be done on section 5.2. Then, a description of the equipment used and modules selected for the analysis will be done on section 5.3. Finally, section 5.5 concludes *with presenting* the final design.

5.1. Design Considerations

The performance monitoring system to be designed under this project can be divided in 2 sub-systems, a photovoltaic system and a data acquisition system. The main design goal of the photovoltaic system was to obtain a well performing and as efficient as possible system. By designing a system with low system level losses, the later analysis process would be simplified as some controllable performance loss factors would see their share decreased, resulting on a more accurate analysis. On the other hand, the main design goal of the data acquisition system was to obtain data on a periodic, sufficient, and reliable way, with an adequate resolution (or frequency between measurements), and with the sufficient endurance to stand the expected operation conditions. Nevertheless, the performance monitoring system design was also constrained by additional factors such as budget, and followed additional design considerations, making the end design a trade-off between all of **this** considerations. The followings list names the main design considerations and later in this section, they will be described in more detail.

- Building a class A monitoring system under IEC 61724-1 standard
- Have an adequate data resolution for analysis
- Budget constrains

- System flexibility for later modifications or modularity
- Maximize the use of available resources
- Level of monitoring capability: System, Sub-system or Module level
- Allow for a comparison between a-Si:H and c-Si technologies
- Design for high system performance
- Availability of resources: Both in-House and external

5.1.1. IEC 61724-1 class A Standard

Building a monitoring station according to the IEC 61724-1 Standard would assure reliability of the resulting acquired data, and could signify a higher value of the end analysis results for the company; it would also make possible a further use of the monitoring station for applications later devised. For this reason, it was of interest of the company to follow a design *according to which complies with* this international standard. Furthermore, the standard classifies the monitoring stations in 3 classes according to their accuracy (Table 5.1), and suggest the ideal class per monitoring application.

As it can be seen on Table 5.2, a Class C standard falls short for the desired application where as class B is sufficient according to the IEC to successfully monitor the system level losses. Although sufficient to cover the initial goal of the project, the possibility of using the built system to precisely measure the system degradation and make a reliable assessment of the second generation PV technology was an interesting possibility, particularly for a company such as HyET Solar *were* a newer technology is produced and is intended to compete against the established c-Si one. Following this consideration, the desired building classification for the monitoring system was a Class A.

Table 5.1
IEC 61724-1 Standard Class Definition

Classification	Accuracy Level
Class A	High Accuracy
Class B	Medium Accuracy
Class C	Basic Accuracy

Table 5.2
Suggested Class Applications

Typical Application	Class A	Class B	Class C
Basic System Performance Analysis			X
System Losses Analysis		X	
PV Technology Assessment	X		
Precise PV System Degradation Measurement	X		

Once the desired Class was established, the required characteristics to comply with Class A are discussed on the IEC 61724-1 standard. Figure 5.1 and 5.2 show the full requirements per system classification. For the particular considered system, the environmental and irradiance measurements the standard requires are the direct measurement of plane of array irradiance I_{POA} and global horizontal irradiance I_{GHI} , measurements of the module temperature T_M with at least 6 temperature sensors, measurements of the ambient temperature, measurement of the wind speed and direction, measurement of the soiling ration in case the losses related to soiling are expected to be higher than 2% of the overall power production on a yearly basis, and an estimation of soiling losses related to rainfall. For the electrical output measurements, the standard requires the measurement of both the DC and AC voltage, current and power at the inverter side, and the overall output energy the inverter delivers.

Parameter	Symbol	Units	Monitoring purpose	Required?			Number of sensors
				Class A High accuracy	Class B Medium accuracy	Class C Basic accuracy	
Irradiance (see 7.3)							
In-plane irradiance (POA)	G_i	W·m ⁻²	Solar resource	√	√ or E	√ or E	Table 4 column 1
Global horizontal irradiance	GHI	W·m ⁻²	Solar resource, connection to historical and satellite data	√	√ or E		Table 4 column 1
Direct normal irradiance	DNI	W·m ⁻²	Solar resource, concentrator	√ for CPV	√ or E for CPV		Table 4 column 1
Diffuse irradiance	G_d	W·m ⁻²		√ for CPV with < 20× concentration	√ or E for CPV with < 20× concentration		Table 4 column 1
Circumsolar ratio	CSR						
Environmental factors (see 7.3)							
PV module temperature	T_{mod}	°C	Determining temperature-related losses	√	√ or E		Table 4 column 2
Ambient air temperature	T_{amb}	°C	Connection to historical data, plus estimation of PV temperatures	√	√ or E	√ or E	Table 4 column 1
Wind speed		m·s ⁻¹	Estimation of PV temperatures	√	√ or E		Table 4 column 1
Wind direction		degrees		√			Table 4 column 1
Soiling ratio	SR		Determining soiling-related losses	√ if soiling losses expected to be > 2 %			Table 4 column 1
Rainfall		cm	Estimation of soiling losses	√	√ or E		Table 4 column 1
Snow			Estimation of snow-related losses				

Figure 5.1 Requirements to comply with IEC 61724-1 class A. Section 1

Parameter	Symbol	Units	Monitoring purpose	Required?			Number of sensors
				Class A High accuracy	Class B Medium accuracy	Class C Basic accuracy	
Humidity			Estimation of spectral variations				
Tracker system (see 7.4)							
Error in dual-axis tracker primary angle	$\Delta\phi_1$	degrees	Tracker system fault detection, dual-axis	√ for CPV with >20× concentration			Table 4 column 1
Error in dual-axis tracker secondary angle	$\Delta\phi_2$	degrees		√ for CPV with > 20× concentration			Table 4 column 1
Single-axis tracker tilt angle	ϕ_T	degrees	Tracker system fault detection, single-axis	√ for single-axis tracker			Table 4 column 1
Electrical output (see 7.5 and 7.6)							
Array voltage (DC)	V_A	V	Energy output, diagnostics and fault localization	√			At each inverter (optionally at each combiner box or each string)
Array current (DC)	I_A	A		√			
Array power (DC)	P_A	kW		√			
Output voltage (AC)	V_{out}	V	Energy output	√	√		At each inverter and at system level
Output current (AC)	I_{out}	A		√	√		
Output power (AC)	P_{out}	kW		√	√	√	
Output energy	E_{out}	kWh		√	√	√	
Output power factor	λ		Utility request compliance	√	√		At each inverter and at system level
Reduced load demand			Determine utility or load request compliance and impact on PV system performance	If applicable	If applicable		At system level
System output power factor request	λ_{req}			If applicable	If applicable		At system level

Figure 5.2 Requirements to comply with IEC 61724-1 class A. Section 2

5.1.2. Data Resolution

The frequency with which a system parameter is measured, and a data point with a timestamp is created, is called data resolution. Monitoring systems vary on their resolution according to the end purpose of the data and the resolution is normally determined by the equipment used for sensing, data acquisition and data logging, and generally speaking, higher resolution equipment follow higher prices. For photovoltaic monitoring purposes, a desirable resolution according to the IEC 61724-1 standard

varies from the order of seconds up to minutes [9], *according to depending on* the application. For the evaluation of performance, a resolution in the order of minutes is reported to be sufficient, while for a system losses analysis and photovoltaic technological assessment, a resolution in the order of seconds is desired as quick variations in environmental factors can rapidly vary the system parameters, such as temperatures due to gusts of wind or incident irradiance due to sudden cloud coverage, creating situations only perceived through a high resolution monitoring capability.

After a commercial analysis of monitoring equipment, it was concluded that obtaining a high resolution monitoring system would not be a problem for environmental parameters, *where as while* for the electrical parameters it seemed a different case. The analyzed electrical performance monitoring systems appeared to have a wide range of resolution sizes, with up to 5 minutes intervals for some less expensive options.

5.1.3. Modularity

The nature of a company producing an innovative product leads to have constant developments *among* of the end baseline product, making a system constrained to the analysis of an old product line, possibly obsolete in the near future. For this reason, an important design consideration was to deliver a monitoring system capable of analyzing different product lines, and also capable of modifying the analyzed photovoltaic modules without the need of mayor modifications to the system.

5.1.4. Available Resources

A way to decrease the end project cost was to make use of as many already available resources the company had as possible. While this consideration should not interfere with the end goal of delivering a reliable performance monitoring system, it could lower the budget expense, as well as decrease the amount of required labour and working hours to build up the system. A brief example of *this* resources include mounting structures, sensing devices and human resources.

For the sake of a swift completion (*?)etition* of the project, the company HyET Solar made available the use of any desired area on a plot of land next of their ownership, next to the main company building. After a preliminary study of the area, 2 main locations where considered for locating the system. Figure 5.3 shows the sky-view of the plot of land and both considered locations, now referred as location number 1 and location number 2.

Location number 1 had an old, out of order monitoring station. While it had a lot of working equipment, it was not operational and was reported to not had been used for at least 9 years. One of the main advantages is that it counted with a sturdy metal structure tilted at 38° and facing south, the optimal position for placing solar modules and obtaining their maximum yearly energy yield in Arnhem, the Netherlands. This presented an opportunity as refurbishing the old monitoring station mounting station would mean spending less time and resources than building a new one from scratch. It had an available area of 35 m², the structure can be seen in more detail in Figure 5.4.

Location number 2 presented a wide open space without any objects nearby, allowing for a free system design. Due to its closeness to the access road to the company building, the location presented the benefit of a high exposure to visitors, making the demonstrator system a noticeable example of a real application for the HyET Solar product.

5.1.5. Level of monitoring

The commercial analysis showed that the level of monitoring offered by the industry varied greatly by equipment and complexity of implementation. A finer level of monitoring requires highly specialized hardware able to monitor the electrical performance of each of the modules contained by the system. *While In spite of* this approach being ideal for a highly in-depth performance analysis as a J-V curve can be periodically obtained per module, the associated cost of the hardware and complexity of implementation made this approach less attractive for the project. This decision was backed by the fact that the IEC 61724-1 Standard advises as sufficient an inverter level monitoring for the goals of the project.

However, less expensive commercially available alternatives *where* found offering sub-system level of monitoring by the use of power optimizers equipped with electric performance monitoring capabilities. This approach seemed to cover plenty of the design considerations as *it* offered the possibility of delivering a modular design as well as having a low impact on the project budget. Nevertheless, this



Figure 5.3

Available area for mounting the monitoring station next to HyET Solar premises. Figure shows direction of north. 2 points were considered. Point number 1 had an abandoned monitoring station with a steel structure that could be reused for the system, also a pre-existing electric line connecting the outdoor setup with the main HyET Solar building. Point number 2 presented enough open field for a totally new system and an easily seen location by visitors to the company.



(a) Front view of structure



(b) Lateral view of structure

Figure 5.4

Pre-existing mounting structure in Hyet Solar premises. The modules and monitoring hardware were not operational anymore. The structure was still in good conditions for re-use after minor refurbishing.

type of technology had a downside as the resolution seemed constrained to sampling on minutes level.

A third option *however* was considered, consisting in the use of commercially available central inverters with monitoring capabilities. This equipment offered a higher sampling rate than their power inverters plus central inverters counterparts but constrained the level of monitoring to a system level instead of per sub-system.

5.1.6. Monitoring compatibility between c-Si and a-Si:H technology

During the literature review phase of the project, the research question "How would the Performance Ratio of a system comprised of HyET Solar a-Si:H modules would compare against a c-Si based one."

was established. Although the performance data of crystalline silicon systems installed in the Netherlands **thus sentence is not complete**, a fairer comparison would be obtained if the monitoring system could measure as well the performance of a c-Si system. This data could also be used for reference of the performance of the second generation photovoltaic technology with respect to the established crystalline silicon based one, therefore making this design consideration an important one.

5.1.7. Design for Performance

As for any photovoltaic system, the design of the performance monitored photovoltaic system also aimed for a high electric performance. A good photovoltaic system design should therefore also minimize as much as possible the losses associated to a power rating mismatch between components ¹, make a good cabling size selection and an optimum electric topology design.

As referred in Chapter 4, a system design with low associated electric losses would also benefit the later analysis of data as less variables would be influencing the system level losses. However, it was noted at an earlier stage of the system design that most of the available inverters were rated at a higher power than the initially desired of 1 kW, which would mean building a system with a rated power drastically lower than the one of the inverter, inducing a high share of power conversion losses. This issue **had to** be tackled without using a high amount of the project budget and more importantly, as described on section 5.1.8, with a constrained supply of HyET Solar modules.

5.1.8. Availability of resources

During the time period that the build up of the monitoring system was planned to begin, the company had several high level on going projects, requiring the totality of the produced modules to be used for this projects. As the high demand for modules was expected to last for at least 2 additional months, an alternative supply had to be found if the construction deadline was to be met.

This lead to the use of "discarded HyET modules" for the system. Among the production line, enough modules that did not comply with the quality standards for sales purposes were found. Many of this modules appeared to have being discarded mainly for not complying with the aesthetic standards required to be sold, yet reporting good electrical performance characteristics. While not being the ideal choice, the use of this discarded modules would allow to accomplish the project in time and make, at the expense of additional uncertainty being introduced into the analysis.

5.2. Analyzed design proposals

After analyzing the design considerations mentioned in section 5.1, a design proposal and an estimated budget was made for the review of the project board. Figure 5.5 better illustrates the physical appearance of this design proposal. The selected location for the system was location 1, as it offered access to plenty of available resources, primarily a mounting structure and an electrical connection. *The existing mounting frame was decided to be used* **It was decided to use the existing mounting frame** after a minor refurbishing of the pre-existing mounting racks to allow for an alternative rigid mounting structure for the modules, that would simulate the surface of a type of rooftop structure, aiming to simulate similar operation conditions **to of one of the main expected most probable (?)** applications for a flexible lightweight HyET Solar system. The lower section of the mounting structure was *decided to be left unmodified and unused by the monitoring system*, allowing the area to be kept used by a different R&D project. The flexible modules would be fixed in a rigid plane structure simulating the fixing characteristics and heat transfer conditions a rooftop covered with a heat and rain insulating membrane **and that** a bitumen covered surface would provide. As the modules are flexible, they need to be fixed **at to** a rigid structure to avoid folding or wrinkling. This rooftop configuration was chosen as it simulates a type of rooftop were the HyET product lightweight characteristic makes it commercially interesting to be implemented. The rigid structure was decided to be built in plywood due to its availability, low cost and easy implementation. Figure 5.6 shows a back view of the system where the plywood structure and its fixation to the steel beams can be appreciated.

¹An industry standard is to size the system power as close as possible to inverter rated power. The inverters efficiency are higher close to their rated operational parameters such as voltage and power.

The proposed electrical design consisted in placing 20 HyET modules for a peak rated power of 1,000 watts² packed in 5 subsystems, each subsystem consisting *in of* 4 modules in series configuration connected to a Solar edge power optimizer. As the Solar edge components count with monitoring capabilities per power optimizer **what do you mean?**, this configuration allows for each group of 5 modules to be tracked and monitored, delivering their electrical performance on a 5 minutes basis. The system topology would therefore be a central inverter with power optimizers configuration allowing for flexibility and scalability. As part of the *fore mentioned aforementioned* flexibility that the inverter with optimizer configuration allows, the system design also includes one crystalline silicon photovoltaic module to serve as a reference and allow for a technology comparison. 6 module temperature sensing points across the system would be implemented in order to comply with the IEC 61724-1 class A Standard, alternating between multiple measurement points for module average temperature, single measurement points for array average temperature and a single measurement point on a c-Si module for reference and comparison.

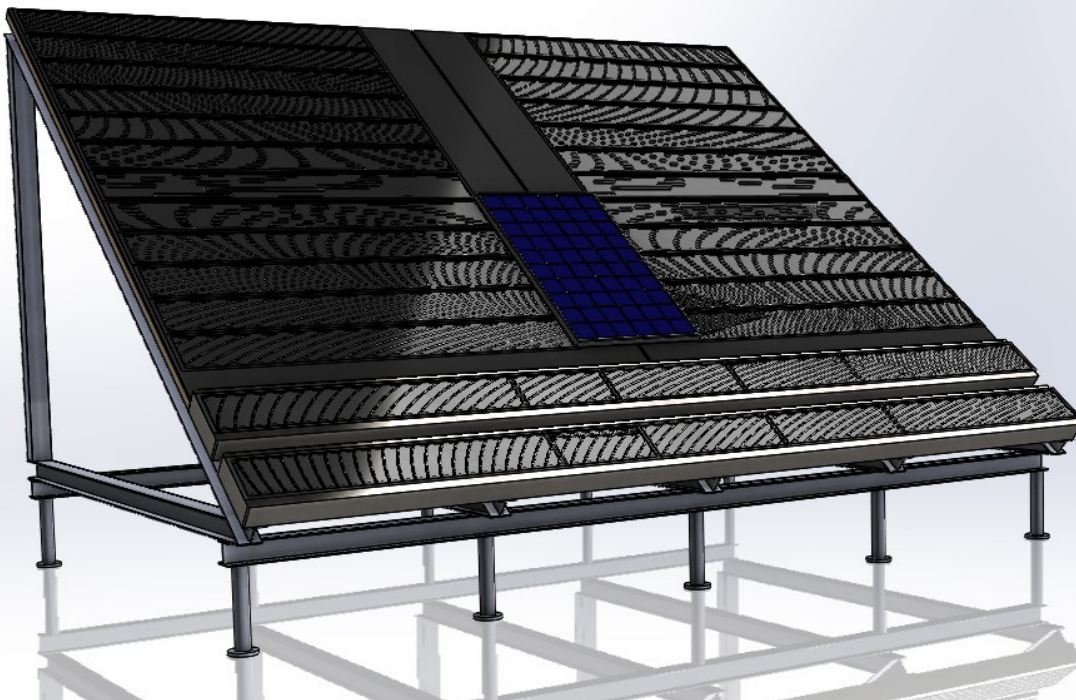


Figure 5.5

Computer assisted design of first proposal. System comprised of 20 a-Si:H modules allowing for the bottom 2 racks of modules to kept being used by the research ad development team for reliability purposes external to the project. The system could include the addition of one or two c-Si modules for reference and technology comparison purposes. The mounting was structure was designed to be built on a wooden frame with a bituminous layer on top to resemble a rooftop and to make use of a material considered less expensive than an environment resistant metal.

As part of the main design proposal, an additional proposal was presented were a modified module mounting structure simulating an alternative rooftop type was used. As the company had an expected project where a large batch of modules would be installed *in on* a particular lightweight prefabricated type of rooftop, the proposal suggested to use the same type of structure to fix the modules in the monitoring station. The electric system design would be identical as the previous proposal, only modifying the type of mounting structure. The reference c-Si module would require to be placed on a lower section of the steel mounting structure as the prefabricated roof was weight sensitive. a computer assisted design model shows the physical appearance of the alternative proposal *on in* figure 5.7.

²Assuming a rough rated power per HyET module of 50 watts. In reality the modules have a slightly lower rated power.

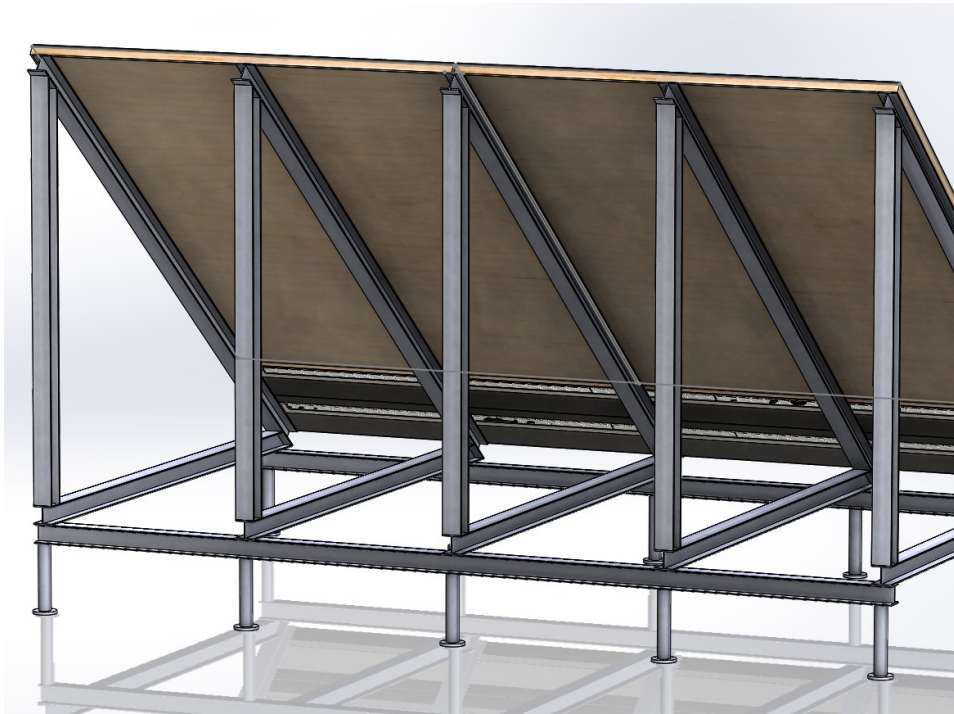


Figure 5.6
Computer assisted design of first proposal. Back view. The back surface of the plywood mounting structure would be fixed to the inclined metal beams of the mounting rack. The render do not show the back slots for positioning the temperature sensors.

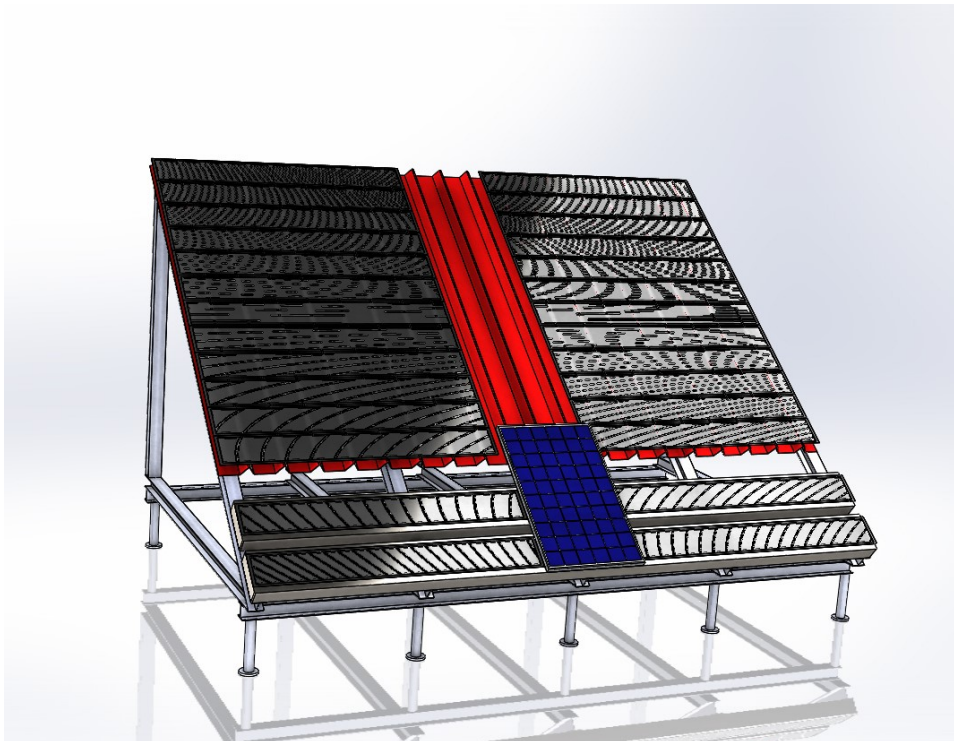


Figure 5.7
Computer assisted design of first proposal, alternative mounting structure. The mounting structure would simulate the operation conditions of HyET module mounted on a prefabricated lightweight rooftop structure similar to the one used on a coming project. c-Si reference module would be mounted on the sturdier lower section.

5.3. Selected equipment

The following section describes the selected equipment used in the final design of the photovoltaic performance monitoring station. The technical specifications and justification of selection can be found within the section. For most of the used equipment, the data sheets are presented in the Appendix section. The section is divided in the following subsystems: Electrical system, data acquisition system, crystalline silicon modules and finally, the mounting system. The parameter description of the analyzed HyET Solar thin film a-Si:H modules is done in a separate section, and can be found in Section 5.4

5.3.1. Electrical System

Power Optimizer

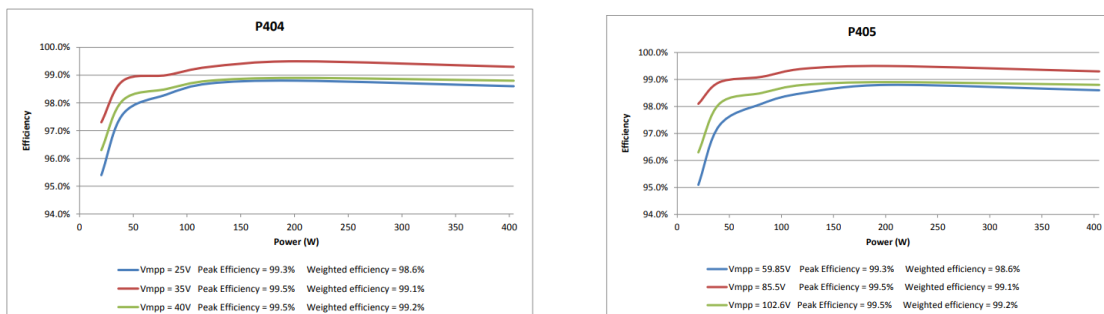
Two different kinds of power optimizers were used, the *Solar edge P404* recommended for use with c-Si modules, and the *Solar edge P405* recommended for use with thin film modules due to higher voltage tolerances than common power optimizers. Both rated at 405 W, this equipment serves as a maximum power point tracker, as well as a voltage V_{mpp} , current I_{mpp} and direct current power P_{mppDC} monitoring (or data acquisition) device. Both optimizers are designed to work with each other regardless of operating at a different input voltage and current as their output parameters are matched. Table 5.3

Table 5.3

Electrical parameters of Solar edge power optimizer P404 and P405. P404 was used with c-Si modules and P405 was used with HyET Solar a-Si:H modules.

Parameters	P404	P405
Rated input power	405 W	405 W
Maximum input voltage (V_{OC})	80 V	125 V
MPPT operating range	12.5 V-80 V	12.5 V-105 V
Maximum input current (I_{SC})	10.1 A	10.1 A
Maximum Efficiency	99.5 %	99.5 %
Weighted Efficiency	98.5 %	98.6 %

As the rated power per HyET Solar a-Si:H module is drastically lower than the rated input power for the *P405*, an arrangement of several modules connected to a single power optimizer had to be done. This would allow the average operational power of the optimizers to fall between their high efficiency range for most of the time. This is a typical characteristic of power conversion equipment, while being functional on a wide input power range, the power conversion efficiency is optimal for a set range of the input power, decreasing as the input power gets further from the rated operation power. Figure 5.8 illustrates this effect on the efficiency vs power curve, also known as power curves, for the mentioned optimizers. For the complete data sheet, please refer to Appendix A.



(a) Powercurve of P404 optimizer

(b) Powercurve of P405 power optimizer

Figure 5.8

This equipment was selected for plenty of reasons such as:

- It allowed to build a flexible system with a-Si and thin film a-Si:H technology under the same inverter.
- It offered a good balance of system price.
- It allowed to build a scalable system as the system can be easily scaled up by simply adding additional power optimizer subsystems.
- It offered decent monitoring capabilities at a low price point.
- Previous systems delivered by HyET Solar were already built using this technology and this brand.
- Other projects at the PVMD reseach group also used this equipment for monitoring purposes [2].

Inverter

The selected inverter was a *Solar edge SE2200H* rated at 2.2 kW. This inverter is designed to work well with the P404 and P405 power optimizers, requiring for a minimum number of 6 optimizers in a string to operate, without a set upper limit³. This inverter, in conjunction with the power optimizers, allows to monitor the electrical performance of the whole system on the DC side, as well as the output power P_{AC} and output energy E_{AC} the inverter delivers to the grid. By an Ethernet or wireless connection, the inverter sends this data to an online monitoring platform run by *Solar edge*, where the data can be visualized and retrieved. Table 5.4 refers to the main electrical parameters. For a full description, please refer to the Appendix B.

Table 5.4

Electrical parameters of Solar edge inverter SE2200H. The rated power is 2,200W, 400W less than the system rated power.

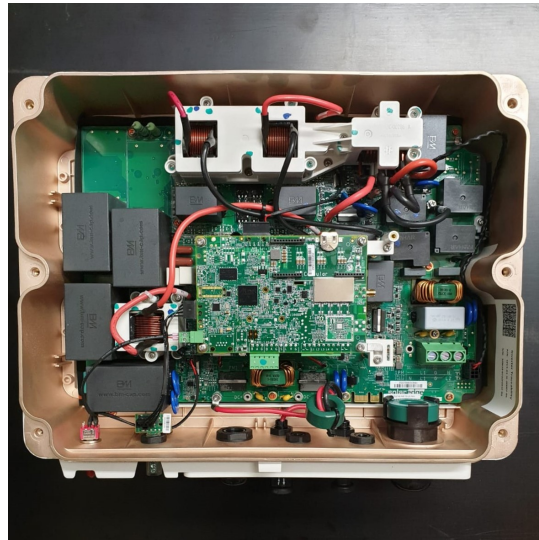
Parameters	SE2200H
Rated output power P_{AC}	2,200 W
Maximum DC power input	3,400 W
Maximum input voltage	480 V
Rated input voltage	380 V
Maximum input current	6.5 A
Weighted Efficiency	98.3 %

While a main reason to use this equipment was the monitoring capabilities it had, the data resolution was reported to be around 5 minutes per sample. This was considered sufficient for the current expected application but low for future applications, therefore the addition of a data acquisition gateway with a higher sampling rate was considered. *Solar edge* offers a gateway device capable of improving the sample retrieving rate. Figure 5.9 shows the inverter once installed and prepared to be connected to the data acquisition gateway.

³The upper operational limit for any inverter is the rated power with an allowed factor for operating above this value, set per each manufacturer.



(a) Installed inverter.



(b) Inverter case open for preparing connection to data acquisition gateway.

Figure 5.9

Solar edge 2200H inverter mounted inside the data house of the HyET Solar monitoring station.

5.3.2. Data Acquisition System

The data acquisition system refers to the group of devices that jointly serve to translate physical or chemical parameters into signals, then read this signals and translate them again into readable forms such as numbers, and lastly record this numeric values with a time stamp for a later analysis. As part of the data acquisition system built for the reported project, the following parameters where recorded:

- Point of array irradiance I_{POA}
- Global horizontal Irradiance I_{GHI}
- Module temperature (a-Si:H) $T_{M_{a-Si:h}}$
- Module temperature (c-Si) $T_{M_{c-Si}}$
- Ambient temperature T_{amb}
- Power DC (Subsystem) $P_{DC_{Sub}}$
- Power DC (System) $P_{DC_{Sys}}$
- Power AC (System) $P_{AC_{Sys}}$
- Voltage (Subsystem) $V_{MPP_{Sub}}$
- Voltage (System) $V_{MPP_{Sys}}$
- Current (Subsystem) i_{DC}
- Current (System) i_{AC}
- Energy yield (Subsystem) E_{Sub}
- Energy yield (System) E_{Sys}

Main Data logger

The data logger used to measure and record the I_{POA} , I_{GHI} , $T_{M_{a-Si:h}}$, $T_{M_{c-Si}}$, T_{amb} was the *Pico Technologies USB TC-08 Temperature Data Logger*. This equipment offers 8 measuring channels with a sampling rate of up to 1 second per measurement with a high resolution of 20 bits. The device is designed to work best with any commercial thermocouple type, offering a temperature resolution of up to 0.025°C. While the inputs are specially designed to work with thermocouple type plugs, the addition of a terminal board, Figure 5.10b, allowed to input the analogical voltage signals of the pyranometers. This in turn allowed to exempt the need of an additional data logging device for the irradiance sensors, and furthermore log all the environmental inputs into one single database. The measured data was then recorded on a computer equipped with the *Picolog 6* software where it could be later retrieved in a CSV format for analysis. Appendix C shows the data sheet of this equipment for further references.



(a) Picologger TC 08



(b) Terminal board

Figure 5.10

Pico Technologies USB TC-08 Temperature Data Logger. 8 channels available for measurements. (b) Terminal board used to modify the input to measure potential differences from the irradiance sensors. With the sensor sensitivity, this potential drop was converted on the datalogger into readable irradiance on $\frac{W}{m^2}$ units.

The Picologger TC 08 data logger retrieves the analogical potential difference signals emitted by the thermocouples and pyranometers, and converts them to digital signals, processed and logged by the attached computer with the *Picolog 6 Software*. The data logger is able to read the signals every second and the logger software is able to read and log also every second. For convenience, the logging procedure was programmed to be performed every 15 seconds, thus having 4 samples per minute. The live measurements were seen in the computer, which allowed to have a quick estimation of the expected energy yield when on site. Figure 5.11 shows the main screen of the logging software. For the analysis, the processing of the data is of higher importance than the simple visualization, therefore the system records a text file on a CSV format which can be post-processed on any kind of software. Figure 5.12 shows the screen view of the live recording process.

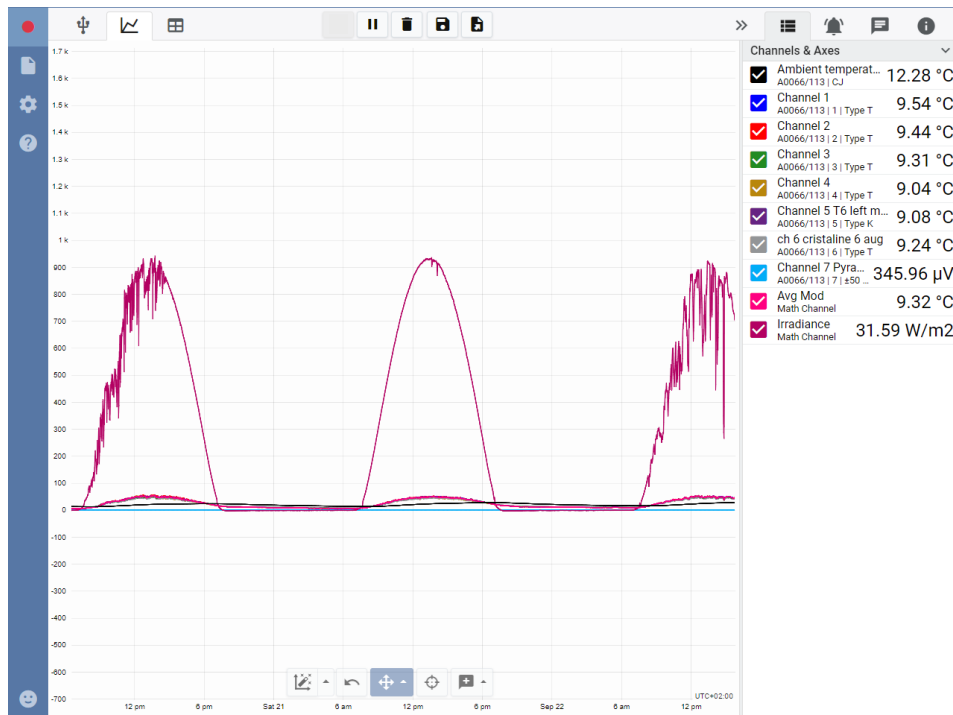


Figure 5.11

Live measurements view of Picolog 6 Software. This is the main view of the data logger dedicated to retrieve environmental parameters. The screen shows the live measurements of the 8 channels including irradiance, ambient temperature, temperature of selected modules and average temperature of the system. The system measures and shows every second any change on the parameters. The log of data is performed every 15 seconds. On the left hand side of the screen a graphical record of the irradiance (Purple) is shown. The temperature is likewise recorded but due to the difference in scale it is hardly appreciated on this image.

Solar edge monitoring platform logging plus gateway system

The datalogger used to measure and record the electric performance parameters P_{DCSub} , P_{DCSys} , P_{ACSys} , V_{MPPSub} , V_{MPPSys} , i_{DC} , i_{AC} , E_{Sub} , E_{Sys} was a combination of the *Solar edge* equipment and its monitoring platform. The equipment, consisting on power optimizers and inverters, counts with the additional feature of registering the electrical operational parameters and then sending this data, via an internet connection, to the online monitoring platform where the live data can be visualized in diagrams, and the raw data can be downloaded in a CSV format for a later analysis. Figures 5.16 and 5.17.

While this design decision allows for a reduced budget expense as expected costs of alternative specialized electric monitoring equipment were estimated to be in the order of 10 times higher than this equipment, it also presents the inconvenient of having a rather poor resolution as the power sampling rate is performed in an aleatory manner every 3 to 6 minutes. This characteristic, while being sufficient for the desired analysis to be performed for this work, would limit a further in-depth analysis of performance losses due to quick changes in the environmental parameters. An additional disadvantage of the low sampling rate was the mismatch between the 2 data sets (One from the Picologger and the second from the monitoring platform). This factor would complicate the analysis since the timestamps of both data sets would not match and a relationship between parameters would be impossible to be performed in an automatized way without a pre-processing step.

These low resolution issues were tackled in 2 manners. Firstly, to make both data sets "compatible" under the same data-stamp regime, a pre-processing step was performed aided by *Matlab* in which the "low resolution" electric performance data set was paired to the "high resolution" environmental parameters data set under the same timestamps by performing an interpolation on the first data set. This was performed in 3 simultaneous ways, by a linear interpolation, a cubic interpolation technique, and a "spline" piecewise polynomial function technique. By graphically analysing the 3 techniques by plotting the 3 trends and comparing them to the original results, the cubic interpolation seems the better

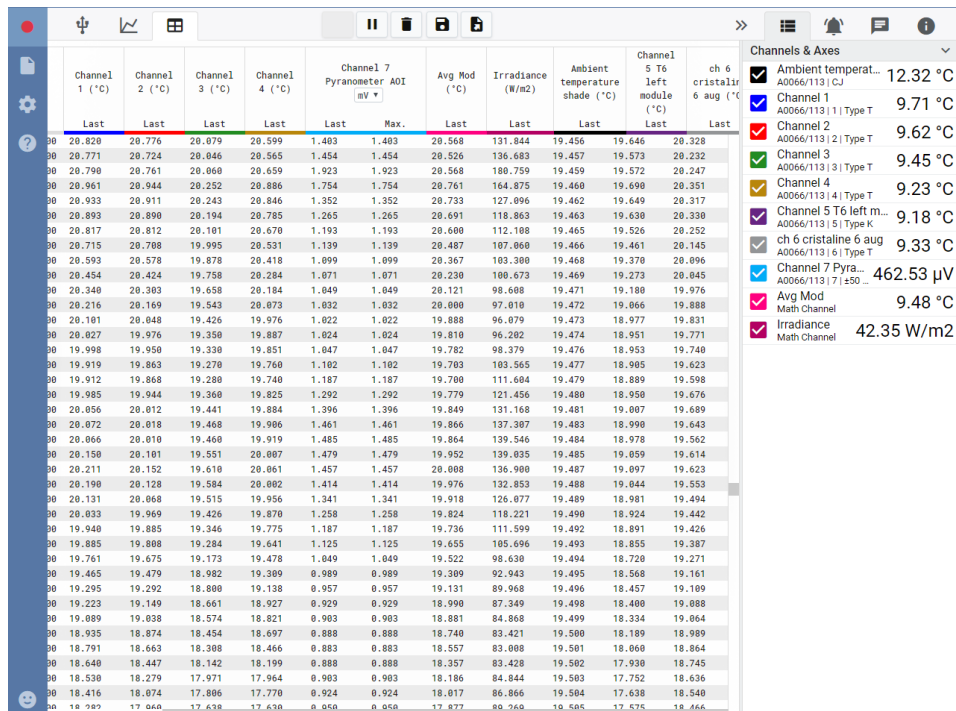


Figure 5.12

Logging of data on the Picolog 6 Software. This is the secondary view of the data logger dedicated to retrieve environmental parameters. The screen shows the live logging of data on steps of 15 seconds. The data can be quickly view on the system and the data set can be imported for a latter analysis on a CSV format.

fit as it offers the closest approximation to real values without having the issue of "overfitting" as the spline interpolation does. The spline interpolation, although generally having a better fit than the cubic interpolation, showed issues when the evaluated values tended to zero by interpolating into forbidden zones⁴. Figure 5.13 shows the mentioned interpolated curves for the 3 different techniques. The poor fit offered by the first technique can be easily noted on Figure 5.14, while the spline technique seems to have a better fit than the cube fit in this zone. Figure 5.15 shows the overfitting due to the spline interpolation when the power output tends to zero.

The second manner to increase the resolution was achieved by adding a gateway to the *Solar edge* inverter, allowing to retrieve the inverter performance data every second. Nevertheless, this approach showed a limitation for the analysis as most of the required data was the recorded by the power optimizers instead of the inverter as the system was comprised of both a-Si:H and c-Si technologies. Although allowing to obtain high resolution sample data, the first approach was preferred to the latter for the aforementioned reasons. Figure ?? shows the physical installation of the gateway device on the monitoring station control room.

Temperature sensors

The chosen module temperature sensing device were type T Thermocouples from the brand RS Components. Their operational temperature ranges from -75°C to 260°C , being more than sufficient for the PV application. The probe termination is a striped point with a diameter of 1/0.2mm. Their tolerance complies with the IEC 584 Class 1 standard making them reliable for research and development applications. This devices are used by the PVMD for module temperature research under additional projects.

Irradiance sensors

For the selection of the temperature sensor, two commercially available technologies were considered, the pyranometer and the reference cell. Both present particular advantages and disadvantages to each other, therefore the selection was done contrasting them to the requirements of the project.

⁴For the evaluation of power performance, the considered "forbidden zones" for the interpolation are the negative values.

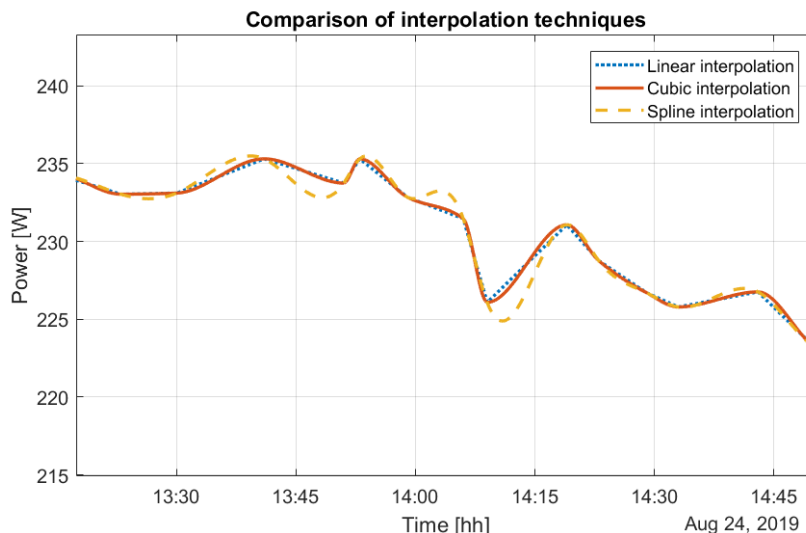


Figure 5.13

Comparison of interpolated techniques. The interpolation analysis is done on a single power optimizer subsystem. A linear, cubic and spline interpolations are compared.

The pyranometer operation principle is based on the change in temperature a black surface presents when exposed to sunlight. This change in temperature creates a potential difference proportional to the incident irradiance level. This potential difference can be read as a signal and, by using the known sensitivity of the device⁵ to translate the potential difference into a readable signal, the irradiance received by the pyranometer can be known. Due to this operation principle, the spectral range the device is sensible to ranges from the ultraviolet to the infrared range. Furthermore, the physical design makes it equally receptive to irradiance at different incident angles. This characteristic makes the technology ideal for measuring the overall irradiance an area is receiving regardless of the application as the output will not be conditioned to a spectral range. [14]

In comparison, the reference cell works based on the photovoltaic effect a semiconductor presents to sunlight. By using a very stable photovoltaic cell where all the working parameters are known, the output current and voltage can be translated into read irradiance. As the working device is a solar cell, the operation characteristics of this applies for the measurements, this means that the band gap of the reference cell will define the spectral response range the device is able to measure, being the non active wavelengths invisible to the device. Another characteristic of the device is the response to difference incident angles, as the response will be dependent of the cell characteristics. This makes it ideal to use for monitoring purposes where the performance of a PV system is being investigated when the reference cell technology is the same as the evaluated system.

Analysing both devices, the pyranometer appeared as the optimum device as it provides the most reliable measurements independent of the type of photovoltaic technology used. The selected devices were the *Kipp & Zonen* CM21 and CM11 pyranometers. Both devices comply with the ISO 9060 Spectrally Flat Class A standard, and the CM 21 is regarded as research grade device. For this reason, the CM21 was used to measure the plane of array irradiance I_{POA} as this is the most important value for the performance analysis. The CM11 was used to measure the global horizontal irradiance as this value is used for historic comparison and reference purposes. Both devices were calibrated by an external company to ensure reliability of measurements and an additional verification was performed by comparing the measurements of the devices with those of a reference pyranometer Figure 5.18 provided by the PVMD.

⁵The sensitivity of an irradiance sensors is the rate of change in electric potential with respect to the incident irradiance. Its units are usually $\frac{\mu V}{\frac{W}{m^2}}$.

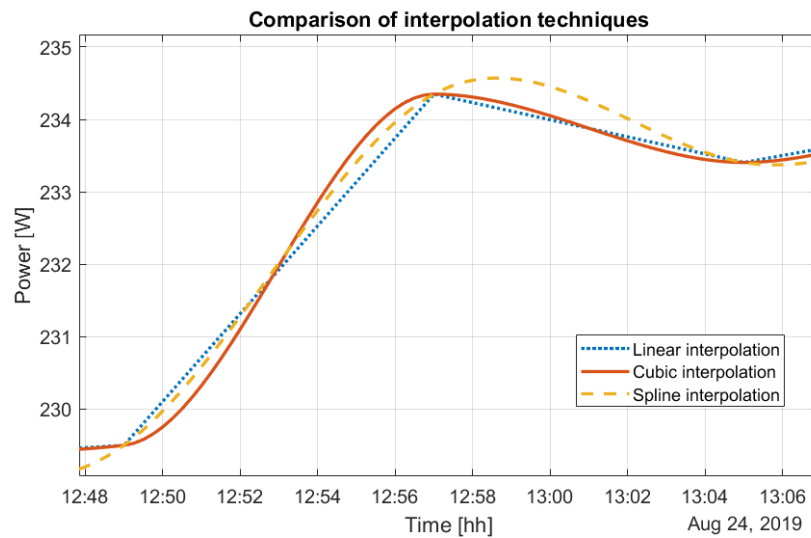


Figure 5.14 Comparison of interpolated techniques. A zoom on a period of 18 minutes shows the differences between the 3 evaluated methods. the linear interpolation presents a basic approximation.



(a) The test was performed in a flat surface at zero tilt



(b) Both measurements were recorded at the same time.

Figure 5.18

Verification of pyranometer measurement reliability. By comparing the instantaneous measurements of both devices for a set period of time, it was verified that the device would perform as expected.

The I_{POA} sensor was placed at the middle of the photovoltaic system as this position would reflect more consistently the average irradiance experienced by the whole system. The mounting can be seen in Figure 5.19. The device was mounted on a metal sheet covered with a black coating to avoid unnecessary reflection, and raised 10 cm above the modules level to ensure the surrounding modules would not disturb the measuring during high angle of incidence periods such as sunrises and sunsets. An additional reason to raise the sensor was to protect it from the heat the system radiates during high irradiance periods.

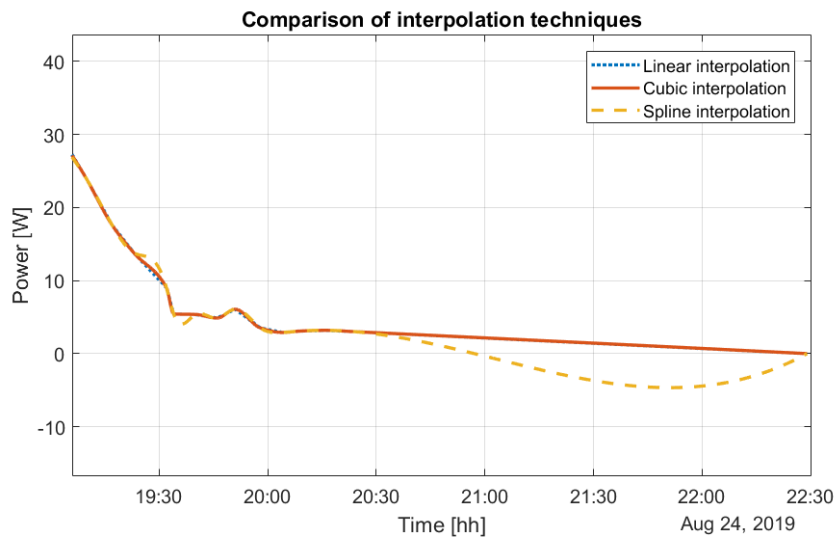


Figure 5.15 Comparison of interpolated techniques. The spline interpolation presents overfitting when the values are close to zero. The interpolation reaches negative values. The chosen technique was the cubic interpolation method.



Figure 5.19 Kip & Zonen CM21 pyranometer mounted in the plane of the array to measure I_{POA} .

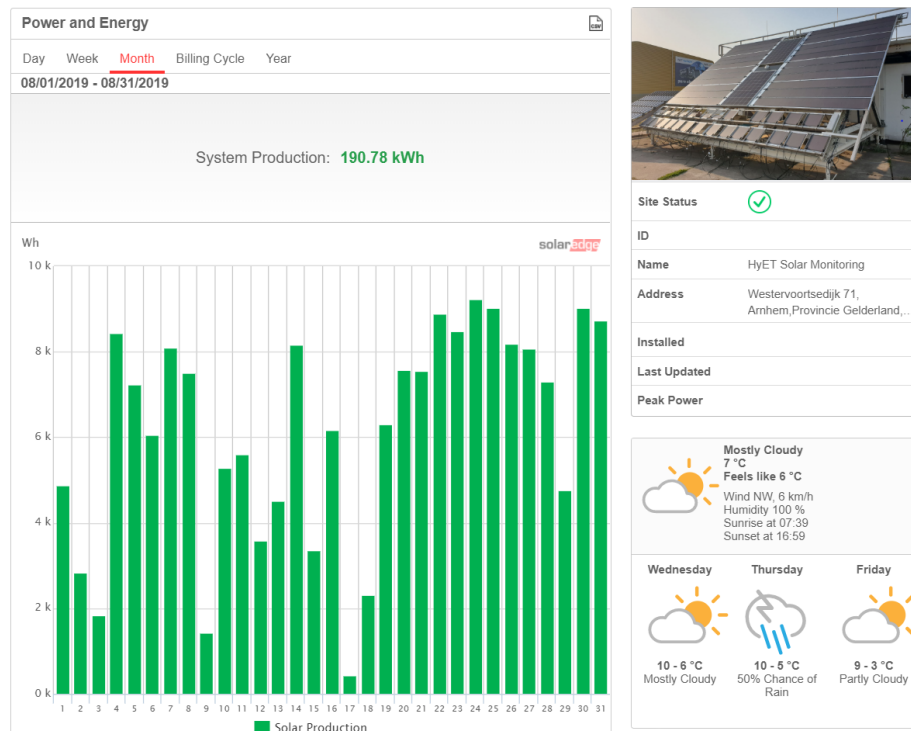


Figure 5.16
Solar edge online monitoring platform.

5.3.3. Crystalline silicone photovoltaic modules

The criteria to select a reference c-Si module was to compare the *HyET Solar* a-Si:H modules to one of the globally most sold modules available. After reviewing the 2019 top manufacturers list, Figure ??, the Trina Honey TSM-PD05 poly-crystalline 270W was selected. This module is sold by the Chinese company Trina Solar, the third largest PV manufacturer globally, and the model is the most basic product in their range. Table 5.5 refers to the relevant electric parameters of these modules for analysis, being of particular attention a rated power of 270 W and a Rated efficiency η_{STC} of 16.5%. The complete parameter description can be found on the data sheet, contained in Appendix D.

Table 5.5
Electrical parameters for Trina Honey 270W poly-crystalline module.

Module parameter	Value
Peak power	270 W
Maximum power point voltage	30.9 V
Maximum power point current	8.73 A
Open-circuit voltage	37.9 V
Short-circuit current	9.22 A
Dimension	1650 × 992 × 35 mm
Weight	18.6 kg
Number of cells	60
Temperature coefficient	- 0.41 $\frac{\%}{K}$
Rated efficiency	16.5 %

5.3.4. Mounting System

The intended mounting procedure of a HyET Solar module is to fix it to a rigid surface by means of an integrated back self adhesive surface, as its intended application is to integrate the module to a rooftop structure, a prefabricated tilted surface or a rigid structure in general. This required the design of a mounting system that would be integrated to the existing rack structure.

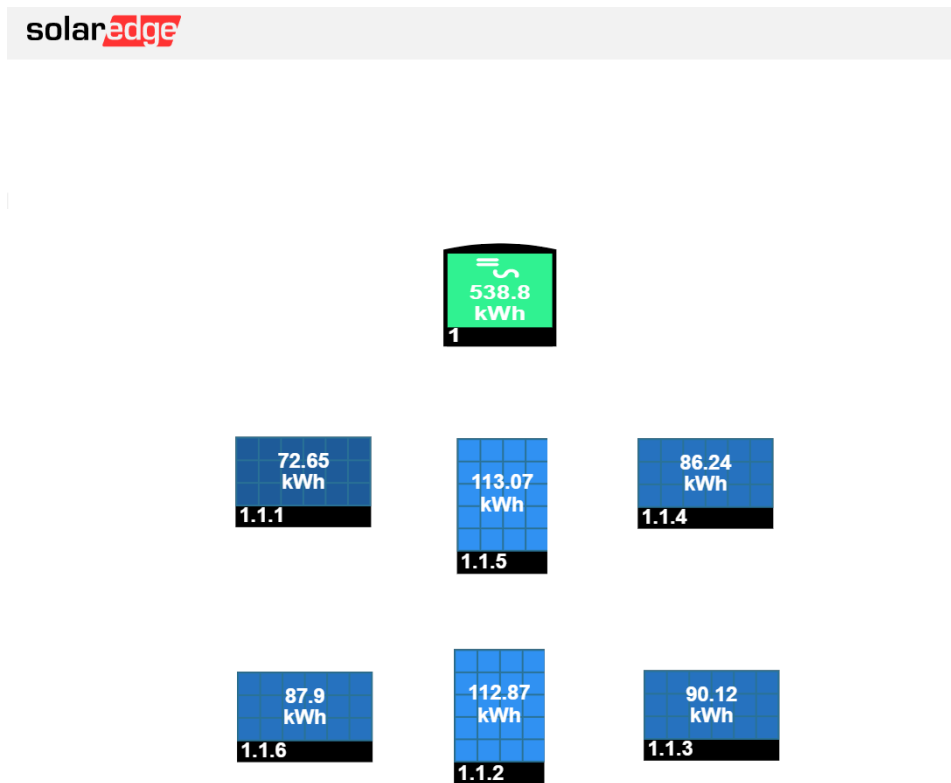


Figure 5.17
Solar edge online monitoring platform.

While wood or a prefabricated rooftop material was originally intended to be used as the mounting system, an in-dept cost analysis of the materials and labour cost showed the cost difference between a wooden structure⁶ and an aluminum one would not be significantly different. Considering this, aiming to make the mounting structure more time and weather resilient, and aiming to improve the passive cooling properties of the mounting by adding a thin material with a high area and a high heat conduction coefficient, the aluminium material was selected.

The mounting plates were designed to hold 3 modules each, making the system comprised of a total of 8 mounting plates holding 24 modules. This disposition would latter allow for an easier mounting procedure. The mounting of the modules into the plates procedure can be seen in Figure 5.20. As the procedure is relatively easy and does not requires specialized training nor equipment, it could be done on-site.

Prior to installation, the plates that would hold the modules to have their temperature monitored were prepared for the placing of the sensor by opening a 5 cm diameter hole on the previously decided location, Figure 5.21. The plates were placed next to the structure and, aided by a cable and a pulley, were then placed starting on the mounting rack from top to bottom. Figure 5.22 shows this process.

⁶The budget comparison for the wooden rooftop was done considering all the materials required to build a wooden structure with a bitumen waterproof layer.



(a) Placing the modules.



(b) Sticking the modules in place.



(c) Fixed modules

Figure 5.20

Fixing the modules to the aluminium mounting plates. The fixing process consist of 2 steps. (a) Placing the modules in the desired location. Tape helped to set the boundaries for a consistent placing. (b) Sticking the modules. Once the modules are in place, the back layer is removed to expose the sticky bituminous layer.(c) The modules are then fixed in the monting plate waiting to be placed in the mounting rack.



(a) Drilling the holes.



(b) Holes on the back of the plate.

Figure 5.21

Last preparations prior to mounting. (a) The sensor holes and connection holes were done on-site to ensure a correct positioning. (b) Holes on the back of the plates ones fixed to the rack.



(a) Plates before installation.



(b) Raising the plates with a pulley.



(c) Fixing top plates.

Figure 5.22

Build up process. (a) The complete plates were placed as close as possible to the mounting rack. (b) A cable and a pulley was used to lift to position the plates. (c) The plates were fixed in place by screws.

5.4. Modules

In order to have a wide sample of modules to analyse and to deliver a photovoltaic system with a peak power large enough to secure a power performance within the inverter efficient range, 24 a-Si:H modules were installed in the photovoltaic performance monitoring platform. The following section describes the used HyET Solar "Powerfoil"⁷ lightweight and flexible thin film a-Si:H modules.

As described briefly on section 5.1, the used modules were those rejected from on-going projects for aesthetically reasons. While these imperfections did not show in the modules parameters, it is still possible the imperfections affect the reliability of the modules, decreasing the lifetime, and thus the performance over the years, of the modules.

The modules were packed in 4 subsystems, each subsystem conformed by a power optimizer and 6 a-Si:H modules. Each subsystem has the capability of monitor the input and output power, input voltage and current. As more rejected modules than required for the project were available, the module log was revised to look for the reason of failing the quality control, choosing the modules that reported only aesthetic defects and whose parameters would be within the expected range for a baseline product.

⁷Powerfoil is the commercial name the company HyET Solar uses for the analyzed thin film a-Si:H modules

Table 5.6
Module dimensions and rated parameters

Parameters	HyET Solar Powerfoil
Length	270 cm
Width	33 cm
Active width	28 cm
Active area	0.756 m ²
Rated power	50 W*
Average rated Efficiency	6-7.5 %

Table 5.7

Modules parameters. Module reference number stated under internal HyET Solar references. Rated efficiency before light soaking as automatically measured and recorded at last production step by **AAA Class** solar simulator. Rated efficiency after light soaking assuming a degradation factor of 15%. Rated power after light soaking assuming a degradation factor of 15%.

Module reference	Subsystem number	Rated efficiency (Before light soaking)	Rated efficiency (Assuming LID of 20%)	Rated power (Assuming LID of 20%)
2802		6.43%	5.59%	42.27
4194		6.65%	5.78%	43.72
7126	1	7.71%	6.70%	50.68
9768		7.42%	6.45%	48.78
2516		6.38%	5.55%	41.94
9002		6.7%	5.83%	44.05
9288			6.89%	5.99%
6590		5.51%	4.79%	36.22
2524	6	6.36%	5.53%	41.81
9858		6.4%	5.57%	42.07
7442		6.2%	5.39%	40.76
7040		7.12%	6.19%	46.81
9472		7.02%	6.10%	46.15
9186		7.38%	6.42%	48.52
9798	4	6.52%	5.67%	42.86
9785		6.83%	5.94%	44.90
8724		6.0%	5.22%	39.44
5308		6.95%	6.04%	45.69
2730		6.8%	5.91%	44.70
9785		6.95%	6.04%	45.69
6176	3	7.19%	6.25%	47.27
5074		6.64%	5.77%	43.65
9196		7.41%	6.44%	48.71
0578		7.0%	6.09%	46.02

5.5. Final System

The final system is comprised of 24 HyET Solar thin film flexible and lightweight a-Si:H modules and 2 c-Si modules. The topology used is power optimizer plus central inverter, for a total of 6 power optimizers. The system is divided in 6 subsystems, each comprised of a module or a group of modules, and a power optimizer. Each power optimizer delivers electrical performance data to the solar edge monitoring platform, therefore the the subsystems can be evaluated separately. A CM 21 kipp and zonnen pyranometer is positioned in the middle of the system to receive the average plane of array irradiance. The physical system can be seen in Figure 5.23. A CM 21 kipp and zonnen pyranometer is positioned on top of the system to measure the global horizontal irradiance.

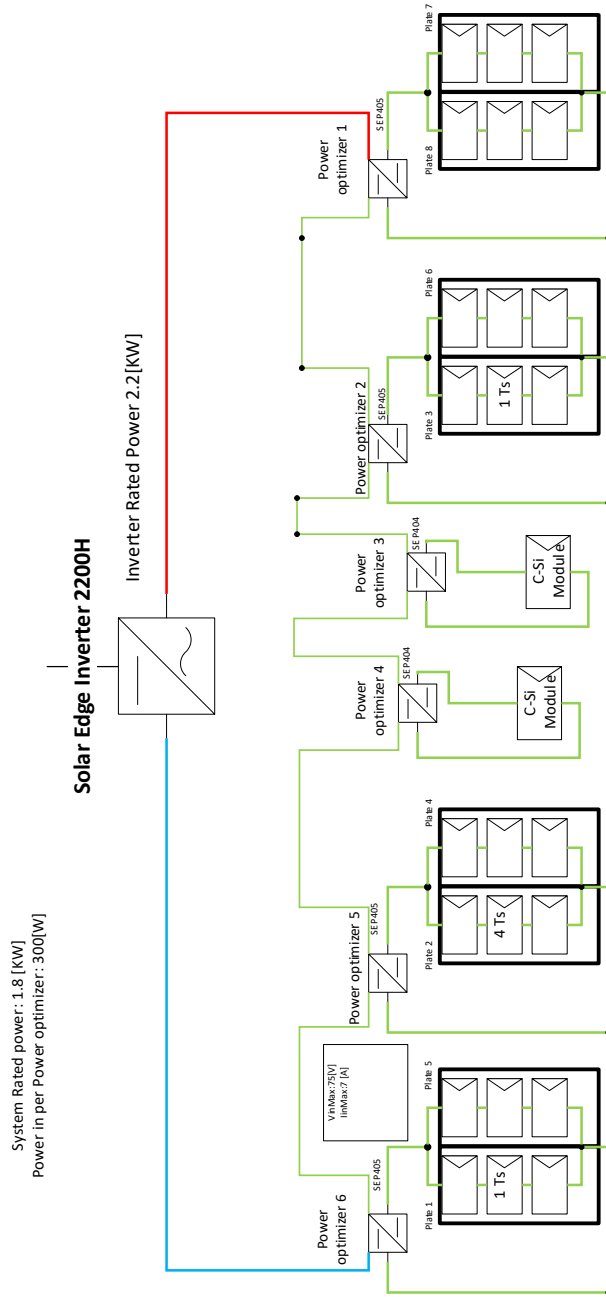
The electrical configuration of the HyET modules is the following: i) The modules are grouped in 2 strings of 3 modules connected in parallel within each other, creating a sub array of 6 modules con-

nected to a power optimizer. This configuration was decided in order to not surpass the maximum input voltage allowed per power optimizer, and deliver a power close to the rated one for the optimizer. ii) Each power optimizer is connected in a string, powering the central inverter. The electrical diagram of the system can be seen on figure 5.24.

A total of 6 temperature measuring point are placed across the system to monitor the array temperature, including the c-Si module. All the irradiance and performance data is logged inside of a protected environment by the TC08 data logger.



Figure 5.23
Completed performance monitoring system.



Emilio Javier Marinique Ambriz

Figure 5.24
System Electrical Diagram

6

Data Analysis

The data obtained by photovoltaic performance monitoring system, whose design is described in chapter 5, was later analyzed, using a mathematical model, the methodology of which is described in Chapter 4. The following chapter discusses the results obtained by the analysis of the performance of the system under real operational conditions from the period from the 6th of August of 2019 until the 16 of October of 2019.

As described in Chapter 1, the primary goal of this work is to investigate the performance of the HyET Solar a-Si:H modules under real operation conditions. This can be divided in 3 sub goals. First, identify the amount of power performance loss the modules are experimenting with respect to the electrical power that would be expected from the modules if the rated efficiency, also referred as STC efficiency, would be constant throughout the operation period, and assuming the associated losses of the power conversion equipment and cabling (Inverter and ohmic losses) to be zero. Second, once the aforementioned difference between the real obtained power P_{REAL} and the idealized STC power P_{STC} , now referred as system losses, is identified, the goal is to quantify the amount of power lost due to the evaluated loss mechanisms or factors, described in Chapter 3. And last, to quantify the impact each loss mechanism is having on the performance ratio of the modules.

Aided by the mathematical model constructed for the HyET Solar modules, this work aims to accomplish the 3 aforementioned sub goals. In order to accomplish the first sub goal, the difference between the P_{STC} and P_{REAL} is identified. As the evaluated data has a range of two and a half months with a sampling rate in the order of seconds, this difference can be contrasted for any time period within this range. This allows to obtain instantaneous system losses, as well as hourly, daily, weekly, monthly and seasonal system losses. By normalizing the output power with respect to the P_{STC} , the performance ratio is calculated, allowing to translate the power losses into of performance ratio losses. As explained in Chapter 2, the performance ratio allows to understand the relative performance response to different environment- and location-specific operation characteristics, as well as making a fair comparison between systems, topologies and PV technologies possible.

To accomplish the second sub goal, the expected power of the modules is modelled after a correction for the influence of the evaluated loss mechanism is made. This outputs a difference in expected power from the STC power P_{STC} to the power corrected for the evaluated loss mechanism $P_{\alpha Corrected}$. The third sub goal is then accomplished by normalizing the corrected predicted power over the P_{STC} , obtaining in this way the value by which the loss mechanism is reducing the performance ratio both instantaneously and over a defined time period.

Some remarks need to be made before reviewing the following analysis. For the evaluation of the modules, a light induced degradation factor of 20% was considered. This value was suggested by internal experimentation made within the HyET Solar company and reflects the expected decrease in power the module experience after being exposed to light soon after being produced. For the evaluation of the HyET Solar a-Si:h subsystem, only 3 out of 4 subsystems (consisting in 6 modules each) are being

evaluated. This decision follows the fact that a subsystem reported a considerably lower performance (in the order of 25% less) compared to the 3 other subsystems from the start of the evaluation period. This factor could be related to the quality of the used modules and, although it would be interesting to analyse the reason of this under-performance, this factor adds additional uncertainty for the evaluation of the project, therefore it was decided to perform the analysis without its influence.

The analysis is divided in 2 main sections, the analysis of the effects of the loss mechanisms is carried out over the period of a day, and the analysis of the variations of the performance ratios over the whole evaluated period. For the first case, the selected day to perform the evaluation was the 24th of August of 2019. This day was selected because it was a cloudless day with a stable measured irradiance, factor which facilitates the evaluation of the share of losses per loss mechanisms as literature suggests the impact of the loss mechanism on the performance changes through the day. Figure 6.1 shows the Plain of Array irradiance Irr_{POA} measured by the performance monitoring station on the mentioned day. The main loss mechanisms are analyzed independently and later together, explaining the share of losses for which each mechanism is responsible on the total system losses. For the latter analysis, the whole period is analyzed and the performance ratios are contrasted between each other.

The mechanisms evaluated by the model on this Chapter will be disused in the following order: Temperature effects, angle of incidence effects, low irradiance effects, power conversion and restive effects through a day, and soiling effects. For the partial shading effects on system losses, the model does not performs an evaluation, but the methodology described in Chapter 4 allows to make a qualitative analysis of its effects. Later on, this Chapter evaluates the whole loss mechanisms effects on the performance of the system over a day. The Chapter concludes with the analysis over the whole period and the comparison with the reference c-Si subsystem.

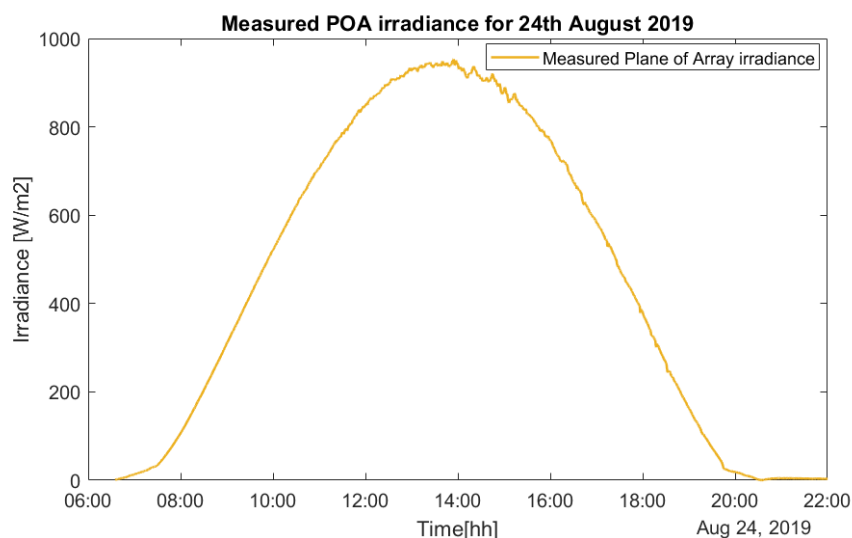


Figure 6.1
Irradiance measured by the monitoring station on the 24th of August 2019. A cloudless sunny day is reflected in a clean irradiance curve.

6.1. Temperature losses

The irradiation characteristics of the 24th of August made it a good day to investigate the effects of higher than standard test conditions temperature on the modules, as the high irradiance and low wind speeds kept the modules at a rather high operation temperature. The reported ambient temperature for this day was 22 °C at 9:00, from where it increased constantly up to 29 °C at 13:00, staying constant until 18:00 where it started to decrease reaching 22 °C again at 18:30 hours. The day was reported to have average windspeeds of 10 km/h from 9:00 to 16:00; after 16:00, the reported average windspeeds dropped to 5 km/h. Figure 6.2 shows how the system average temperature started operations at 12 °C and rapidly reached STC temperature at around 9:00 hours, from where the constant irradiance

increase promoted a steep temperature increase, up to levels of 55 °C to 60 °C during the hours with peak incident irradiance. The module temperature started to decrease slowly from 16:00 until 18:00 hours, one hour after the incident irradiance started decreasing, suggesting that the system followed a thermal capacitive effect during the aforementioned period.

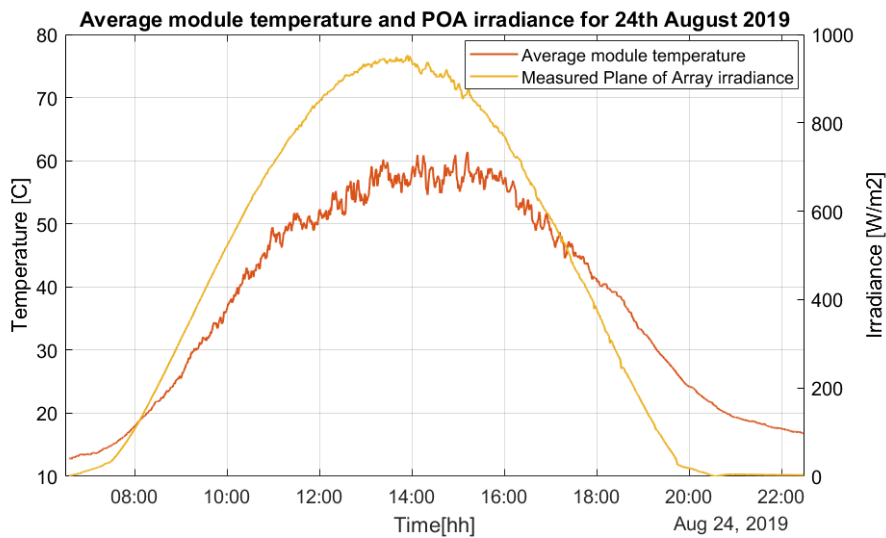


Figure 6.2 Average module temperature measured for the a-Si:H modules. The irradiance is contrasted with the module temperature suggesting a strong correlation between each other.

Analyzing the average system temperature with the model, Figure 6.3 shows a decrease in the efficiency from the rated 5.62% for most of the operation period. It is noted how, during the hours of peak power production on this summer day (from 11:00 to 17:00), the overall temperature corrected efficiency was modelled to be between 5.43% and 5.33%, averaging a decrease of 0.25% absolute decrease in efficiency related to temperature.

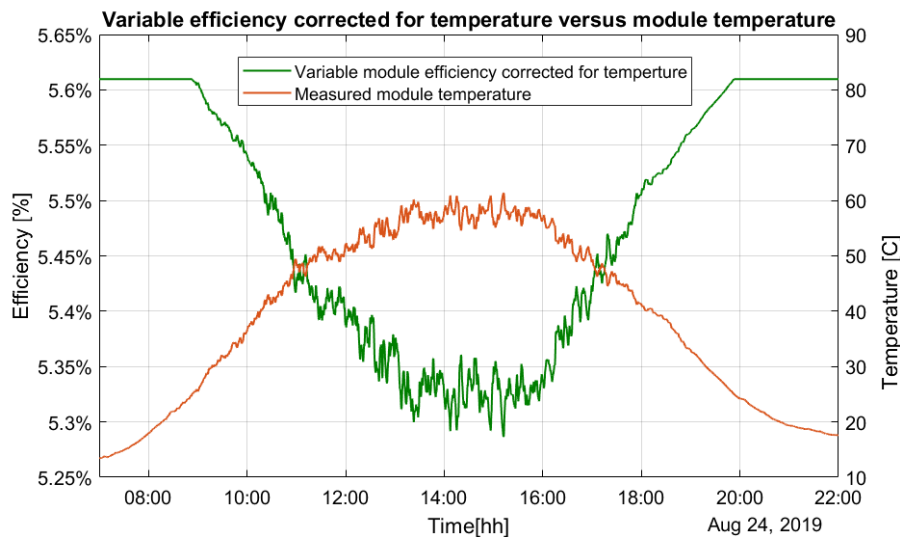


Figure 6.3 Comparison of the live variations of the module efficiency with respect to the module temperature. The variation function responds to 2 heat coefficients, one for lower than 40 °C temperatures, and one for high temperatures.

The effect of temperature on performance can be seen on Figure 6.4 (a) and (b). The figure shows how the losses due to temperature are dismissable until 10:00 and after 18:00 hours. Comparing this effects with the Figure 6.3, it can be seen how a change in the steepness of the variable efficiency curve (in green) also happens at around the same time, when the modules reach 40 °C. This behaviour is

explained by remarking that the model is comprised of two temperature coefficients, having a change between coefficients at 40 °C. The energy lost due to temperature can be seen in Figure 6.4 as the area between the STC power and Expected power corrected for temperature curves. Sub figure (b) makes a close up on the graph where it can be seen how the maximum difference between these curves is present at the peak energy production period, reporting power losses due to temperature of 32.5 Watts. Comparing this value with the measured DC power of 640 W, it can be concluded that temperature losses account for up to 42% of the system losses before power conversion. This can be better noticed on Figure 6.5, where the normalized temperature losses are presented. Here, it is easier to notice how the impact of increased module temperature is variable through the day, accounting for a larger share of losses during the most energy productive times. The graph shows how the heat accounts for up to a 6 % decrease of the performance ratio from 13:00 to 16:00 hours. This loss mechanism by itself explains almost half of the system losses present during high irradiance periods, but none of the observed system losses on low production periods such as sunrise and sunset.

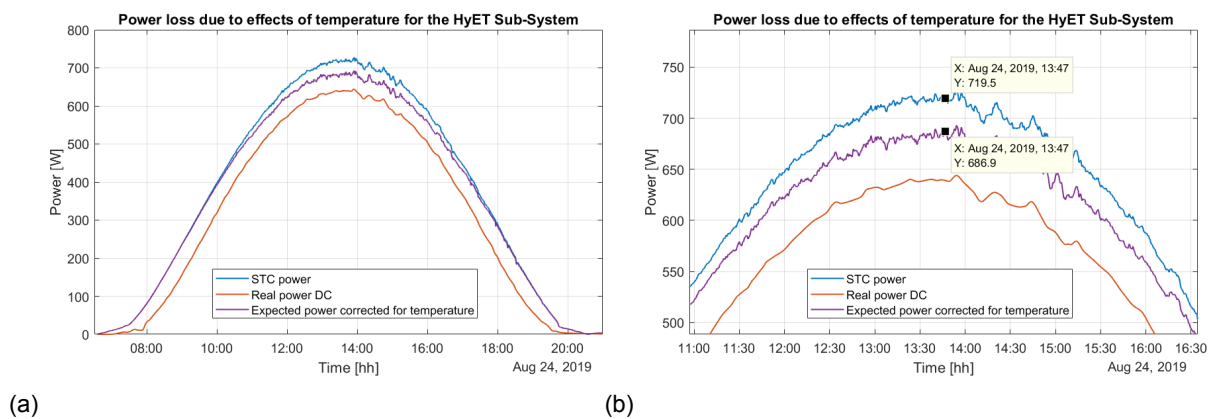


Figure 6.4 Effects of temperature on the output power for the a-Si:H modules. It can be noted how a high share of losses are related to temperature effects during peak energy production periods.

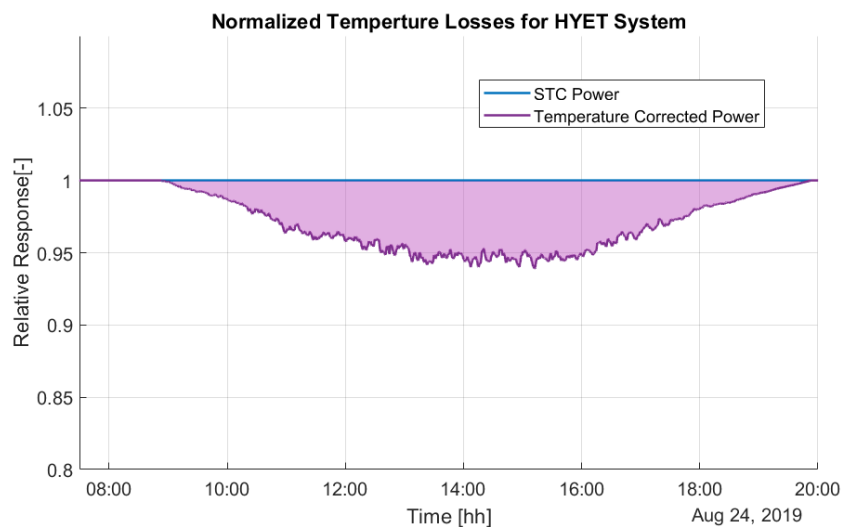


Figure 6.5 Normalized effect of the temperature on a-Si:H modules. The impact is notably higher closer to 13:00 hours.

6.2. Angle of incidence losses

To analyze the system level losses associated to the angle of incidence, the model relates this angle with the measured module angle dependant reflectance. In Figure 4.23, the described behaviour is presented for this day. The angle of incidence graph in turquoise shows how the AOI before 8:00 is

higher than 90°, being this moment the sunrise experienced by the system. Both at the sunrise and sunset, the direct sunlight reflected by the modules is maximum as the modules are not optimized to receive light at such high angles, nevertheless the high texturing in the modules surface make the losses be minimum at a close to 60°AOI. For the evaluated day, the minimum AOI never reached 0° and happened close to 14:00 hours.

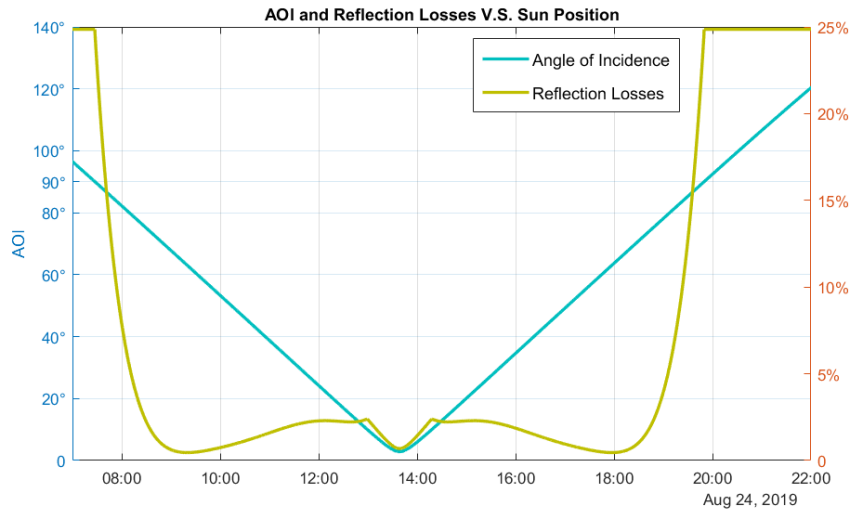


Figure 6.6 Comparison of the variation of the angle of incidence through the day, and the increase in the experienced reflection.

The analysis shows how the power losses related to the AOI are present in 2 main periods: during sunrise and sunsets, and close to peak power production time. Figure 6.7 (a) shows the energy yield lost due to AOI reflection is higher during high production periods than during sunrise and sunset periods, although it's relative impact is higher during the sunrise and sunset periods (close to 25% of the losses). This is simply due to the high power production difference, even a small percentage of losses are accounted to AOI, this percentage is affecting the highest production period, whereas the high percentage of losses associated to AOI at sunset and sunrise are happening during the lowest production periods. By analyzing Figure 6.7 (b), the addition of the AOI correction to the temperature power correction reduces the gap between explained losses and unexplained losses during high production periods, but, still lacks to relate a loss mechanism, to the losses on medium and low production periods. (06:00 to 11:00 hours and 17:00 to 22:00 hours). This can be better visualised on Figure 6.8 by seeing how the area between the temperature correction and the measured DC power, the energy yield, is still not fully covering the full amount of losses on this time periods.

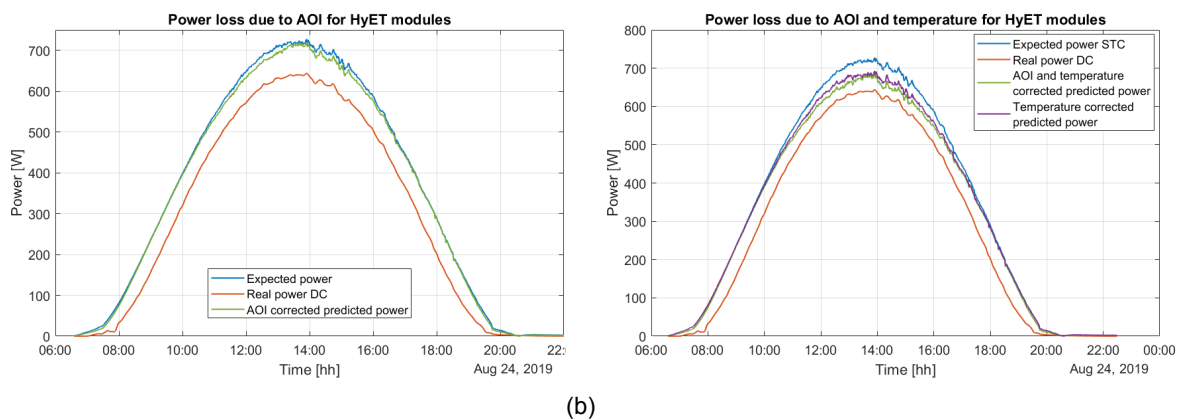


Figure 6.7 Effects of angle of incidence on the output power for the a-Si:H modules. Subfigure (a) shows the corrected power for AOI influence, where as figure (b) shows the sum of the effects of AOI and temperature effects.

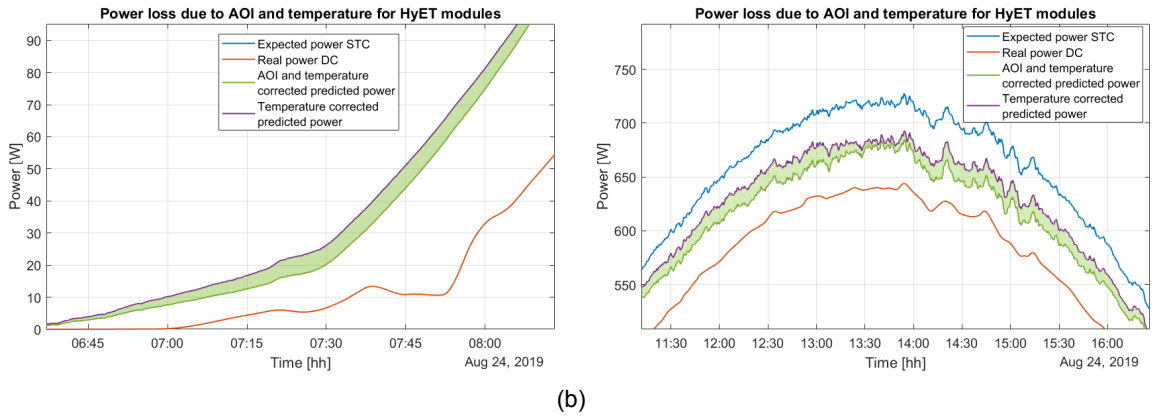


Figure 6.8

Effects of temperature on the output power for the a-Si:H modules. A close up shows the energy lost due to angle of incidence induced reflection.

6.3. Low irradiance losses

The model evaluated the performance of the modules at a lower than STC irradiance ($1,000 \frac{W}{m^2}$) by decreasing the relative efficiency with respect to the incident irradiance level. The predicted power after the correction for low irradiance is performed can be seen in Figure 6.9. It is easily noted how the low irradiance corrected predicted power diverges from the STC predicted power during sunrise and sunset. This indicates that the low irradiance is the main loss mechanism accounting for losses in periods where the modules are exposed to low and mild levels of irradiance and therefore, as expected, the power losses associated to low irradiance are minimum close to the high production periods.

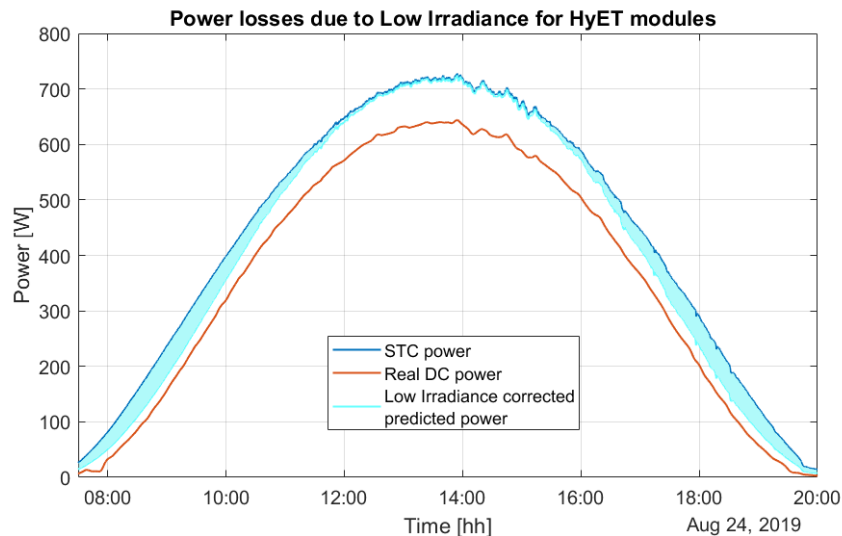


Figure 6.9

Effects of low irradiance conditions on the output power for the a-Si:H modules. The figure shows how this loss mechanism is highly present during sunsets and sunrises. The area in turquoise notes the energy lost due to low irradiance.

Figure 6.10 helps better visualize the impact of low irradiance on the system level losses. It can be seen how an exponential increase in the losses is seen closer to sunrise and sunset, when this mechanism alone accounts for almost 50% of the performance ratio losses. The energy yield losses can be seen in Figure 6.9, represented by the area filled with a translucent turquoise color. While only being present during the low and mild power production periods, the lost energy yield appears to be dominated by this factor for the aforementioned periods.

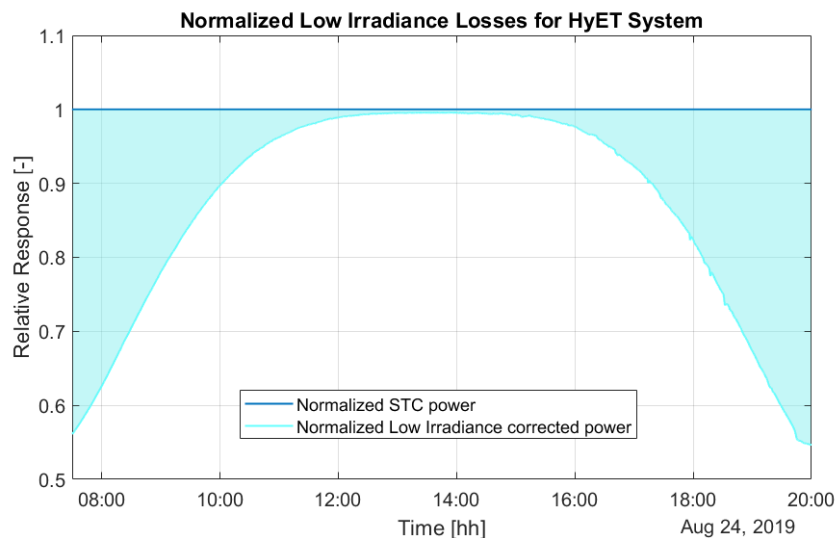


Figure 6.10
Normalized effect of low irradiance on low performance. The figure illustrates how the performance ratio exponentially decreases during sunsets and sunrises.

6.4. Power conversion and ohmic losses

By analyzing the difference between the measured DC and AC power produced by the system, a time dependent loss function was obtained. It appears that a large share of the energy yield lost due to both factors happened at peak production, Figure 6.11. Nevertheless, is the moment of the day where the share of associated losses are minimum, Figure 6.12. Contrarily, while the energy yield loss at sunrise and sunset associated to inverter losses is minimal, the normalized analysis shows how this period is exponentially ruled by the power lost due to an efficiency reduction at the inverter by operating at such a low power level. This behaviour is described by the inverter power curve, shown in Appendix B.

Analyzing the Figure 6.12, it can be seen how the measured AC power drops to zero before the DC power does. This can be explained by the fact that the inverter is receiving such a low power that it shuts down. The observed value for shutting down is 25 W or less. This represents 1.15% of the inverter rated power. An additional analysis shows how the inverter efficiency quickly drops from 70% to 0% once the input DC power is less than 90%. Overall, the system shows how the performance on a sunny day keeps the inverter plus ohmic losses on a constant level of less than 4% for most of the day.

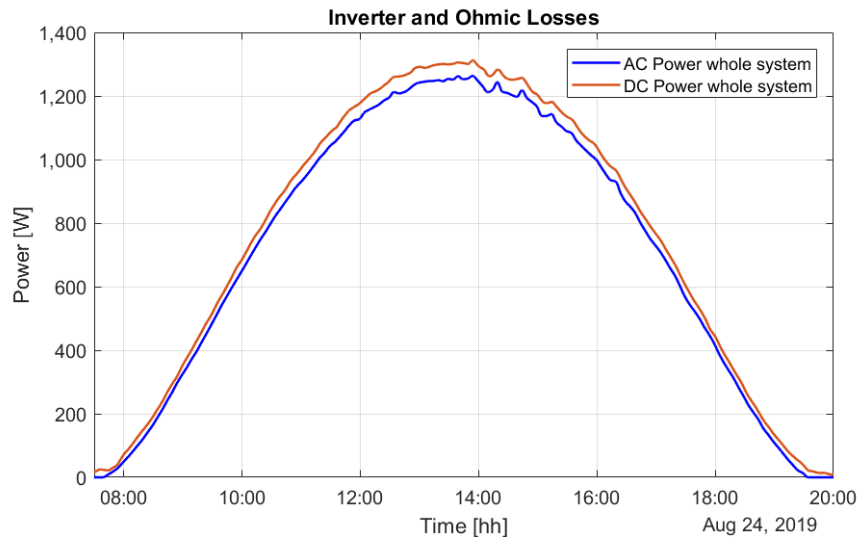


Figure 6.11
Effects of Power conversion and resistance on the output power for the a-Si:H modules.

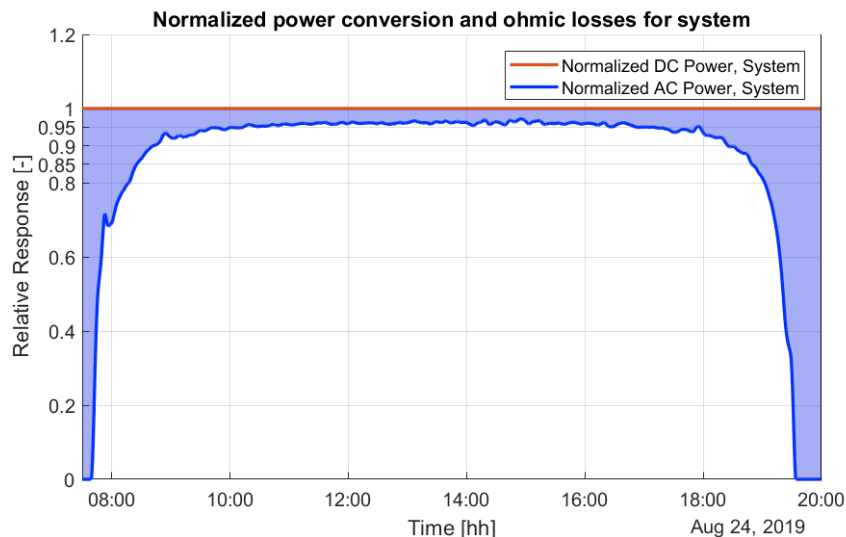


Figure 6.12
Normalized effects of power conversion and cabling on the module performance. The figure shows a stable performance for most of the operational period, with a high decrease of performance as the system output power decreases.

6.5. Intra-day Analysis

By analyzing the combined effect of the loss mechanisms on the modules on a day, the origin of the system level losses can be determined and an estimate of their impact on performance can be obtained. By adding the effects of each mechanism, one after each other, the source of most system level losses is determined, Figure 6.13. This can be viewed as the area between the STC power (blue curve), and the power corrected for all effects including soiling (magenta curve). The figure allows to visualize how the dominant loss mechanisms at midday (high production period) is the temperature effect, while the dominant loss mechanism during sunrise and sunset is the low irradiance performance. Overall, for the evaluated day these 2 mechanisms are responsible for 42.8% of the performance losses (Accounted both as performance ratio and yield losses). Power conversion and ohmic losses account for 22.82% of the performance losses leaving AOI and soiling a combined percentage impact on performance of 13.77%. This leaves a remaining 20.6% of unexplained losses, perhaps as a result of additional degradation to the initial 20% Light Induced Degradation (LID) factor considered for the analysis. As Figure 6.12 showed the impact of the power conversion was fairly stable for most of the power production pe-

riod, the joint analysis of the power conversion losses are done later in Figure 6.17. The performance ratio reported for the 24th of August for the HyET System was 0.8306 without considering power conversion effects, and 0.7805 after including them. The performance ratio reported for the reference c-Si system was 0.9176 without considering power conversion effects, and 0.8675 after including them.

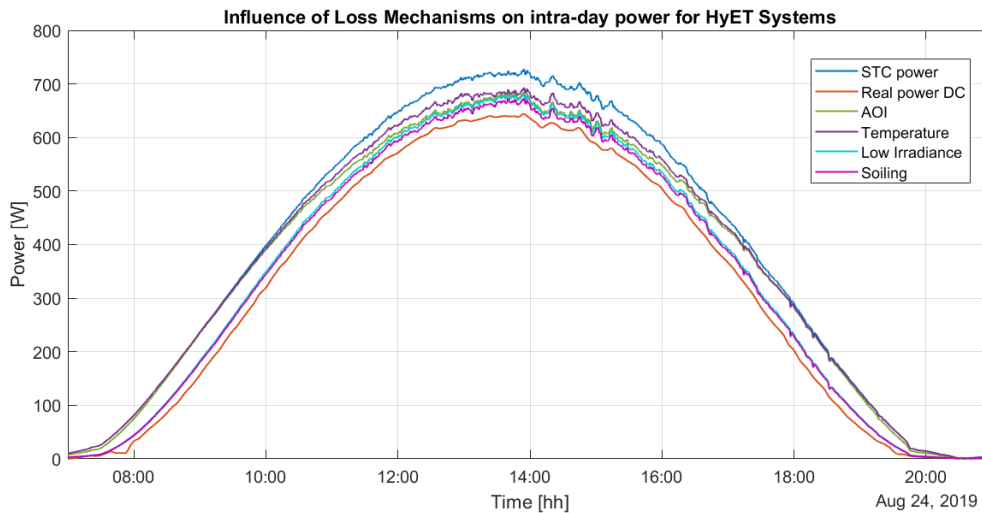


Figure 6.13 Influence of evaluated loss mechanisms on the a-Si:H modules. The evaluation was performed for the 24th of August of 2019. The figure shows how most of the losses were identified. It is notable how the temperature losses complement with the low irradiance losses, resulting on a stable power decrease for the whole period. The remaining losses are assumed to be due to degradation effects.

Figures 6.14 and 6.15 show a close up of the influence each loss mechanism has on the energy yield. It can be noted on Figure 6.14 (a) how all loss factors contribute to a decreased yield at peak production periods, being this period clearly dominated by the temperate losses. Figures 6.14 (b) and 6.15 (b) shows a clear dominance of the effects of low irradiance at low production periods, being followed only by AOI effects during sunrise, and interestingly not as much during sunset. Figure 6.15 (a) shows the transition period between a dominance in the influence of low irradiance, with a growing influence of AOI reflection and temperature effects. The inflection point occurs at 11:00 when temperature effects equal low irradiance effects, and slightly later AOI effects equal low irradiance effects.

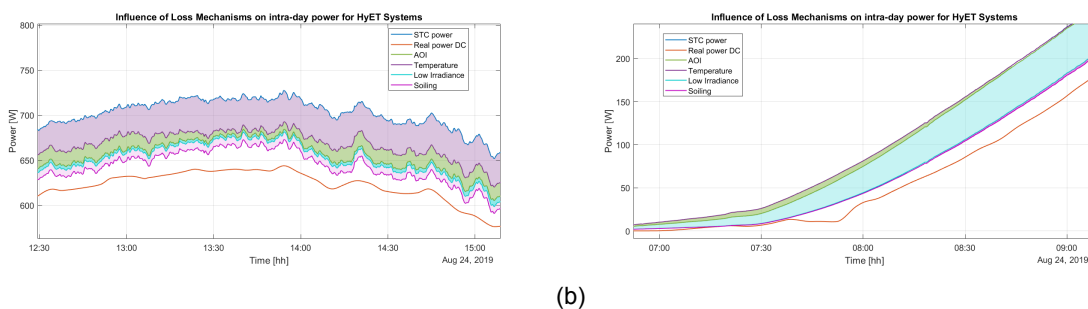


Figure 6.14 Influence of the evaluated loss mechanisms on the a-Si:H module. A close up on the early morning and midday period shows how the dominant loss effect changes throughout the day, being initially low irradiance and later temperature effects.

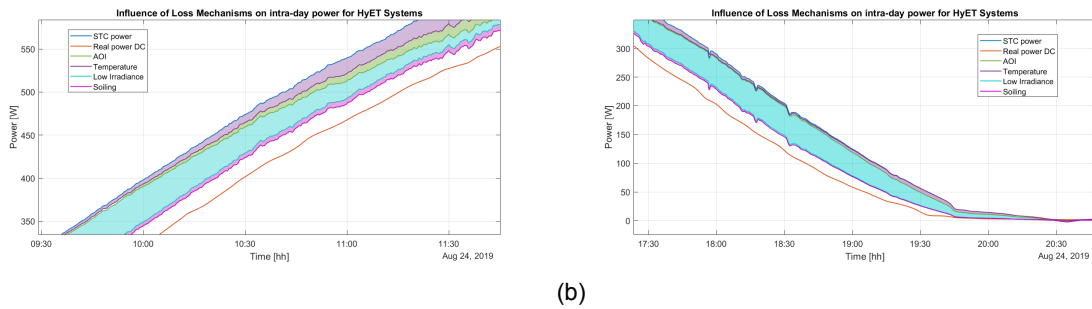


Figure 6.15

Influence of the evaluated loss mechanisms on the a-Si:H module. (a) shows a close up of the transition period from morning to midday. The transition between the dominant loss mechanism can be appreciated. (b) shows a complete dominance of low irradiance at sunset, with AOI influence in a far second place.

On Figure 6.16, the area between the power corrected for all evaluated loss mechanisms, including soiling effect (Magenta curve), and the real power DC is highlighted. This area accounts for the yield loss that is not yet explained by the model. As explained on Chapter 4, these losses are assumed to be related to the effects of degradation, particularly light induced degradation. The degradation effect seems rather constant through the operation period, having a slightly larger impact during peak power production.

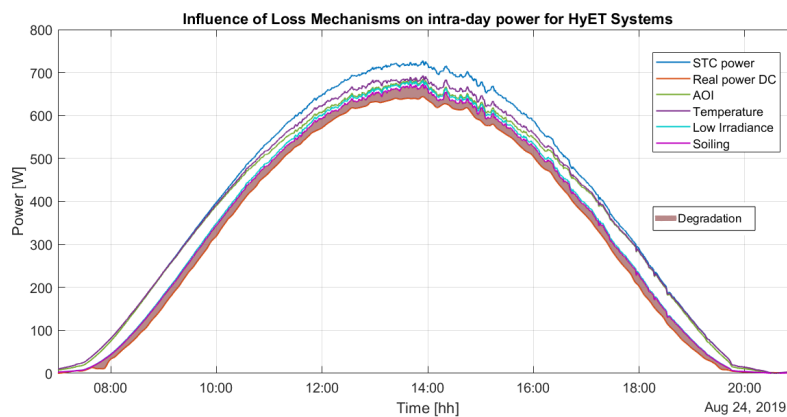


Figure 6.16

Assumed degradation of the modules. The red area represents the losses not explained by the previously assessed loss mechanisms. This work infers this losses to be related to degradation of the modules.

The normalized plot of the influence of each loss mechanisms on performance can also be seen as the remaining performance ratio the system has, after the effects of the evaluated loss mechanisms are taken into account, Figure 6.17. This shows the instantaneous performance ratio of the system, and the time dependent effects of the loss mechanisms on it. It must be noted that integrating this time dependant performance ratio over time will not return the performance ratio for the evaluated period (in this case a day), as the influence in yield is not taken into account on the normalized function. Nevertheless, the normalized plot helps better understand how each loss mechanism is influencing the power decrease at a different rate based on the time. This time dependant effects can be better seen if we take a zoom into the plot. Figure 6.18 (a) shows a close up of the period from 12:00 to 15:00. A quick evaluation on the mechanism corrected performance ratio shows how at 13:30 the influence on performance from the joint effects of temperature, AOI and low irradiance, is decreasing the performance ratio up to a value of 0.938. Comparing this to the reported performance ratio before power conversion is taken into account, illustrated as the normalized real power DC curve, the value of 0.8875 shows a performance ratio decrease of 0.03608 related to degradation, after the correction for soiling of 1.442% is accounted for. The performance ratio lost due to power conversion at the same period is reported to be of 0.0319, similar to the degradation effects.

However, evaluating the effects at a different time period, 18:00 hours when the reported irradiance rounds $400 \frac{W}{m^2}$, the share of the effects changes drastically, relating performance ratio losses of 0.1761 just for the effects of low irradiance, performance ratio losses of 0.08828 due to degradation, and performance ratio losses of 0.0452 due to power conversion.

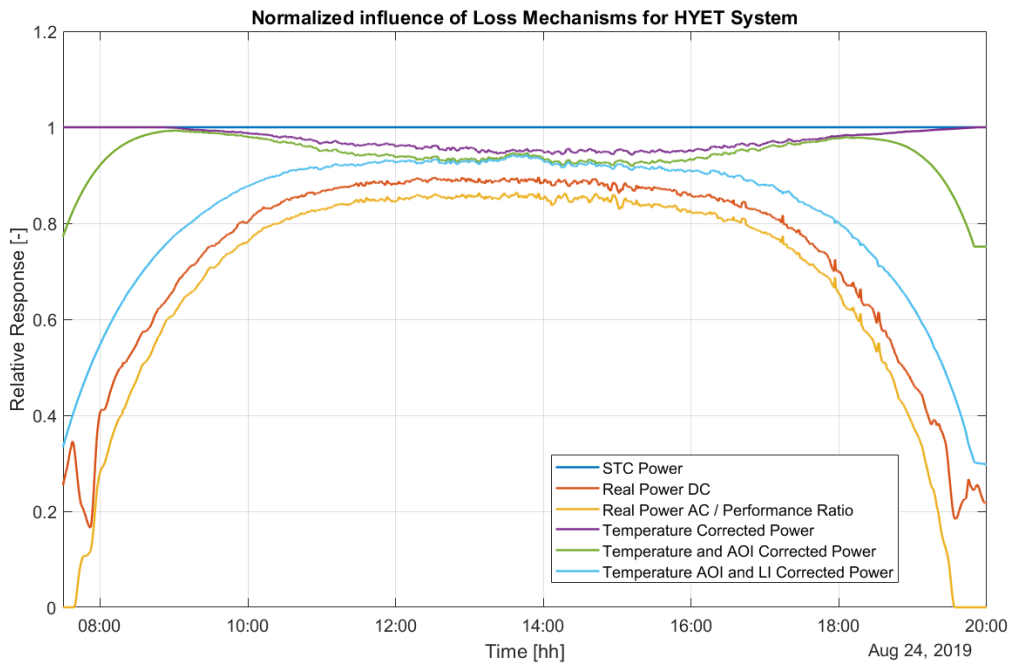
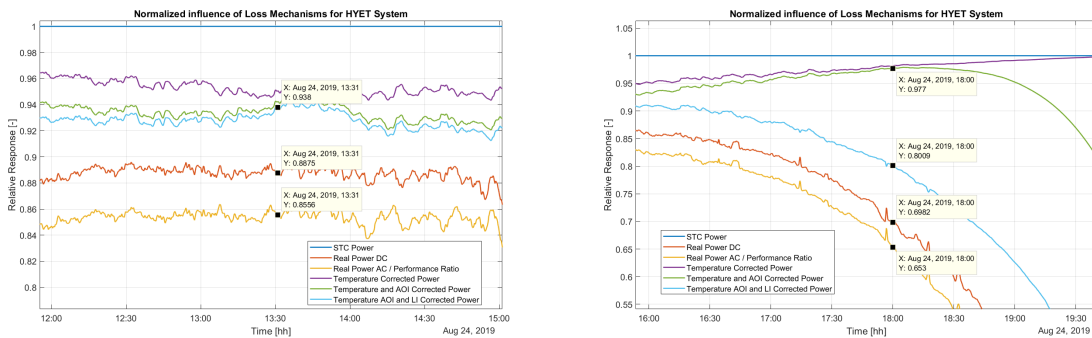


Figure 6.17 Normalized influence of the loss mechanisms on the a-Si:H modules. 2 patterns can be appreciated. The Temperature, AOI and low irradiance influence varies drastically through the day, where ass degradation and power conversion losses are stable for the most part.



(a) (b)

Figure 6.18 A zoom in the normalized influence of the loss factors on a-Si:H modules.

Nevertheless, the high production period is one of the most relevant to analyze as most of the energy is generated during it. For this, Figure 6.19 illustrates the behaviour of the modules in a clear way as it shows the mentioned production period having a fairly constant behaviour. Again, the temperature has a dominant effect followed by the power conversion and ohmic influence. It is interesting to see how reflection losses due to AOI have also a significant effect during this period.

To finalize the intra-day analysis, Figure 6.20 shows the share each loss mechanism is accounted for in the total performance losses. Recalling the definition of the performance ratio, the showed per-

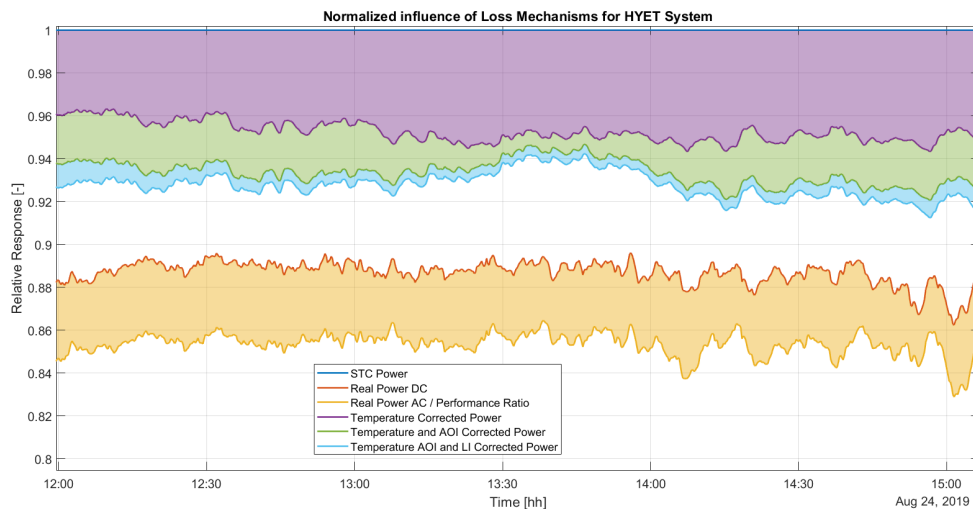


Figure 6.19

A zoom in the normalized influence of the loss factors on a-Si:H modules. The selected period is the high production one, from 12:00 to 15:00 hours. The highlighted areas give an indicative of the share of influence of each mechanism. Degradation is represented without any highlighted area.

centages can be understood as both energy yield losses and performance ratio losses. It is interesting to note how the low irradiance performance has the higher influence on losses with a 27%. After degradation, power conversion and ohmic losses comes third with a 19%, and temperature effects comes in a notorious 4Th place, being this the expected dominant mechanism for a summer day. The angle of incidence has a minor impact, accounting for 9% of the total losses, and the expected losses related to soiling in the Netherlands come last with a 5% share. The value of reduced PR per loss mechanism can be noted on Figure 6.21.

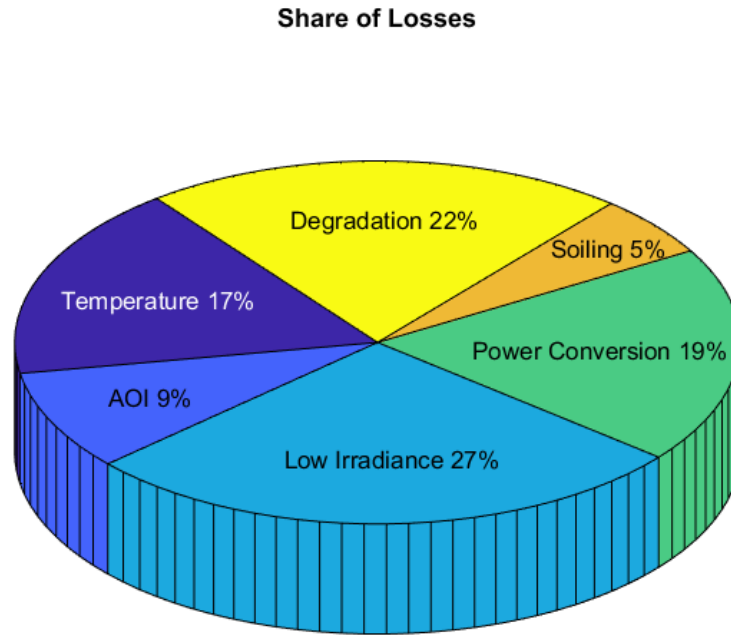


Figure 6.20 Share of energy losses on an a-Si:H. Notably, the low irradiance losses are the dominant factor for the modules. Temperature effects are far back with a 17%.

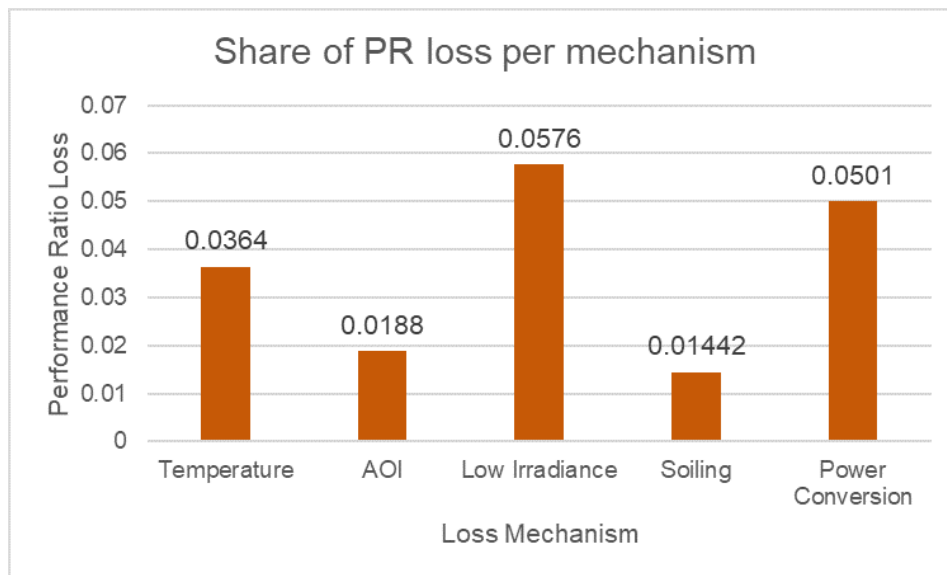


Figure 6.21 Share of performance ratio decreased per loss factor.

6.6. Full Period Analysis

The evaluation of the a-Si:H modules performance over the full period was performed by obtaining the performance ratio delivered daily by the system, and comparing it among the full period. Figure 6.22

shows the performance ratios variation over the whole evaluated period. It should be noted that the overall performance ratio reported from the 4th of August until the 16th of October is of 0.7885. On the other hand, the reported performance ratio for the c-Si modules for the same period is 0.9217. Analyzing the daily performance ratios, a trend can be identified of higher values obtained during the sunnier month of August 2019, while still having 4 days of August with low performance ratios. The trend during September and October shows a decrease on the average maximum values from 0.85 to 0.8 levels during September, and 0.75 levels reaching October. The number of low performing days also increases as the day moves further from summer. It should be noted that a setback caused the loss of data for 5 days at the end of August and beginning of September. This points are seen as the days with a performance ratio of zero, and are taken out of the evaluated average.

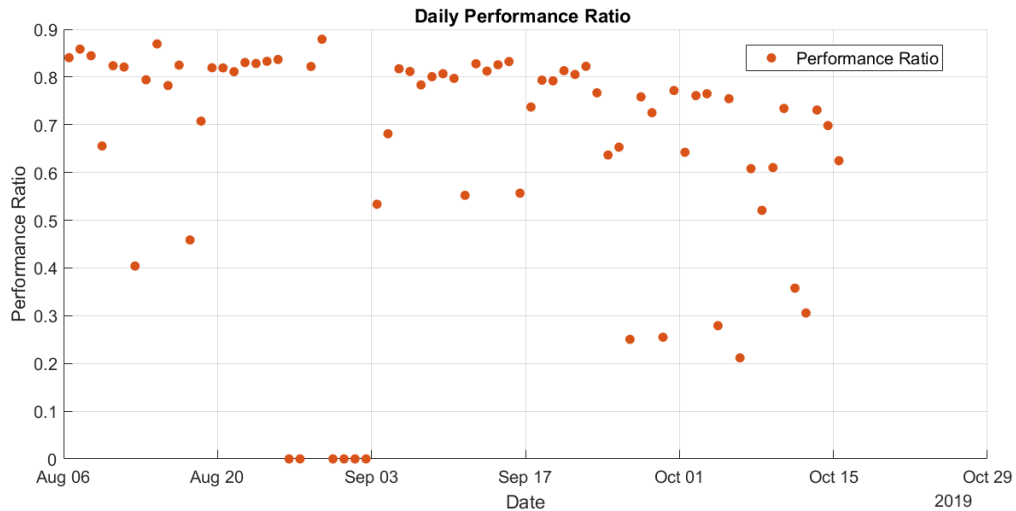


Figure 6.22

Daily performance ratios for the period of the 4th of August 2019 until the 16 of October 2019. The 5 points with a reported performance ratio of zero are a consequence of a malfunction on the data logger for a period of 5 days. Higher performance ratios can be seen during August, compared to September and October.

By comparing the reported daily performance ratios to the irradiation measured the same day, Figure 6.23 shows a clear trend where most of the days with measured irradiation higher than $4,000 \frac{Wh}{m^2 day}$ have the highest reported performance ratios surpassing the 0.8 mark. On the other hand, a low measured irradiance shows an exponentially decreasing performance ratio on the modules.

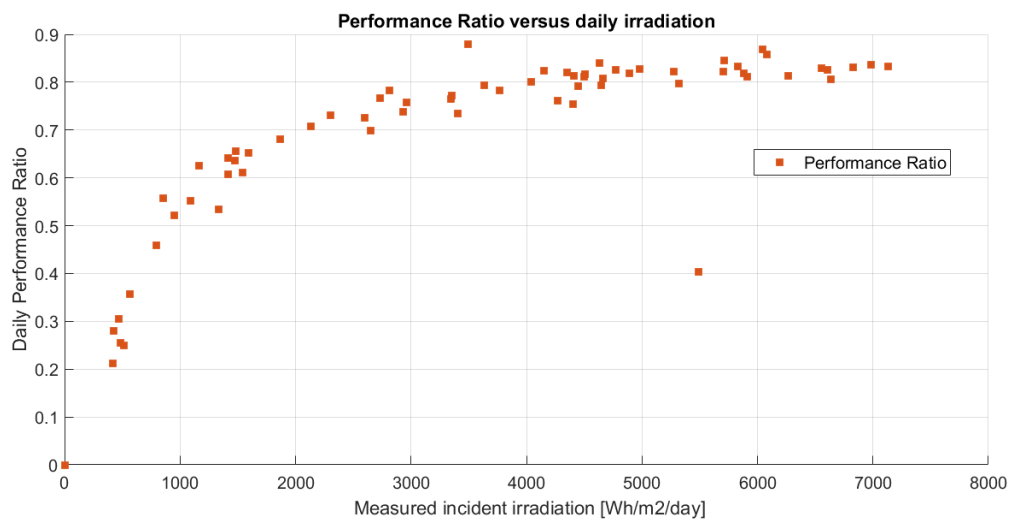


Figure 6.23

Performance ratio versus daily irradiation. A clear trend can be appreciated of the dependence of the performance ratio to the incident irradiation. Days that reported high irradiation also reported high performance ratios.

Conclusion

This work presented a methodology to evaluate the performance of an a-Si:H based photovoltaic system. The main factors decreasing the performance of a system built with the evaluated photovoltaic devices were identified and referred as loss mechanisms. Experiments were performed on the characterisation of the evaluated modules, from which their response to the identified loss mechanisms was obtained. This characterisation data was used to build a mathematical model that describes the operation of a photovoltaic system built with a-Si:H technology. A preliminary research was performed to understand the capabilities that a performance monitoring station would require in order to evaluate the performance and the impact of the loss mechanisms on a photovoltaic system. A photovoltaic system integrated in a monitoring station, comprised of 24 a-Si:H modules and 2 c-Si modules was built with the purpose of obtaining real performance and environmental data of the performance of a system under real operation conditions. This measured electrical and environmental data was used together with the built model to make an assessment on instantaneous, daily and monthly performance. Then, through this data assessment, the 4 proposed research questions were intended to be solved. The conclusions obtained by the data analysis are here presented.

Which factors affect the system level performance of a photovoltaic system comprised of HyET Solar a-Si:H flexible and lightweight modules? To answer the first research question, the literature review showed how up to eleven factors shape the real performance of a photovoltaic system, each having a different influence on the total share of system losses. These factors, called by this work as loss mechanisms were:

- Effect of the module temperature on a decreased energy conversion efficiency.
- Effect of the angle of incidence of the sunlight on increased reflection, therefore higher optical losses.
- Effect of a lower than AM 1.5 standard test conditions efficiency on a decreased energy conversion efficiency.
- Effect of the resistance to the electrical current flow on the output power delivered by the photovoltaic system.
- Effect of the power conversion loss, inherent to inverter and power conditioning devices, on the output power delivered by the photovoltaic system.
- Effect of the accumulation of dirt particles attached on the module surface, on a decreased energy conversion efficiency.
- Effect of partial shading on a photovoltaic array on the overestimation of incident sunlight for a photovoltaic system.
- Effect of partial shading on a photovoltaic module on reducing the array energy yield by limiting the current.
- Effect of a mismatch between the rated AM 1.5 spectral power distribution, and a different spectral power distribution resultant of a higher air mass.
- Effect of light induced degradation on the photo-active layers, on material recombination associated with the creation of higher trap states particles promoting higher internal losses and a decreased energy conversion efficiency on the modules.

- Effect of a potential induced degradation promoted by large potential differences between the module surface and the electric ground of the array, inducing a material recomposition on the photo-active layers associated with the creation of higher trap states particles promoting higher internal losses and a decreased energy conversion efficiency on the modules¹

What is the quantitative influence of these factors on the decreased performance experience by an a-Si:H based system, located in Arnhem, the Netherlands? By reviewing the data delivered by the constructed model, this research question was answered for the system built for the project. The daily analysis showed how the energy lost by the system that day, represented by its performance ratio, was of 0.7805. This means that a 21.95% of the energy the system was able to deliver under the sun conditions presented over the day, was lost. It is very interesting to note also the performance ratio of the system without taking into account the performance lost on the power conversion and cables, particularly from a photovoltaic technology research point of view because this power transmission and conversion factor is unavoidable for the current state of the art technology. This claim is supported by the reported performance ratio loss of 5.01% accounted for this 2 factors. Literature suggest a normal performance decrease for cabling to be not lower than 1%, and up to 3%, while the yield lost expected for an inverter is of 2 to 4 %, making the 5.01% value fall within expected parameters. Considering this, the reported performance ratio of 0.8306 indicates that a 16.94% of the possible energy yield is lost due to the environment, operation, and technology related conditions.

A remarkable finding by this work was the identification of the hierarchy of the loss mechanisms for the a-Si:H system. Literature suggested the temperature effect to be the dominant loss mechanism for most photovoltaic systems, while also pointed a better expected performance under heat conditions from a-Si:H technologies compared to c-Si, factor that was validated with the characterization experiments performed by this work on HyET Solar modules. Nevertheless, the analysis showed temperature effects are far from being the dominant effect for HyET Solar a-Si:H modules. Instead, the dominant factor probed to be the effect of low irradiance on the modules.

Going deeper on this results, this strong dominance of low irradiance levels on the performance of the modules could be partially related to a reported high level of "shunts" on the evaluated modules. The shunts relate to the internal parallel resistance in the modules that serve as a gateway for the current flow, keeping the internal current losses low. The HyET Solar modules evaluated reported a low shunt resistance value, making the current losses higher in proportion when the overall power production rate was lower, which relates to the same period as a low irradiance input.

The second loss mechanism reported in importance was the degradation losses. While this mechanism reported a 22% share of the total losses, it is also true that the not evaluated spectral mismatch losses are also influencing this proportion. Regardless, the degradation losses are reported to be significant for the energy production, factor that should be addressed by the manufacturer if the energy yield is to be increased.

Concluding on the angle of incidence losses, it was interesting to note how the reflection versus angle of incident behaviour of the modules followed a trend on which the reported reflection at 60 ° was lower than at a lower angles. This could be explained by the surface texturing performed on the HyET Solar modules for light trapping purposes, which seems to be having a positive effect on the losses at medium angles of incidence. This is a positive effect because the modules will operate at these angles for a larger period of time then at lower angles of incidence, which are present mostly during midday. This statement is supported by the low reported yield loss related to reflection losses.

What would be the performance ratio of an a-Si:H based system, located in Arnhem, the Netherlands? The work satisfactorily answers this research question by giving the average performance ratio for the HyET Solar System for the evaluated period, being 0.7885. The analysis showed a clear positive relationship between high irradiation levels and a higher observed daily performance ratios.

¹This factor was purposely not further investigated by this work as internal documentation in HyET Solar suggested a minimal impact of this effect on the evaluated modules derived to the use of a non-silicon material as a top encapsulant.

The work tried to visualize if a degradation could be observed by the daily performance ratio decrease, but conclusive results could not be obtained on this as the soft decrease observed on the performance ratio values could be easily explained by lower irradiance observed as the days went further from summer time. It is most likely that the variation observed in the performance ratio are related to environmental variation effects rather than to a continuous light induced decrease. Nevertheless, by using the performance monitoring station built for the purpose of accomplishing this work, data points can be obtained in the future on which days with similar environmental conditions can be compared between 2 different periods, and a good assessment of degradation with time can be obtained.

How would the performance ratio of an a-Si:H based system, located in Arnhem, the Netherlands compare to the performance ratio on an c-Si based system, located in Arnhem, the Netherlands?

By comparing both technologies, it is conclusive that the c-Si technology delivers a higher performance ratio than the a-Si:H. The gap between the two technologies could have been drastically decreased if the modules used for the studies would have been from a higher tier, since modules rejected for commercialisation introduced additional variables to the study. Nevertheless, the factors associated to the decrease the performance ratio are now identified and further development on this area can bring down the impact of these factors on the losses, therefore improving the performance ratio for HyET Solar a-Si:H modules.

Final conclusions After answering the proposed research questions, this work delivered additional conclusions not proposed at the beginning of it. The monitoring station built for the purpose of this work proved to be a reliable source of data, and its future operation will continue to deliver interesting results if further analysis is performed.

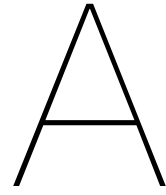
It needs to be considered that, although the evaluated modules delivered a lower performance ratio than the c-Si technologies, the current state of development indicate that, if the resources available for a continuous development of the thin film a-Si:H technology are sufficient, the gap between a competitive and cost effective a-Si:H and c-Si device is not large. The unique physical characteristics of the thin film technologies also make them a more attractive option for particular applications where c-Si implementation is not straight-forward. The analysis here performed helped validate one of the claimed benefits of the a-Si:H technology compared with c-Si, a 4 times better temperature coefficient compared with the one of c-Si modules. If further development is performed on these modules, a matching application for the implementation of these modules would be in high irradiance, warm weather locations, where the characteristics of the module when exposed to high temperature would yield a better performance than other photovoltaic technologies.

Outlook

This work created a data acquisition system that, as of the 25th of November of 2019, is recording the performance of the system described by this work. The continuity of this project will yield further knowledge on the behaviour of the HyET Solar thin film flexible and lightweight a-Si:H modules. A continuity on the analysis of this data is highly advised.

The monitoring station design allows for an easy change of the evaluated modules, this characteristic can prove to be beneficial in the future if different variations within the same a-Si:H modules want to be researched. Nevertheless, it is highly advised that at least one of the 4 subsystems delivered with this project are kept permanently on the monitoring station as the obtained data will yield valuable knowledge on the degradation process experienced by the modules when exposed to real operation conditions.

On the model created, the time factor resulted in the non inclusion of the spectral mismatch evaluation. Including this loss mechanism in the model evaluation will improve the model reach.



Power Optimizers Datasheets



Power optimizer

P300 / P370 / P404 / P405 / P500 / P505



POWER OPTIMIZER

Vermogensoptimalisatie op paneelniveau

- Speciaal ontworpen om te werken met SolarEdge omvormers
- Tot 25% meer opbrengst
- Superieur rendement (99,5%)
- Verhelpt elk verlies dat ontstaat door 'mismatch', variërend van produkttoleranties tot schaduwvorming
- Flexibel systeemontwerp voor optimaal gebruik van de beschikbare ruimte
- Snelle montage door één enkele bevestiging
- Geavanceerd onderhoud dankzij monitoring op paneelniveau
- Spanningsafschakeling op paneelniveau voor de veiligheid van installateurs en brandweer

Optimizer model (geschikte paneeltypes)	P300 (60-cels panelen)	P370 (hoog vermogen 60- en 72-cels panelen)	P500 (96-cels panelen)	P404 (60- en 72-cels panelen, korte strings)	P405 (dunne film panelen)	P505 (panelen met hoge stromen)	
INGANG							
Nominale DC-ingangsvermogen ⁽¹⁾	300	370	500	405	405	505	W
Absolute maximale ingangsspanning (Voc bij laagste temperatuur)	48	60	80	80	125	83	Vdc
MPPT-werkbereik	8 - 48	8 - 60	8 - 80	12,5 - 80	12,5 - 105	12,5-83	Vdc
Maximale kortsluitstroom (Isc)	11		10,1		14		Adc
Maximaal rendement				99,5			%
EU rendement				98,8			%
Overspanningscategorie				II			
UITGANG TIJDENS GEBRUIK (POWER OPTIMIZER IS AANGESLOTEN OP WERKENDE SOLAREDEGE OMVORMER)							
Maximale uitgangsstroom				15			Adc
Maximale uitgangsspanning	60			85			Vdc
UITGANG TIJDENS STAND-BY (POWER OPTIMIZER IS LOSGEKOPPELD VAN OMVORMER OF OMVORMER IS UIT)							
Veilige uitgangsspanning per power optimizer				1 ± 0,1			Vdc
NORM- EN REGELGEVING							
EMC	FCC deel 15 klasse B, IEC61000-6-2, IEC61000-6-3						
Veiligheidseisen	IEC62109-1 (klasse II veiligheid), UL1741						
RoHS	Ja						
Brandveiligheid	VDE-AR-E 2100-712:2013-05						
INSTALLATIE SPECIFICATIES							
Maximale toegestane systeemspanning	1.000						Vdc
Afmetingen (B x L x H)	128 x 152 x 28		128 x 152 x 36		128 x 152 x 50	128 x 152 x 59	mm
Gewicht (inclusief kabels)	630	655	750	775	845	1.064	gr
Ingangsconnector	MC4 ⁽²⁾				Enkele of dubbele MC4 ⁽³⁾	MC4 ⁽²⁾	
Uitgangsconnector	MC4						
Lengte uitgangskabels	0,95					1,2	m
Bedrijfstemperatuur	-40 - +85						°C
Beschermingsklasse	IP68						
Relatieve vochtigheid	0 - 100						%

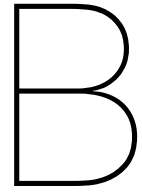
⁽¹⁾ Nominale STC-waarde van het paneel. Panelen met +5% tolerantie zijn toegestaan.

⁽²⁾ Neem contact op met SolarEde indien u andere type connectoren wilt gebruiken.

⁽³⁾ Dubbele ingang voor parallelle aansluiting van 2 dunne film panelen; P/N: P405-SRMDMRM. Bij een oneven aantal panelen in een string is het toegestaan om een P405 met dubbele ingang aan te sluiten op één paneel, waarbij de ongebruikte ingangsconnectoren afgesloten dienen te worden met de bijgeleverde afsluitdoppen.

PV-SYSTEEMONTWERP MET EEN SOLAREDEGE OMVORMER ⁽⁴⁾		1-FASE HD-WAVE	1-FASE	3-FASE	3-FASE (MET 480V TRANSFORMATOR)	
Minimale stringlengte (power optimizers)	P300, P370, P500 P404, P405, P505	8	6	16	18	
Maximale stringlengte (power optimizers)		25		50	50	
Maximaal vermogen per string		5.700	5.250	11.250	12.750	W
Parallele strings van ongelijke lengtes of oriëntaties		Ja				

⁽⁴⁾ Het is niet toegestaan om P404/P405/P505 in dezelfde string te plaatsen als de P300/P370/P500/P600/P700/P800.



Solar edge SE2200H Datasheet

Single Phase Inverter with HD-Wave Technology

SE2200H, SE3000H, SE3500H, SE3680H,
SE4000H, SE5000H, SE6000H

INVERTERS



Optimized installation with HD-Wave technology

- Specifically designed to work with power optimizers
- Record-breaking efficiency
- Extremely small, lightweight and easy to install
- High reliability
- Built-in module-level monitoring
- Outdoor and indoor installation
- Fixed voltage inverter for longer strings
- Smart Energy Management control
- Advanced safety feature - integrated arc fault protection
- Compatible with the StorEdge Interface for StorEdge™ applications

/ Single Phase Inverter with HD-Wave Technology

SE2200H, SE3000H, SE3500H, SE3680H, SE4000H, SE5000H, SE6000H

	SE2200H	SE3000H	SE3500H	SE3680H	SE4000H	SE5000H	SE6000H	
OUTPUT								
Rated AC Power Output	2200	3000	3500	3680	4000	5000 ⁽¹⁾	6000	VA
Maximum AC Power Output	2200	3000	3500	3680	4000	5000 ⁽¹⁾	6000	VA
AC Output Voltage (Nominal)	220/230							Vac
AC Output Voltage Range	184 - 264.5							Vac
AC Frequency (Nominal)	50/60 ± 5							Hz
Maximum Continuous Output Current	10	14	16	16	18.5	23	27.5	A
Utility Monitoring, Islanding Protection, Configurable Power Factor, Country Configurable Thresholds	Yes							
INPUT								
Maximum DC Power	3400	4650	5425	5700	6200	7750 ⁽²⁾	9300	W
Transformer-less, Ungrounded	Yes							
Maximum Input Voltage	480							Vdc
Nominal DC Input Voltage	380							Vdc
Maximum Input Current	6.5	9	10	10.5	11.5	13.5	16.5	Adc
Reverse-Polarity Protection	Yes							
Ground-Fault Isolation Detection	600kΩ Sensitivity per Unit							
Maximum Inverter Efficiency	99.2							%
European Weighted Efficiency	98.3	98.8				99		%
Nighttime Power Consumption	< 2.5							W
ADDITIONAL FEATURES								
Supported Communication Interfaces	RS485, Ethernet, ZigBee (optional), WiFi (optional), Cellular (optional)							
Smart Energy Management	Export Limitation, Smart Energy, StorEdge Applications							
Arc Fault Protection	Integrated, User Configurable (According to UL1699B)							
STANDARD COMPLIANCE								
Safety	IEC-62109-1/2, AS-3100							
Grid Connection Standards	AS-4777, VDE-AR-N-4105, VDE 0126-1-1, UTE C15-712, G83/2, G59/3, CEI-021, EN 50438, IEC61727, IEC62116, ÖNORM, TF3.2.1, C10-11, NRS 097-2-1							
Emissions	IEC61000-6-2, IEC61000-6-3, IEC61000-3-11, IEC61000-3-12, FCC Part 15 Class B							
INSTALLATION SPECIFICATIONS								
AC Output - Supported Cable Diameter	9-16							mm
AC - Supported Wire Cross Section	1-13							mm ²
DC Input	1 x MC4				2 x MC4 pair			
Dimensions (H x W x D)	280 x 370 x 142							mm
Noise	< 25							dB(A)
Weight	7.8				9	10.6		kg
Cooling	Natural Convection							
Operating Temperature Range	-20 to +60 ⁽³⁾ (-40°C option)							°C
Protection Rating	IP65 — Outdoor and Indoor							

⁽¹⁾ 4600VA in Germany

⁽²⁾ 7130VA in Germany

⁽³⁾ For power de-rating information refer to: <https://www.solaredge.com/sites/default/files/se-temperature-derating-note.pdf>

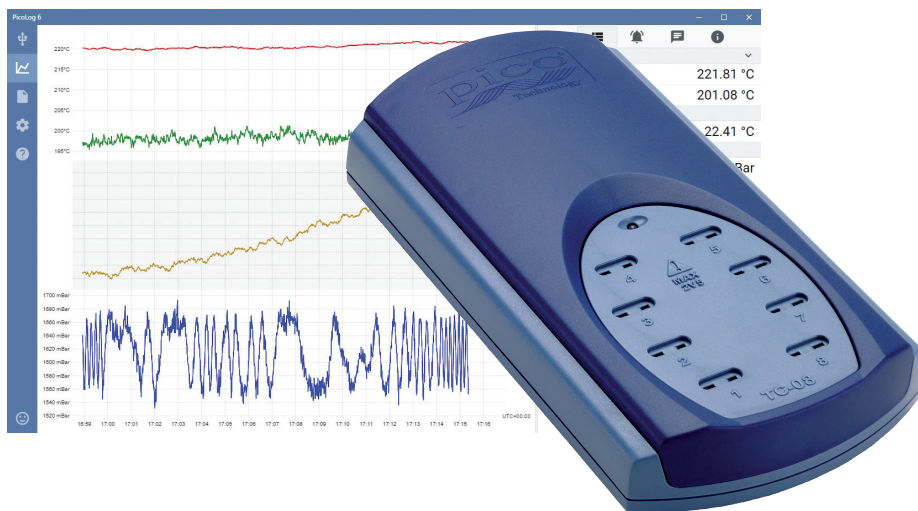
C

Datalogger



TC-08

8-channel thermocouple data logger



Low cost, high resolution

- Measures and records up to eight thermocouples at once
- 20-bit resolution and high accuracy
- Supports all commonly used thermocouple types
- Measures from $-270\text{ }^{\circ}\text{C}$ to $+1820\text{ }^{\circ}\text{C}$
- Built-in cold junction compensation
- Up to 10 measurements per second
- USB-connected and powered
- Run multiple units on a single PC
- Free to download PicoLog 6 and PicoScope 6 software
- Free software development kit
- Example programs available to download
- Free technical support
- Free software updates
- Compatible with Windows, macOS and Linux

www.picotech.com

TC-08 thermocouple data logger

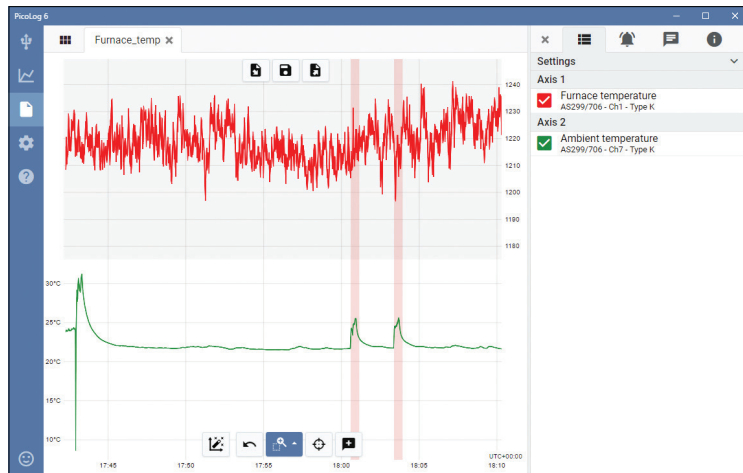
The USB TC-08 thermocouple data logger offers industry-leading performance and a cost-effective temperature measurement solution. With eight direct thermocouple inputs, the USB TC-08 can take accurate, rapid readings. In addition, you can use up to 20 units simultaneously on one PC. The logger can measure and record temperatures ranging from $-270\text{ }^{\circ}\text{C}$ to $+1820\text{ }^{\circ}\text{C}$ using the appropriate thermocouple type (B, E, J, K, N, R, S, T). It draws power from your computer's USB port, so no external power supply is necessary.

Wide temperature range

The TC-08 thermocouple data logger is designed to measure a wide range of temperatures using any thermocouple that has a miniature thermocouple connector. Pico supplies a wide range of suitable thermocouples (see **Ordering information**).

All types of thermocouple in common use today are supported, allowing an effective temperature range of $-270\text{ }^{\circ}\text{C}$ to $+1820\text{ }^{\circ}\text{C}$ (the actual temperature range depends on the thermocouple being used).

You can also use the built-in cold junction compensation (CJC) circuit as a ninth channel to measure ambient temperature.



Fast and accurate temperature data acquisition

With the TC-08 thermocouple data logger, you can make temperature measurements both quickly and accurately.

The short conversion time of the TC-08 means that it can take up to 10 temperature measurements every second (CJC counts as an additional measurement), while the high (20-bit) resolution ensures that the TC-08 can detect minute changes in temperature. For Type K thermocouples, the TC-08 can maintain a better than $0.025\text{ }^{\circ}\text{C}$ resolution over a $-250\text{ }^{\circ}\text{C}$ to $+1370\text{ }^{\circ}\text{C}$ range.

PicoLog 6 software – straightforward from the start

PicoLog 6 is a complete data acquisition software package for the TC-08 data logger, and is fully compatible with Windows, macOS and Linux. With its clear and user-friendly layout, ideal for use with a mouse or a touchscreen, PicoLog 6 allows you to set up the logger and start recording with just a few clicks of the mouse, whatever your level of data logging experience. Set up simple or advanced acquisitions quickly, and record, view and analyze your data with ease.

Capture controls
Separate Record, Pause and Reset buttons make it harder to press any of them by mistake.

Save and Export options
Copy your graph to the clipboard, save it as a PDF, export the raw data to a CSV file, or save the data and configuration as a robust .picoLog database file.

Alarms
Set up alarms to alert you to a range of events. Alarms can take the form of sounds, visual notifications, graph annotations and more.

Notes & annotations
Add notes about the dataset as a whole or annotations about particular points on the graph.

Device settings view
Easily set up and adjust acquisition and math channels on one or more data loggers and check their status at a glance.

Graph view
Display your data in real time, as it is collected, on up to four independent Y axes simultaneously: set them up by dragging and dropping the entries in the Channels & Axes panel on the right.

Give instant feedback
We want to hear from you! Click here to contact Pico with your comments.

Pullout information panel
Manage your channel and axis settings, alarms, notes and capture information in this easy-to-read layout. Close the panel to make more room for the capture graph, and reopen it at any time.

Multiple devices
Log data on up to 20 devices at the same time. Here, three separate data loggers are in use: two USB TC-08s and one ADC-24 voltage input logger.

Data view
Display all the data collected so far or keep the graph scale the same and pan along as new samples appear.

Pan and zoom controls
Zoom in, zoom out, zoom to a selection or pan through the data with these tools. If you make a mistake, just click Undo.

Cursors and annotations
Use cursors to highlight the data value and time at any point on the graph, or click Add annotation to mark that point with a text note.

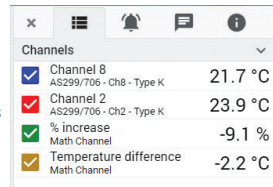
Settings Panel Data:

Axis	Channel	Value
Axis 1	Tank - top (A0024/014 1 Type K)	112.85 °C
	Tank - base (A0024/014 2 Type K)	101.88 °C
Axis 2	Lab ambient temperature (AS299/706 1 Type K)	24.99 °C
Axis 3	Differential 1 - 2 (EV377/014 1 - 2 ±1.25 V)	883.34 mBar

Math channels

Sometimes you need to use data from one or more measurement channels to graph and record a calculated parameter. You can use the PicoLog 6 equation editor to set up simple math channels such as A-B or more complex functions such as log, sqrt, abs, round, min, max, mean and median.

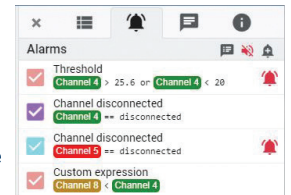
PicoLog 6 treats math channels like any other channel, so you can still set alarms and annotate them.



Channel	Value
Channel 8 AS299/706 - Ch8 - Type K	21.7 °C
Channel 2 AS299/706 - Ch2 - Type K	23.9 °C
% Increase Math Channel	-9.1 %
Temperature difference Math Channel	-2.2 °C

Alarms

In PicoLog 6, you can set up alarms to alert you to various events. These can be as simple or as complex as you like: alarms can trigger on a signal threshold or disconnection of the data logger, or you can set up a logic expression of your own. Alarms can play sounds, display visual alerts, run applications or mark when the event occurred on the graph.

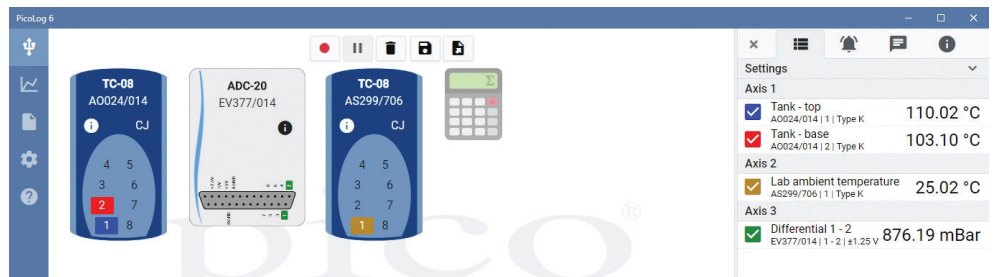


Alarm	Value
Threshold Channel 4 > 25.6 or Channel 4 < 20	
Channel disconnected Channel 4 == disconnected	
Channel disconnected Channel 5 == disconnected	
Custom expression Channel 1 > Channel 4	

Intuitive logger and channel setup

The Devices view lets you set up a multichannel acquisition system in a simple way, with the option to use multiple different Pico data loggers simultaneously. PicoLog shows you an image of each connected device, so you can quickly and easily enable or disable channels and set up their properties.

On the right, you can see the device setup for the acquisition on the previous page: two TC-08s and one ADC-20 voltage input logger.



The screenshot shows the PicoLog 6 interface with three virtual devices: two TC-08 thermocouples (A0024/014 and AS299/706) and one ADC-20 voltage input logger (EV377/014). On the right, the Settings panel is open, showing three axes of data being logged:

Axis	Channel	Value
Axis 1	Tank - top A0024/014 1 Type K	110.02 °C
Axis 1	Tank - base A0024/014 2 Type K	103.10 °C
Axis 2	Lab ambient temperature AS299/706 1 Type K	25.02 °C
Axis 3	Differential 1 - 2 EV377/014 1 - 2 ±1.25 V	876.19 mBar

Robust file format

At the heart of PicoLog 6 is the file system, which stores live capture data directly to a robust database, rather than to a single file that is vulnerable to corruption and data loss. If the computer is shut down and rebooted, PicoLog will only lose the data during the outage – saving resumes when you restart the software.

This file system also means that the size of the dataset you can capture you is virtually unlimited – the only restriction is the size of your computer's hard disk!

The .picolog file format is compatible across all operating systems, and there is no need to set up a file to save to before the capture is complete. You can also save mid-capture if you wish to share the data collected so far. Since anyone can download and install PicoLog 6 for free, you can easily share saved data with co-workers, customers and suppliers for offline post-analysis.

Data can be exported as CSV. In addition, you can export a PDF containing a graph, channel configuration, capture notes, annotation notes and alarm trigger history.

PicoSDK®

Pico's software development kit, PicoSDK, is available free of charge and allows you to write your own software and interface to third-party software packages.

Pico also maintains repositories of example code on GitHub (github.com/picotech), showing how to use PicoSDK with software packages such as Microsoft Excel, National Instruments LabVIEW and MathWorks MATLAB, or with programming languages including C, C++, C# and Visual Basic .NET.

PicoSDK and the *TC-08 Programmer's Guide* are available to download from www.picotech.com/downloads.



Try the PicoLog 6 software today!

PicoLog 6's built-in demo mode allows you to try out the full functionality of the software with a choice of virtual devices and simulated live data. You also can use PicoLog 6 to view previously saved data, even with no device connected. Visit www.picotech.com/downloads and select **PicoLog Data Loggers** to get your copy.

USB TC-08 thermocouple data logger

Specifications

Hardware	
Number of channels (single unit)	8
Maximum number of channels (using up to 20 units)	160
Conversion time	100 ms per thermocouple channel + 100 ms for CJC (this can be disabled if all channels are used as voltage inputs)
Temperature accuracy	Sum of $\pm 0.2\%$ of reading and $\pm 0.5\text{ }^{\circ}\text{C}$
Voltage accuracy	Sum of $\pm 0.2\%$ of reading and $\pm 10\text{ }\mu\text{V}$
Overvoltage protection	$\pm 30\text{ V}$
Maximum common-mode voltage	$\pm 7.5\text{ V}$
Input impedance	2 M Ω
Input range (voltage)	$\pm 70\text{ mV}$
Resolution	20 bits
Noise-free resolution	16.25 bits
Thermocouple types supported	B, E, J, K, N, R, S, T
Input connectors	Miniature thermocouple
General	
Connectivity	USB 2.0
Device connector type	USB 2.0, Type B
Power requirements	USB port
Dimensions	201 x 104 x 34 mm (7.91 x 4.09 x 1.34 in)
Temperature range, operating	0 $^{\circ}\text{C}$ to 50 $^{\circ}\text{C}$
Temperature range, operating, for quoted accuracy	20 $^{\circ}\text{C}$ to 30 $^{\circ}\text{C}$
Temperature range, storage	-20 $^{\circ}\text{C}$ to 60 $^{\circ}\text{C}$
Humidity range, operating	5 to 80 % RH non-condensing
Humidity range, storage	5 to 95 % RH non-condensing
Altitude	Up to 2000 m
Pollution degree	Pollution degree 2
Water resistance	Not water-resistant
Safety approvals	Designed to 2014/35/EU: Low Voltage Directive
EMC approvals	Tested to 2014/30/EU: Electromagnetic Compatibility Directive
Environmental approvals	RoHS and WEEE compliant
Software	PicoLog 6, PicoSDK (available from www.picotech.com/downloads) Example code (available from Pico's GitHub organization page, github.com/picotech)

General (continued)	
PC requirements	Windows 7, 8 or 10, 32-bit or 64-bit macOS 10.9 (Mavericks) or later, 64-bit only Linux (tested on OpenSUSE and Ubuntu), 64-bit only Hardware as required by the operating system
Documentation	Quick Start Guide User's Guide Programmer's Guide EU Declaration of Conformity All relevant documentation is available for download from www.picotech.com/downloads

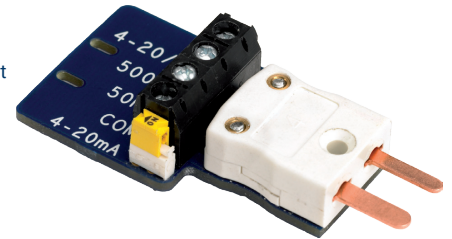
Compatible thermocouples

The TC-08 is compatible with all commonly used thermocouples, offering high accuracy without compromising acquisition speed. Thermocouple types and temperature ranges are shown in the table below.

Type	Overall range (°C)	0.1 °C resolution	0.025 °C resolution
B	20 to 1820	150 to 1820	600 to 1820
E	-270 to 910	-270 to 910	-260 to 910
J	-210 to 1200	-210 to 1200	-210 to 1200
K	-270 to 1370	-270 to 1370	-250 to 1370
N	-270 to 1300	-260 to 1300	-230 to 1300
R	-50 to 1760	-50 to 1760	20 to 1760
S	-50 to 1760	-50 to 1760	20 to 1760
T	-270 to 400	-270 to 400	-250 to 400

Also measures voltage and current!

The optional TC-08 single-channel terminal board plugs into one channel on the data logger and has a set of screw terminals, allowing you to connect sensors with voltage or current outputs to the data logger without any need for soldering. The four input ranges (± 50 mV, ± 500 mV, ± 5 V and 4–20 mA) allow you to measure a wide range of signals.



USB TC-08 thermocouple data logger

Ordering information

Pico offers both off-the-shelf and built-to-order thermocouples for use with the TC-08. If you require a custom build for your application, our Technical Support team is available to discuss your requirements. You can contact the team via email (support@picotech.com),

Type K and T thermocouples

Order code	Product name	Description	USD*	EUR*	GBP*
SE059	SE059 thermocouple type K	High-temperature, exposed tip, fiberglass insulated, 1 m	26	22	18
SE060	SE060 thermocouple type K	High-temperature, exposed tip, fiberglass insulated, 2 m	36	31	25
SE061	SE061 thermocouple type K	High-temperature, exposed tip, fiberglass insulated, 3 m	45	38	31
SE062	SE062 thermocouple type K	High-temperature, exposed tip, fiberglass insulated, 5 m	65	55	45
SE002	SE002 thermocouple type K	Probe, air, 4.5 mm tip	48	41	33
SE001	SE001 thermocouple type K	Exposed tip, fiberglass insulated, 1 m	10	9	7
SE030	SE030 thermocouple type K	Exposed tip, fiberglass insulated, 2 m	14	12	9
SE031	SE031 thermocouple type K	Exposed tip, fiberglass insulated, 5 m	20	17	15
SE000	SE000 thermocouple type K	Exposed tip, PTFE insulated, 1 m	10	9	7
SE027	SE027 thermocouple type K	Exposed tip, PTFE insulated, 2 m	14	12	9
SE028	SE028 thermocouple type K	Exposed tip, PTFE insulated, 3 m	15	13	10
SE029	SE029 thermocouple type K	Exposed tip, PTFE insulated, 10 m	30	26	21
SE003	SE003 thermocouple type K	Insertion, 3.3 mm tip	40	34	28
SE004	SE004 thermocouple type K	Ribbon surface, 8 mm tip	48	41	33
SE056	SE056 thermocouple type T	5 mm × 50 mm stainless steel waterproof tip, silicone insulated, 3 m	40	34	28
SE057	SE057 thermocouple type T	5 mm × 50 mm stainless steel waterproof tip, silicone insulated, 5 m	55	46	38
SE058	SE058 thermocouple type T	5 mm × 50 mm stainless steel waterproof tip, silicone insulated, 10 m	96	79	66
SE051	SE051 thermocouple type T	Exposed tip, fiberglass insulated, 1 m	10	9	7
SE052	SE052 thermocouple type T	Exposed tip, fiberglass insulated, 2 m	13	11	9
SE053	SE053 thermocouple type T	Exposed tip, fiberglass insulated, 3 m	16	14	11
SE054	SE054 thermocouple type T	Exposed tip, fiberglass insulated, 5 m	22	19	15
SE055	SE055 thermocouple type T	Exposed tip, fiberglass insulated, 10 m	30	26	21
SE046	SE046 thermocouple type T	Exposed tip, PTFE insulated, 1 m	10	9	7
SE047	SE047 thermocouple type T	Exposed tip, PTFE insulated, 2 m	13	11	9
SE048	SE048 thermocouple type T	Exposed tip, PTFE insulated, 3 m	16	14	11
SE049	SE049 thermocouple type T	Exposed tip, PTFE insulated, 5 m	22	19	15
SE050	SE050 thermocouple type T	Exposed tip, PTFE insulated, 10 m	30	26	21

* Prices correct at the time of publication. Sales taxes not included. Please check www.picotech.com for the latest prices before ordering.

Ordering information (continued)

Order code	Product name	Description	USD*	EUR*	GBP*
PP222	TC-08	Thermocouple data logger with Pico blue USB 2.0 cable, 1.8 m	409	349	289

Optional accessories

Order code	Product name	Description	USD*	EUR*	GBP*
PP624	TC-08 single-channel terminal board	Single-channel terminal board for use with USB TC-08 thermocouple data logger	30	26	21
MI106	USB 2.0 cable, 1.8 m**	Replacement Pico blue USB 2.0 cable, 1.8 m	9	7	6
TA268	USB 2.0 cable, 0.5 m**	Pico blue USB 2.0 cable, 0.5 m	9	7	6
MI121	USB 2.0 cable, 4.5 m**	Pico blue USB 2.0 cable, 4.5 m	17	14	12
CC001	Calibration certificate for thermocouple loggers	Calibration service offered by Pico on its temperature data loggers	83	70	58



* Prices correct at the time of publication. Sales taxes not included. Please check www.picotech.com for the latest prices before ordering.

** Pico blue USB cables are designed and built specifically for use with Pico Technology oscilloscopes and data loggers in order to minimize voltage drop and noise. Take care to use your TC-08 data logger with Pico blue USB cables only.

UK global headquarters:

Pico Technology
James House
Colmworth Business Park
St. Neots
Cambridgeshire
PE19 8YP
United Kingdom
☎ +44 (0) 1480 396 395
✉ sales@picotech.com

North America regional office:

Pico Technology
320 N Glenwood Blvd
Tyler
Texas 75702
United States
☎ +1 800 591 2796
✉ sales@picotech.com

Asia-Pacific regional office:

Pico Technology
Room 2252, 22/F, Centro
568 Hengfeng Road
Zhabei District
Shanghai 200070
PR China
☎ +86 21 2226-5152
✉ pico.china@picotech.com

Errors and omissions excepted. *Pico Technology*, *PicoLog*, *DrDAQ* and *PicoSDK* are internationally registered trademarks of Pico Technology Ltd.

LabVIEW is a trademark of National Instruments Corporation. *Linux* is the registered trademark of Linus Torvalds, registered in the U.S. and other countries. *macOS* is a trademark of Apple Inc., registered in the U.S. and other countries. *MATLAB* is a registered trademark of The MathWorks, Inc. *Windows* and *Excel* are registered trademarks of Microsoft Corporation in the United States and other countries.

MM001.en-9. Copyright © 2004–2019 Pico Technology Ltd. All rights reserved.

www.picotech.com



Pico Technology



@LifeAtPico



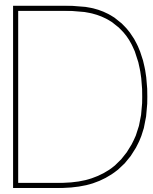
@picotechnologyltd



Pico Technology



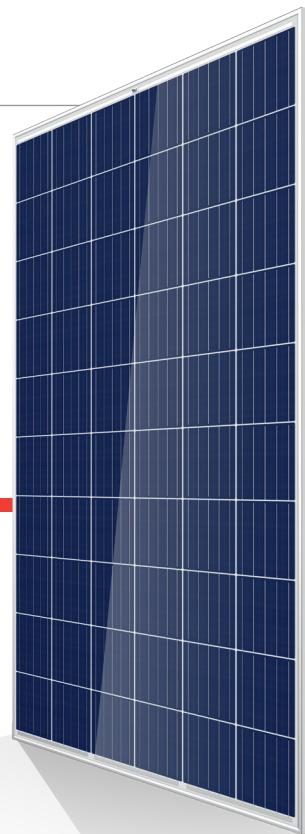
@picotech



Crystalline silicon modules data sheet

Honey MODULE

TSM-PD05



60 CELL
MULTICRYSTALLINE MODULE

270-285W
POWER OUTPUT RANGE

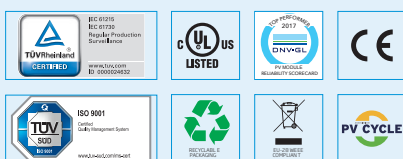
17.4%
MAXIMUM EFFICIENCY

0/+5W
POSITIVE POWER TOLERANCE

Founded in 1997, Trina Solar is the world's leading comprehensive solutions provider for solar energy. We believe close cooperation with our partners is critical to success. Trina Solar now distributes its PV products to over 60 countries all over the world. Trina Solar is able to provide exceptional service to each customer in each market and supplement our innovative, reliable products with the backing of Trina Solar as a strong, bankable partner. We are committed to building strategic, mutually beneficial collaboration with installers, developers, distributors and other partners.

Comprehensive Product And System Certificates

IEC61215/IEC61730/UL1703/IEC61701/IEC62716
 ISO 9001: Quality Management System
 ISO 14001: Environmental Management System
 ISO14064: Greenhouse Gas Emissions Verification
 OHSAS 18001: Occupational Health and Safety Management System



Excellent low light performance on cloudy days, mornings and evenings

- Advanced surface texturing
- Back surface field
- Selective emitter



Maximize Limited Space

- 60-cell module power output up to 285 W
- Up to 174 W/m² power density



Highly reliable due to stringent quality control

- All modules have to pass electroluminescence (EL) inspection
- Over 30 in-house tests (UV, TC, HF, and many more)
- In-house testing goes well beyond certification requirements
- PID resistant
- 1000 V UL/1000 V IEC certified

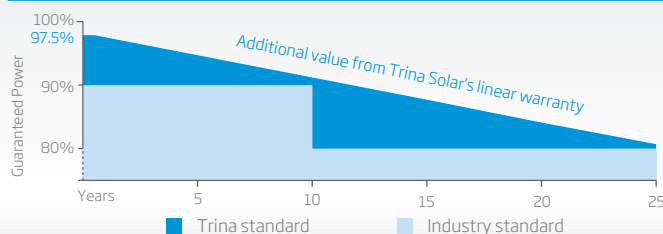


Certified to withstand challenging environmental conditions

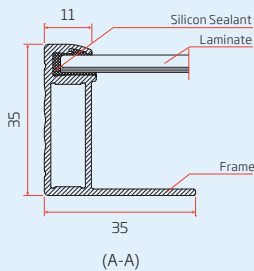
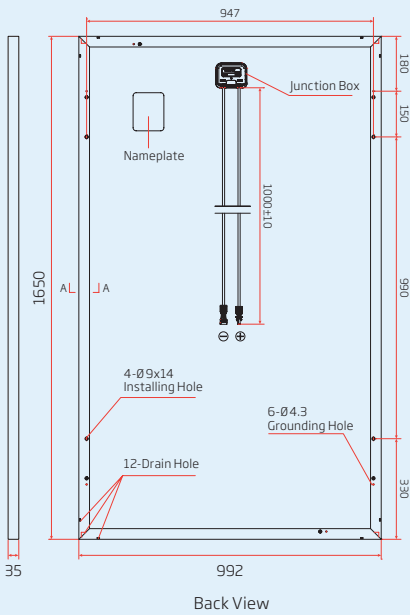
- 130 km/h wind load (2400 Pa)
- 900 kg snow load per module (5400 Pa)
- 35 mm hail stones at 97 km/h
- Ammonia resistance
- Salt mist resistance
- Resistance to sand and dust abrasion

LINEAR PERFORMANCE WARRANTY

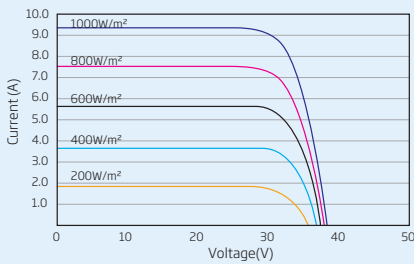
10 Year Product Warranty · 25 Year Linear Power Warranty



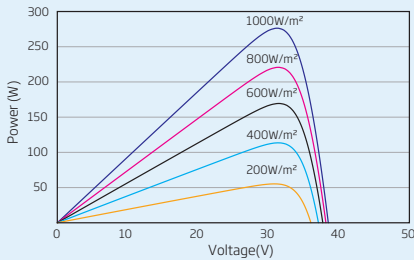
DIMENSIONS OF PV MODULE
TSM-PD05
(unit: mm)



I-V CURVES OF PV MODULE (280W)



P-V CURVES OF PV MODULE (280W)



ELECTRICAL DATA @ STC	TSM-270 PD05	TSM-275 PD05	TSM-280 PD05	TSM-285 PD05
Peak Power Watts- P_{MAX} (Wp)*	270	275	280	285
Power Output Tolerance- P_{MAX} (W)	0/+5	0/+5	0/+5	0/+5
Maximum Power Voltage- V_{MPP} (V)	30.9	31.1	31.4	31.6
Maximum Power Current- I_{MPP} (A)	8.73	8.84	8.92	9.02
Open Circuit Voltage- V_{OC} (V)	37.9	38.1	38.2	38.3
Short Circuit Current- I_{SC} (A)	9.22	9.32	9.40	9.49
Module Efficiency η_m (%)	16.5	16.8	17.1	17.4

STC: Irradiance 1000 W/m², Cell Temperature 25°C, Air Mass AM1.5
* Measuring tolerance: ±3%

ELECTRICAL DATA @ NOCT	TSM-270 PD05	TSM-275 PD05	TSM-280 PD05	TSM-285 PD05
Maximum Power- P_{MAX} (Wp)	200	204	208	211
Maximum Power Voltage- U_{MPP} (V)	28.6	28.8	29.0	29.2
Maximum Power Current- I_{MPP} (A)	7.00	7.09	7.15	7.23
Open Circuit Voltage- U_{OC} (V)	35.1	35.3	35.4	35.5
Short Circuit Current- I_{SC} (A)	7.44	7.52	7.59	7.66

NOCT: Irradiance at 800 W/m², Ambient Temperature 20°C, Wind Speed 1 m/s.

MECHANICAL DATA

Solar Cells	Multicrystalline 156.75 × 156.75 mm
Cell Orientation	60 cells (6 x 10)
Module Dimensions	1650 × 992 × 35 mm
Weight	18.6 kg
Glass	3.2 mm, high transparency, AR coated and heat tempered solar glass
Backsheet	White
Frame	Silver Anodized Aluminium Alloy
J-Box	IP 67 or IP 68 rated
Cables	Photovoltaic Technology Cable 4.0mm ² , 1000 mm
Connector	EU Countries: 28 MC4 / UTX / TS4, Non-EU Countries: 28 QC4 / TS4

TEMPERATURE RATINGS

Nominal Operating Cell Temperature (NOCT)	44°C (±2K)
Temperature Coefficient of P_{MAX}	- 0.41%/K
Temperature Coefficient of V_{OC}	- 0.32%/K
Temperature Coefficient of I_{SC}	0.05%/K

MAXIMUM RATINGS

Operational Temperature	-40 to +85°C
Maximum System Voltage	1000VDC (IEC) 1000VDC (UL)
Max Series Fuse Rating*	15 A
Mechanical Load	5400 Pa
Wind Load	2400 Pa

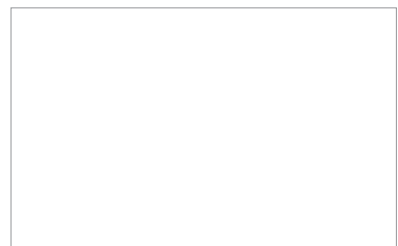
* DO NOT connect fuse in combiner box with two or more strings in parallel connection

WARRANTY

10 year Product Workmanship Warranty
25 year Linear Performance Warranty
(Please refer to product warranty for details)

PACKAGING CONFIGURATION

Modules per box:	30 pieces
Modules per 40' container:	840 pieces



TSM_EN_2017_LB

Bibliography

- [1] Dispositivi e sistemi fotovoltaici, 2013. Provided by Gianluca Limodio.
- [2] Ignacio Narvaez Alavez. Monitoring of bifacial floating pv systems and validation of a toolbox for its simulation., 2019.
- [3] Reinhart Appels, Buvaneshwari Lefevre, Bert Herteleer, Hans Goverde, Alexander Beerten, Robin Paesen, Klaas De Medts, Johan Driesen, and Jef Poortmans. Effect of soiling on photovoltaic modules. *Solar energy*, 96:283–291, 2013.
- [4] Michael Buday. Measuring irradiance, temperature, and angle incidence effects on photovoltaic modules in auburn hills, michigan. Master's thesis, 2011.
- [5] Chris Deline. Partially shaded operation of a grid-tied pv system. In *2009 34th IEEE Photovoltaic Specialists Conference (PVSC)*, pages 001268–001273. IEEE, 2009.
- [6] Yanping Du, Christopher J Fell, Benjamin Duck, Dong Chen, Kurt Liffman, Yinan Zhang, Min Gu, and Yonggang Zhu. Evaluation of photovoltaic panel temperature in realistic scenarios. *Energy Conversion and Management*, 108:60–67, 2016.
- [7] Swapnil Dubey, Jatin Narotam Sarvaiya, and Bharath Seshadri. Temperature dependent photovoltaic (pv) efficiency and its effect on pv production in the world—a review. *Energy Procedia*, 33: 311–321, 2013.
- [8] Maria Fennis. Task 413: Temperature coefficient measurements, 2016.
- [9] IEC. 61724-1: 2017, photovoltaic system performance-part 1: Monitoring, 2018.
- [10] David L King, Jay A Kratochvil, and William E Boyson. Measuring solar spectral and angle-of-incidence effects on photovoltaic modules and solar irradiance sensors. pages 1113–1116, 1997.
- [11] David L King, Jay A Kratochvil, and William E Boyson. Temperature coefficients for pv modules and arrays: measurement methods, difficulties, and results. pages 1183–1186, 1997.
- [12] David L King, Jay A Kratochvil, and William Earl Boyson. Photovoltaic array performance model. 2004.
- [13] Bill Marion, J Adelstein, K ea Boyle, H Hayden, B Hammond, T Fletcher, B Canada, D Narang, A Kimber, L Mitchell, et al. Performance parameters for grid-connected pv systems. pages 1601–1606, 2005.
- [14] Jenya Meydbray. Pyranometers and reference cells, what's the difference? *PV Magazine*, 2012.
- [15] Pramod Nepal. Effect of soiling on the pv panel kwh output. 2018.
- [16] Takashi Oozeki, Kenji Otani, and Kosuke Kurokawa. An evaluation method for pv system to identify system losses by means of utilizing monitoring data. 2:2319–2322, 2006.
- [17] Mauricio D Perez and Nima E Gorji. Modeling of temperature profile, thermal runaway and hot spot in thin film solar cells. *Materials Science in Semiconductor Processing*, 41:529–534, 2016.
- [18] Y Riesen, M Stuckelberger, F-J Haug, C Ballif, and N Wyrsh. Temperature dependence of hydrogenated amorphous silicon solar cell performances. *Journal of Applied Physics*, 119(4):044505, 2016.
- [19] Santiago Silvestre, Alfredo Boronat, and A Chouder. Study of bypass diodes configuration on pv modules. *Applied Energy*, 86(9):1632–1640, 2009.

- [20] Arno HM Smets, Klaus Jäger, Olindo Isabella, RACMM van Swaaij, and Miro Zeman. *Solar Energy: The physics and engineering of photovoltaic conversion technologies and systems*. UIT, 2016.
- [21] DL Staebler and C R_ Wronski. Optically induced conductivity changes in discharge-produced hydrogenated amorphous silicon. *Journal of Applied Physics*, 51(6):3262–3268, 1980.
- [22] DL Staebler and CR Wronski. Reversible conductivity changes in discharge-produced amorphous si. *Applied physics letters*, 31(4):292–294, 1977.
- [23] M Stutzmann, WB Jackson, and CC Tsai. Kinetics of the staebler–wronski effect in hydrogenated amorphous silicon. *Applied Physics Letters*, 45(10):1075–1077, 1984.
- [24] Quinten Swanborn. Heat transfer model for hyet solar single junction modules, 2019.
- [25] Hairen Tan. *Materials and Light Management for High-Efficiency Thin-Film Silicon Solar Cells*. PhD thesis, 09 2015.
- [26] Elias Urrejola, Javier Antonanzas, Paulo Ayala, Marcelo Salgado, Gonzalo Ramírez-Sagner, Cristian Cortés, Alan Pino, and Rodrigo Escobar. Effect of soiling and sunlight exposure on the performance ratio of photovoltaic technologies in santiago, chile. *Energy Conversion and Management*, 114:338–347, 2016.
- [27] WGJHM Van Sark, Nils Holger Reich, Björn Müller, Alfons Armbruster, Klaus Kiefer, and Christian Reise. Review of pv performance ratio development. pages 4795–4800, 2012.
- [28] Wilfried van Sark, Lex Bosselaar, Pierre Gerrissen, KBD Esmeijer, Panagiotis Moraitis, Menno van den Donker, and Gerjan Emsbroek. Update of the dutch pv specific yield for determination of pv contribution to renewable energy production: 25% more energy! *Proceedings of the 29th EUR-PSEC*, pages 4095–4097, 2014.
- [29] A Virtuani, E Lotter, M Powalla, U Rau, and JH Werner. Highly resistive cu (in, ga) se₂ absorbers for improved low-irradiance performance of thin-film solar cells. *Thin Solid Films*, 451:160–165, 2004.
- [30] Yaw-Juen Wang and Po-Chun Hsu. An investigation on partial shading of pv modules with different connection configurations of pv cells. *Energy*, 36(5):3069–3078, 2011.
- [31] J Zorrilla-Casanova, M Piliouge, J Carretero, P Bernaola, P Carpena, L Mora-López, and M Sidrach-de Cardona. Analysis of dust losses in photovoltaic modules. In *World Renewable Energy Congress-Sweden; 8-13 May; 2011; Linköping; Sweden*, number 057, pages 2985–2992. Linköping University Electronic Press, 2011.